EXPERIMENTAL STUDY OF A TWO-DOF FIVE BAR CLOSE-LOOP MECHANISM

A Thesis Submitted to the

College of Graduate Studies and Research

In Partial Fulfillment of the Requirements

for the Degree of Master of Science

in The Department of Mechanical Engineering

University of Saskatchewan

Canada

By

Reza Moazed

©Copyright R. Moazed, August 2006. All rights reserved.

PERMISSION TO USE

In presenting this thesis in partial fulfillment of the requirements for a Postgraduate degree from the University of Saskatchewan, I agree that the Libraries of this University may make it freely available for inspection. I further agree that permission for copying of this thesis in any manner, in whole or in part, for scholarly purposes may be granted by the professor or professors who supervised my thesis work or, in their absence, by the Head of the Department or the Dean of the College in which this thesis was done. It is understood that any copying or publication or use of this thesis or parts thereof for financial gain shall not be allowed without my written permission. It is also understood that due recognition shall be given to me and to the University of Saskatchewan in any scholarly use which may be made of any material in my thesis.

Requests for permission to copy or to make other use of material in this thesis in whole or part should be addressed to:

Head of the Department of Mechanical Engineering

University of Saskatchewan

Saskatoon, Saskatchewan

Canada S7N 5A9

ABSTRACT

This research is to carry out an experimental study to examine and verify the effectiveness of the control algorithms and strategies developed at the Advanced Engineering Design Laboratory (AEDL). For this purpose, two objectives are set to be achieved in this research. The first objective is to develop a generic experiment environment (test bed) such that different control approaches and algorithms can be implemented on it. The second objective is to conduct an **e**xperimental study on the examined control algorithms, as applied to the above test bed.

To achieve the first objective, two main test beds, namely, the real-time controllable (RTC) mechanism and the hybrid machine, have been developed based on a two degree of freedom (DOF) closed-loop five-bar linkage. The 2-DOF closed-loop mechanism is employed in this study as it is the simplest of multi-DOF closed-loop mechanisms, and control approaches and conclusions based on a 2-DOF mechanism are generic and can be applied to a closed-loop mechanism with a higher number of degrees of freedom. The RTC mechanism test bed is driven by two servomotors and the hybrid machine is driven by one servomotor and a traditional CV motor.

To achieve the second objective, an experimental study on different control algorithms has been conducted. The Proportional Derivative (PD) based control laws, i.e., traditional

PD control, Nonlinear-PD (NPD) control, Evolutionary PD (EPD) control, non-linear PD learning control (NPD-LC) and Adaptive Evolutionary Switching-PD (AES-PD) are applied to the RTC mechanism; and as applied to the Hybrid Actuation System (HAS), the traditional PD control and the SMC control techniques are examined and compared.

In the case of the RTC mechanism, the experiments on the five PD-based control algorithms, i.e., PD control, NPD control, EPD, NPD-LC, and AES-PD, show that the NPD controller has better performance than the PD controller in terms of the reduction in position tracking errors. It is also illustrated by the experiments that iteration learning control (ILC) techniques can be used to improve the trajectory tracking performance. However, AES-PD showed to have a faster convergence rate than the other ILC control laws. Experimental results also show that feedback ILC is more effective than the feedforward ILC and has a faster convergence rate. In addition, the results of the comparative study of the traditional PD and the Computed Torque Control (CTC) technique at both low and high speeds show that at lower speeds, both of these controllers provide similar results. However, with an increase in speed, the position tracking errors using the CTC control approach become larger than that of the traditional PD control.

In the case of the hybrid machine, PD control and SMC control are applied to the mechanism. The results show that for the control of the hybrid machine and the range of speed used in this experimental study, PD control can result in satisfactory performance. However, SMC proved to be more effective than PD control.

ACKNOWLEGMENTS

I would like to take this opportunity to express my sincere thanks to my supervisors, Professor C. Zhang and Professor D. Chen, for their valuable guidance and continuous encouragement in the whole research as well as the critical review of the manuscript.

I would like to extend my special thanks to the other members of my advisory committee: Professor M. M. Gupta, Professor R. Fotouhi for their valuable support and constructive suggestions throughout the course of this project.

I also acknowledge Dr. P. Ouyang, a former graduate student at the AEDL for his valuable suggestions and advice. I would also like to thank Mr. R.J. Wilson for making the HAS prototype used in this experimental study, and Mr. D. Bitner for his help with the experimental set-up of the RTC mechanism.

Dedicated to my mom and dad

Dr. Hadi Moazed and MRS. Malikeh Jafar Nejadi

Table of Contents

PERMISSION TO USE……i

ABSTRACT……...……ii

ACKNOWLEDGMENTS……..iv

TABLE OF CONTENTS…….....vi

LIST OF TABLES……...x

LIST OF FIGURES……xi

ACRONYMS……...…….xiv

CHAPTER 1 Introduction……1

1.1 Background and motivation……...1

1.2 Traditional Mechanisms Vs Mechatronic Mechanisms…….3

1.3 Research objectives and scopes…….5

1.4 General Methodology……6

1.5 Organization of the thesis……..8

CHAPTER 2 Literature Review……10

2.1 Introduction……..10

2.2 Servo mechanisms and hybrid actuation systems……....11

2.3 Dynamics of multi-DOF closed-loop mechanisms……..13

2.4 Control Schemes for Multi-DOF Closed-loop Mechanisms……...22

2.4.1 PD based control methods……....22

2.4.2 Model based control methods……...24

2.5 Previous works developed at the AEDL at the University of Saskatchewan……..25

2.6 Trajectory planning methods……...26

2.7 Summary……..27

CHAPTER 3 Test Beds for Experimental Study

3.1 Introduction……..28

3.2 Two DOF Five Bar Linkage Close-loop Mechanism……..29

3.3 RTC mechanism test bed…….33

3.4 Hybrid Actuation system test bed……36

3.5 User interface of the test beds……..40

3.6 Position and Velocity measurements……...42

3.7 Summary……..43

CHAPTER 4 Control Algorithms……..44

4.1 Introduction……..44

4.2 PD and NPD control laws……45

4.3 Iteration Learning Control (ILC)…….47

4.3.1 Iterative learning……...47

4.3.2 Evolutionary PD (EPD) control law…….49

4.3.3 Adaptive Evolutionary Switch Gain PD Control (AES-PD)……50

4.3.4 Adaptive Nonlinear PD learning control (NPD-LC)……52

4.4 Computed Torque Control (CTC) algorithm……...53

4.5 Summary and Discussion…….54

CHAPTER 5 EXPERIMENTS AND RESULTS ON THE RTC MECHANISM……...56

5.1 Introduction……..56

5.2 Trajectory planning for the two servomotors……...57

5.3 PD and NPD control laws……59

5.4 EPD control law……...65

5.5 NPD-LC control law……71

5.6 AES-PD control law……76

5.7 Comparison of the PD, NPD, EPD, AES-PD, NPD-LC Control methods……..82

5.8 Comparison of Feedforward ILC control to Feedback ILC control……86

5.9 Comparison of CTC control law to PD control law……89

5.10 Comments on the experiment……92

5.10.1 Initial position error……92

5.10.2 Sampling period……..93

5.10.3 Estimations of velocity……...93

5.11 Conclusion…….94

CHAPTER 6 EXPERIMENTS AND RESULTS ON THE HAS MECHANISM……...96

6.1 Introduction……..96

6.2 Dynamic model of the hybrid actuation system……..97

6.3 Sliding Mode Control (SMC) for nonlinear systems…….100

6.4 Trajectory Planning for the CV and Servomotor……...104

6.5 Experimental Results of the HAS……..105

6.7 Conclusion…….113

Chapter 7 Conclusion and Recommendation……..114

7.1 Overview of the thesis……...114

7.2 Major Conclusions…….115

7.3 Future Work……...116

References……...118

LIST OF TABLES

Table 3.1 Parameters of the five-bar mechanism……...31

Table 5.1 Performance improvement with the EPD control at the low speed case……...69

Table 5.2 Performance improvement with the EPD control at the high speed case……..70

Table 5.3 Performance improvement with the NPD-LC control at the low speed case…75

Table 5.4 Performance improvement with the NPD-LC control at the high speed case ……75

Table 5.5 Performance improvement with the AES-PD control at the low speed case….80

Table 5.6 Performance improvement with the AES-PD control at the high speed case ……80

Table 5.7: Experimental Results for PD, NPD, EPD, NPD-LC, AES-PD at the low speed case (maximum errors and torques in the actuators)…….80

Table 5.8: Experimental Results for PD, NPD, EPD, NPD-LC, AES-PD at the high speed case (maximum errors and torques in the actuators)…….85

Table 5.9 Performance improvement comparison of feedforward ILC and feedback ILC ……88

Table 6.1 The parameters of the two motors……...107

LIST OF FIGURES

Figure 2.1: The structure of a 2 DOF parallel robot……..15

Figure 3.1: Five-bar linkage mechanism……...29

Figure 3.2: Schematic of a five-bar linkage mechanism (Ouyang, 2002)…….30

Figure 3.3: Individual links of the five-bar mechanism: (a) Link 1, (b) Link 2, (c)Link 3, and (d) Link 4…….31

Figure 3.4: RTC mechanism test bed…….34

Figure 3.5: Control diagram of the RTC mechanism……35

Figure 3.6: Hybrid actuation system test bed…….37

Figure 3.7: Control diagram of the HAS mechanism……38

Figure 3.8: User Interface developed in C^{++} in the case of the RTC mechanism……..40

Figure 4.1: Iterative scheme of the iteration learning control algorithm……...48

Figure 5.1: Experimental results by applying PD and NPD controllers for the low speed case: (a) angle error of Actuator 1 and (b) angle error of Actuator 2……61

Figure 5.2: Experimental results by applying PD and NPD controllers for the low speed case: (a) torque of Actuator 1 and (2) torque of Actuator 2……...62

Figure 5.3: Experimental results by applying PD and NPD controllers for the high speed case: (a) angle error of Actuator 1 and (b) angle error of Actuator 2……63

Figure 5.4: Experimental results by applying PD and NPD controllers for the high speed case: (a) torque of Actuator 1 and (2) torque of Actuator 2……...64

Figure 5.5: Experimental results by applying EPD controller for the low speed case (Iterations 1 to 3): (a) angle error of Actuator 1 and (b) angle error of Actuator 2……..67

Figure 5.6: Experimental results by applying EPD controller for the low speed case (Iterations 3 to 6): (a) angle error of Actuator 1 and (b) angle error of Actuator 2……..68

Figure 5.7: Experimental results by applying EPD controller for the high case (Iterations 1 to 4): (a) angle error of Actuator 1 and (b) angle error of Actuator 2……69

Figure 5.8: Experimental results by applying NPD-LC controller for the low speed case (Iterations 1 to 3): (a) angle error of Actuator 1 and (b) angle error of Actuator 2……..72

Figure 5.9: Experimental results by applying NPD-LC controller for the low speed case (Iterations 3 to 6): (a) angle error of Actuator 1 and (b) angle error of Actuator 2……..73

Figure 5.10: Experimental results by applying NPD-LC controller for the high speed case (Iterations 1 to 4): (a) angle error of Actuator 1 and (b) angle error of Actuator 2……..74

Figure 5.11: Experimental results by applying AES-PD controller for the low speed case (Iterations 1 to 3): (a) angle error of Actuator 1 and (b) angle error of Actuator 2……..77

Figure 5.12: Experimental results by applying AES-PD controller for the low speed case (Iterations 3 to 6): (a) angle error of Actuator 1 and (b) angle error of Actuator 2……..78

Figure 5.13: Experimental results by applying AES-PD controller for the high speed case (Iterations 1 to 4): (a) angle error of Actuator 1 and (b) angle error of Actuator 2……..79

Figure 5.14 Comparison of the trajectory tracking performance with PD-based controllers at the low speed case: (a) angle error of Actuator 1 and (b) angle error of Actuator 2….83

Figure 5.15 Comparison of the trajectory tracking performance with PD-based controllers at the high speed case: (a) angle error of Actuator 1 and (b) angle error of Actuator 2…84

Figure 5.16: Experimental results by applying Feedforward ILC for the low speed case (Iterations 1 to 6): (a) angle error of Actuator 1 and (b) angle error of Actuator 2……..88

Figure 5.17: Experimental results by applying CTC and PD control for the low speed case: (a) angle error of Actuator 1 and (b) angle error of Actuator 2……...90

Figure 5.18: Experimental results by applying CTC and PD control for the high speed case: (a) angle error of Actuator 1 and (b) angle error of Actuator 2……...91

Figure 6.1: Measured position tracking errors in the motors for the low speed case using PD controller: (a) angle error of Servomotor and (b) angle error of CV motor…….108

Figure 6.2: Measured position tracking errors in the motors for the high speed case using PD controller: (a) angle error of Servomotor and (b) angle error of CV motor…….109

Figure 6.3: Measured position tracking errors in the motors for the low speed case using SMC: (a) angle error of Servomotor and (b) angle error of CV motor……110

Figure 6.4: Measured position tracking errors in the motors for the high speed case using SMC: (a) angle error of Servomotor and (b) angle error of CV motor……111

ACRONYMS

AEDL	Advanced engineering design laboratory
CTC	Computed torque control
DOF	Degree of freedom
EPD	Evolutionary PD
NPD	Nonlinear PD
PD	Proportional derivative
RTC	Real-time controllable
CV	constant velocity
SMC	sliding mode control
ILC	Iteration learning control
NPD-LC	nonlinear-PD learning control
AES-PD	Adaptive evolutionary switching PD control
HAS	Hybrid actuation system

Chapter 1

Introduction

1.1 Background and motivation

Mechanisms can be classified into two main categories based on their structures, namely, serial and parallel. A serial type mechanism has its links sequentially connected, constructing an open loop. In general, the first link of the open chain structure originates from a fixed base and it is subsequently connected to the other links with the last one having an open end. The end effector is usually mounted to the last link. In contrast with the open loop structure, the end effector of a close-loop mechanism is linked to the fixed base by the use of multiple kinematic chains. Normally all the actuators of these mechanisms are located on or close to the base (Li and Wu, 2004). Closed-loop structure mechanisms are also sometimes referred to as parallel mechanisms in the literature.

Serial type structures have some inherent disadvantages such as low position accuracy and mechanical stiffness. For instance, the position accuracy of a serial mechanism with many links is considerably low, since a small amount of error at each joint is enlarged

and accumulated by its subsequent links (Li et al., 2000). As well, the mechanical stiffness of the open-loop structure is essentially poor considering that each link has to carry the mass of its subsequent links and their actuators. In comparison to their serial counterparts, parallel structures have a high stiffness, high motion accuracy and high load-structure ratio. Due to their advantages over serial structure mechanisms, parallel structure mechanisms have been receiving increasing interest from both academia and industries in recent years.

To obtain the same number of degrees of freedom (DOF), a closed-loop structure is far more complex than an open-loop one, thereby resulting in a more complex dynamic model in general. It is common knowledge in the field of controls that for the control of a mechanism with a more complex dynamics a more sophisticated control algorithm is usually required. Therefore, it is clear that for the control of a parallel mechanism a more advanced control algorithm is necessary in comparison to the serial structure mechanism. Due to the complexity of the dynamic model of parallel mechanisms, the control of these structures is a challenging and difficult task. Numerous control algorithms and methods are proposed for the control of these structures, including several control algorithms that have been developed for the control of parallel mechanisms throughout the years in the Advanced Engineering Design Laboratory (AEDL) at the University of Saskatchewan. The need of research to generalize these developments and to develop experimental means in conjunction with the theoretical work is the main motivating factor behind this study.

This study will focus on the experimental work to verify the theoretical works recently completed in the AEDL. In particular, the test bed developed for the experimental study, which consists of a 2 degree of freedom (DOF) parallel mechanism will be described; as well the results of the experiments conducted will be presented and discussed in order to illustrate and validate the effectiveness of the different control algorithms previously developed at the AEDL.

1.2 Traditional Mechanisms Vs Mechatronic Mechanisms

According to the International Federation for the Promotion of Mechanism and Machine Science (IFToMM), a mechanism is defined as a set of connected components to perform a definite motion and force transfer (IFToMM, 1991). Traditionally, a mechanism is viewed as a structure that has at least one DOF and is driven by one or more constant velocity motors. These motors are not real-time controllable (RTC) or adjustable and such a traditional mechanism is termed a non-RTC mechanism.

If a mechanism is driven by real-time controllable (RTC) motors or servomotors, then it is called an RTC mechanism. Due to the use of servomotors, the RTC mechansim can be planned and programmed in real-time. RTC mechanisms are also called mechatronic mechanisms in the literature and in general are multi-degrees of freedom systems. There are many advantages associated with the use of servomotors in machines as the mechanism can be used for more diversified purposes due to its programmablitliy. Robotic applications in which a manipulator produces flexible motions under various payloads is a good example of this concept (Ouyang, 2002).

RTC motors are used in many advanced robots and machine tools. This is due to their real time controllability which enables them to adapt to different applications without the need to redesign the mechanical structure of the mechanism. One of the typical applications of RTC mechanisms is to track motion, in which a trajectory of the end-effector is desired and given as a function of time and then the mechanism is controlled such that the end-effector follows the given trajectory. Another typical application of RTC mechanisms is to track a set of points, in which the motion between any two points is not of interest. The point-set tracking problem can be viewed as a simplified version of the trajectory tracking problem, so tracking of a trajectory is generally more demanding than tracking of a set of points. This thesis concentrates on trajectory tracking. Although RTC motors can be programmed to follow a desired trajectory, it is important to note that in the case of non-RTC mechanisms, trajectory generation is a generic design problem. This problem, however, does not usually involve the time factor, and nor is the feedback control involved (Klein, 1987; Ouyang, 2002).

It is possible for a mechanism to incorporate both RTC and non-RTC motors for its drive. In this thesis, a mechanical system where its drive includes two types of motors, a servomotor and a constant velocity (CV) motor, is referred to as the hybrid actuation system. Hybrid actuation systems provide a middle ground between the traditional inflexible machines and the modern flexible robots. These systems will be discussed in more details in the following chapters.

1.3 Research objectives and scopes

The research presented in this thesis focuses on experimentally verifying some of the control algorithms and approaches developed at the AEDL as well as reported in the literature. In particular, the following research objectives are set to be achieved.

Objective 1: Develop a generic experiment environment (test bed) such that different control approaches and algorithms can be implemented on it.

It is remarked that a 2 DOF mechanism is used as a generic experiment environment. The term generic here is used since the 2 DOF closed loop mechanism is the simplest of multi-DOF closed loop systems and the approaches, methods and conclusions based on a 2 DOF mechanism can all be applied to a structure with a higher number of degrees of freedom (Wang, 2000).

It is also remarked that the 2 DOF closed loop mechanism is studied under two different experimental setups. In the first case, the mechanism is driven by two RTC motors (i.e., servomotors) and therefore is real time controllable. In the second case, the mechanism is a hybrid actuation system and is driven by a traditional non-RTC constant speed motor and a servo motor. It is noted that existing research on hybrid actuation systems usually employs two servomotors, one of which is used to mimics the behavior of a constant velocity motor. It is obvious that this is different than the real situation where a CV motor is in place. This study differs from existing ones in that a CV motor and a servomotor are used for the hybrid actuation system.

Objective 2: Conduct an **e**xperimental study on different control algorithms, including error-based control algorithms, such as proportional derivative (PD), non-linear PD (NPD), iterative learning methods (ILC), and model-based control algorithms such as computed torque control (CTC) and Sliding Mode Control (SMC), as applied to the above test beds.

It is remarked that in this thesis, *model based control* refers to those control approaches in which the dynamic model of the plant is employed into their control law. In comparison, *error based control* methods refer to those control approaches that are based just on the errors of the system and do not take the dynamic model of the plant into consideration. At high speeds, the calculation of the dynamic model poses a challenge due to its heavy computational time. Therefore, model based control approaches might not result in satisfactory performance at higher speeds.

To measure the performance trajectory tracking, two indices are used in this study, i.e., (i) the error between the predefined motion and the actual one and (ii) the peak driving torque required from the servo motors.

1.4 General Methodology

To achieve Objective 1, a five-bar (closed loop) mechanism with two degrees-of-freedom is to be designed and developed. The five-bar mechanism has a wide range of

applications and its motion control has been intensively investigated (Youcef-Toumi and Kuo, 1993; Guo et al., 1999; Ghorbel, 1995). It should be noted that the five-bar mechanism is the typical structure of multi-DOF and closed-loop mechanical systems, and the results obtained from it would be of generalized implications (Wang, 2000).

It should be noted that with respect to objective 1, two different experimental setups are developed. The first case is an RTC mechanism driven by two servomotors which is used to test the effectiveness of different control methods such as the traditional PD control, NPD control, ILC iterative control techniques and the well known CTC control strategy. For the second case, a CV motor and a servomotor are used to develop a hybrid actuation system. This prototype is to be employed to carry out an experimental study of hybrid actuation machines. A control method known as the sliding mode control will be implemented on the system. The prototype developed and the results of the experiments conducted will be discussed in chapters 3 and 5 respectively.

To achieve Objective 2, the generic experiment environment developed will be used to conduct experiments in order to verify the effectiveness and validity of the control algorithms mentioned in the objective. Experiments are conducted to test the effectiveness of the ILC learning control methods proposed at the AEDL. ILC control used in the previous literature is feedforward or off-line learning control. In this type of iterative learning control, information for computing the current torque profile does not come from the present iteration, but from the previous one. ILC control proposed at the AEDL, however, is an online learning control in that the controlled torque of the current

iteration consists of a combination of the current controlled torque (feedback) and also the torque profile produced in the previous iteration (feedforward). It is expected that the latter type of ILC control provides more satisfactory results since its torque profile is a combination of the current and previous iterations. Experiments are conducted to see the effectiveness of feedforward and feedback ILC and the results are presented in Chapter 5.

It is remarked that for the control of a complex mechanical structure for precise and fast performance, an advanced controller based on an accurate system dynamic model is usually desired. In the case of controlling parallel robots, however, the intensive computation due to the complexity of the dynamic model can result in difficulties in the physical implementation of the controllers for high-speed performance. Therefore more complex control methods, such as model based control approaches might not yield satisfactory results at higher speeds due to heavy computational time. In chapter 5, the traditional PD control law (i.e., error based control) is compared to the CTC control law (i.e., model based control) at low and high speeds, to get a measure of the effectiveness of error based and model based control algorithms at these two operating conditions.

1.5 Organization of the thesis

This thesis consists of seven chapters. In chapter 2, a literature review of the dynamics and control of the 2 DOF five-bar closed loop mechanism is presented, with a goal to further analyze and justify the objectives of this thesis.

Chapter 3 presents the design and development of the test beds for experiments. In particular, motor, amplifier, servo drive and controller configuration and specifications will be discussed in detail; and the design of the test beds will be presented.

In Chapter 4, different control approaches examined in this study will be reviewed and outlined. These control approaches include proportional derivative (PD), non-linear PD (NPD), iterative learning methods (ILC), and computed torque control (CTC).

In chapter 5, the results of the experiments conducted on the RTC mechanism will be presented and analyzed.

In chapter 6, the hybrid actuation system is considered and discussed in details. As well, sliding mode control for the control of hybrid actuation systems will also be introduced. The results of the experiments conducted using the hybrid machine test bed and applying sliding mode control are also presented and discussed in this chapter.

Chapter 7 presents the conclusions drawn from this research, which is followed by suggestions and recommendations for possible future work.

Chapter 2

Literature Review

2.1 Introduction

This chapter is to provide a brief review of past and recent developments in the design, modeling, and control of servo and hybrid mechanisms. The objective is to examine various approaches that have been developed in this research topic and to identify the issues involved, thereby justifying the necessity of the present research. Particularly, in Section 2.2 servo mechanisms and hybrid actuation systems are discussed in detail, and compared to identify their advantages and disadvantages. In Section 2.3, a dynamic model of the 2 DOF closed loop mechanism used in this study is introduced and outlined. In Section 2.4, two types of control which are of interest in this study, i.e., error based and model based control schemes, are introduced. Section 2.5 presents the previous relevant works that have been developed at the AEDL. This is followed by section 2.6, discussing commonly-used approaches for trajectory tracking.

2.2 Servo mechanisms and hybrid actuation systems

A machine that is driven by two types of motors, namely, the servomotor and the constant speed motor is called a hybrid machine. The advantage of this kind of machines is their high reliability and power. In contrast, machines driven by only constant speed motors suffer from the lack of task flexibility. Since all motions of non-RTC machines are recognized in the hardware of the system (as they are not controllable and therefore lack a control mechanism and a controller), an expensive and time consuming reconstruction of the hardware is necessary for any modification to the motion of these machines.

In comparison to the traditional mechanism, machines driven by servomotors are flexible in operation by reprogramming of the servomotor. For servo mechanisms to achieve and fulfill new task requirements, only the control program needs to be modified. For this reason, these types of machines are often referred to as programmable machines in the literature (Ouyang, 2004). Applications of such machines can be found in packaging machinery, stamping, and machine tools.

The use of servomotors in machines has also drawbacks. One of these drawbacks is the low ratio of the payload to the motor power capacity. Also, these machines provide poor motion precision under high-speed operations. Servomotor-driven mechanisms operate in a wide range of motion, which may include an extreme acceleration profile. This imposes

severe torque requirements on the motors, producing excessive torque variations that will most likely create significant heat in the motor windings. Certain motor specifications also constrain the range and speed of reachable output motions. Such characteristics include the motor's rated torque and peak power capability (Ouyang, 2002; Li and Wu, 2004). The use of servomotors in combination with the traditional constant speed motors in closed loop mechanisms can alleviate these problems. The structure of a closed loop mechanisms allows for the concept of hybrid machine which combines the power of the traditional non-RTC motors with the programming and real time controllability of today's modern servomotors.

A few researchers have worked on the hybrid machine systems. Greenough et al (1995) developed a hybrid machine system, which consists of a CV motor, a flywheel, and a servomotor to construct a closed loop 2-DOF mechanism. The mechanism is driven by the servomotor and the constant speed motor, both of which drive a single output and are coupled through a 2-DOF mechanism. While the two motors drive the two independent shafts supplying power to an output member, the trajectory of the servomotor is controlled with a user specified motion and the CV motor is uncontrollable. In hybrid machines, the CV motor supplies the mechanism with the majority of the power while the servomotor acts as a driver providing low modulating torque.

Hybrid machines can also be a combination of several motors and mechanisms. Due to the lower cost of CV motors in comparison to their servomotor counterparts as well as their capability of energy recuperation, the use of hybrid machines makes it possible to

significantly reduce the operating cost (Tokuz and Jones, 1991; Tokuz 1992; Van de Straete and De Schutter, 1996).

2.3 Dynamics of multi-DOF closed-loop mechanisms

In order to develop an effective controller for optimal trajectory tracking performance, the dynamics of a mechanism must first be thoroughly analyzed. In this section the dynamic model that describes the dynamical behavior of the 2-DOF closed loop mechanism is introduced. The development of an accurate dynamic model plays a significant role in the control of a mechanism in several ways. First, a precise dynamic model is required to predict how a mechanism will react in response to the forces and torques acting on it. Second, an accurate dynamic model is necessary for the development of suitable control strategies.

Numerous methods and approaches have been developed in previous works for deriving the dynamic equations of a mechanism (Thomson, 1993; Codourey, 1998; Ghorbel, 1994 and 1997). Newtonian mechanics and Lagrange's method are the two most widely used approaches to derive the dynamic model of mechanisms. The superiority of one approach over another is solely based on the accuracy and computational efficiency of the model.

Whilst there has been numerous studies on the dynamic modeling of serial structures, but little work has been done on modeling of parallel mechanisms. (Fitcher, 1986; Raghavan et al., 1989; Reboulet et al., 1991; Liu et al., 1993; Ghorbel, 1994 and 1997; Gautier et al.,

1995; Ghorbel and Srinivasan, 1998). The difficulty in the dynamic modeling of closed-loop mechanisms is due to the fact that some dependant joints are highly coupled with the independent joint variables. Hall (1981) developed the dynamic model for a four bar, single-DOF closed-loop mechanism using Lagrange's equations of motion. Nguyen and Cipra (1999) and Wang (2000) developed the dynamic model of a 2 DOF closed loop planar mechanism following the same approach as in Hall (1981).

Reduced order model analysis method proposed by Ghorbel (1994, 1997) and modified by Ouyang (2002) is another approach for the dynamic modeling of closed loop mechanisms. This approach is described in full details in the remainder of this section and is used to develop the dynamic model of the 2-DOF five-bar closed loop mechanism used in this study. Ghorbel originally developed the dynamic model of a closed loop 2-DOF mechanism using the reduced order model method, however, in his study the mass centers are in-line with the link, meaning the center of mass of each link lies on the axis of the link, i.e., δ_i =0 in Figure 2.1. Ouyang (2002) extended Ghorbel's method to a more general situation, with off-line link mass centers. In Ouyang's study the mass center of each link in the mechanism is arbitrarily distributed with respect to the link's reference coordinate system (see Figure 2.1). The dynamic model developed by Ouyang (2002) is adopted and used in this study. The development of the model is outlined as follows.

Consider a 2 DOF parallel robot shown in Figure 2.1. m_i is the mass of the individual linkages, r_i is the distance to the center of mass from the joint of link i, L_i is the length of link i, and I_i is the inertia of link i. As mentioned previously, the center of mass of

each link is assumed to be offline with an angle δ_i for the more general application. The motion of the 2-DOF closed loop mechanism is governed by Ghorbel 1994, 1997 and Ouyang, 2002.

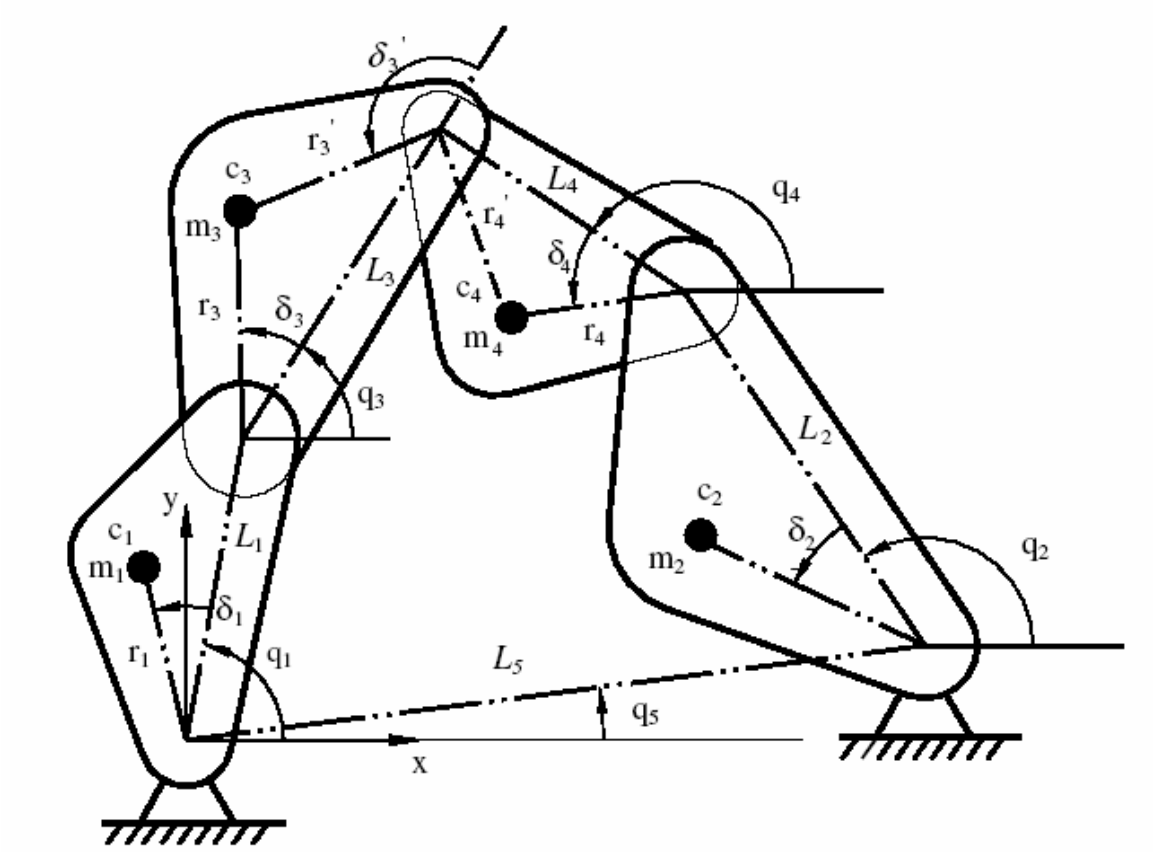

Figure 2.1: The structure of a 2 DOF parallel robot

$$\begin{cases} D(q')\ddot{q} + C(q',\dot{q}')\dot{q} + g(q') = \tau \\ \dot{q}' = \rho(q')\dot{q} \\ q' = \sigma(q) \end{cases} \tag{2.1}$$

where

$$q = \begin{bmatrix} q_1 & q_2 \end{bmatrix}^T, \qquad q' = \begin{bmatrix} q_1 & q_2 & q_3 & q_4 \end{bmatrix}^T$$

$$\dot{q} = \begin{bmatrix} \dot{q}_1 & \dot{q}_2 \end{bmatrix}^T, \qquad \dot{q}' = \begin{bmatrix} \dot{q}_1 & \dot{q}_2 & \dot{q}_3 & \dot{q}_4 \end{bmatrix}^T$$

$$D(q') = \rho(q')^T D'(q')\rho(q') \tag{2.2}$$

$$C(q', \dot{q}') = \rho(q')^T C'(q', \dot{q}')\rho(q') + \rho(q')^T D'(q')\dot{\rho}(q', \dot{q}') \tag{2.3}$$

$$g(q') = \rho(q')^T g'(q') \tag{2.4}$$

In equations 2.2 through 2.4, the matrix $D'(q')$, contains the inertial forces of the free system, $C'(q', \dot{q}')$ represents the Coriolis and centrifugal matrix of the free system, and $G'(q')$ is the gravity vector of the free system. The determination of $D'(q')$, $C'(q', \dot{q}')$, $g'(q')$, $\dot{\rho}(q', \dot{q}')$, $\rho(q')$, and $\sigma(q)$ are given as follows (Ghorbel, 1997; Ouyang, 2002).

By means of the Lagrangian method, one has

$$D'(q') = \begin{bmatrix} d_{1,1} & 0 & d_{1,3} & 0 \\ 0 & d_{2,2} & 0 & d_{2,4} \\ d_{3,1} & 0 & d_{3,3} & 0 \\ 0 & d_{4,2} & 0 & d_{4,4} \end{bmatrix} \tag{2.5}$$

where

$$d_{1,1} = m_1 r_1^2 + m_3(L_1^2 + r_3^2 + 2L_1 r_3 \cos(q_3 + \delta_3)) + I_1 + I_3,$$

$$d_{1,3} = m_3(r_3^2 + L_1 r_3 \cos(q_3 + \delta_3)) + I_3,$$

$$d_{2,2} = m_2 r_2^2 + m_4 (L_2^2 + r_4^2 + 2L_2 r_4 \cos(q_4 + \delta_4)) + I_2 + I_4,$$

$$d_{2,4} = m_4 (r_4^2 + L_2 r_4 \cos(q_4 + \delta_4)) + I_4,$$

$$d_{3,1} = d_{1,3},$$

$$d_{3,3} = m_3 r_3^2 + I_3,$$

$$d_{4,2} = d_{2,4},$$

$$d_{4,4} = m_4 r_4^2 + I_4$$

$$C'(q', \dot{q}') = \begin{bmatrix} h_1 \dot{q}_3 & 0 & h_1(\dot{q}_1 + \dot{q}_3) & 0 \\ 0 & h_2 \dot{q}_4 & 0 & h_2(\dot{q}_2 + \dot{q}_4) \\ -h_1 \dot{q}_1 & 0 & 0 & 0 \\ 0 & -h_2 \dot{q}_2 & 0 & 0 \end{bmatrix} \tag{2.6}$$

in which

$$h_1 = -m_3 L_1 r_3 \sin(q_3), \text{ and}$$

$$h_2 = -m_4 L_2 r_4 \sin(q_4)$$

$$g'(q') = g \begin{bmatrix} (m_1 r_1 + m_3 L_1) \cos(q_1 + \delta_1) + m_3 r_3 \cos(q_1 + q_3 + \delta_3) \\ (m_2 r_2 + m_4 l_2) \cos(q_2 + \delta_2) + m_4 r_4 \cos(q_2 + q_4 + \delta_4) \\ m_3 r_3 \cos(q_1 + q_3 + \delta_3) \\ m_4 r_4 \cos(q_2 + q_4 + \delta_4) \end{bmatrix} \tag{2.7}$$

where g represents the gravitational acceleration constant.

Considering the fact that the 2-DOF five-bar linkage closed loop mechanism is constructed from two open-chain serial links, one has the following two independent scleronomic holonomic constraint equations

$$\phi(q') = \begin{bmatrix} \phi(1) \\ \phi(2) \end{bmatrix} = 0 \tag{2.8}$$

where

$$\phi(1) = L_1 \cos(q_1) + L_3 \cos(q_1 + q_3) - L_5 - L_2 \cos(q_2) - L_4 \cos(q_2 + q_4) \tag{2.9}$$

$$\phi(2) = L_1 \sin(q_1) + L_3 \sin(q_1 + q_3) - L_2 \sin(q_2) - L_4 \sin(q_2 + q_4) \tag{2.10}$$

Note that $\alpha(q') = q$, which presents a transformation from $q' = \begin{bmatrix} q_1 & q_2 & q_3 & q_4 \end{bmatrix}^T$ to $q = \begin{bmatrix} q_1 & q_2 \end{bmatrix}^T$, as shown in the following equation.

$$\alpha(q') = \begin{bmatrix} 1 & 0 & 0 & 0 \\ 0 & 1 & 0 & 0 \end{bmatrix} q' = q \tag{2.11}$$

In the above equation, the vector q' represents the generalized coordinate vector of the free system and vector q is the generalized coordinate vector of the constrained system.

Defining the following quantities:

$$\psi(q') \overset{\Delta}{=} \begin{bmatrix} \phi(q') \\ \alpha(q') \end{bmatrix}, \qquad \psi_{q'}(q') \overset{\Delta}{=} \frac{\partial \psi}{\partial q'}$$

From Equations (2.9), (2.10), and (2.11), $\psi_{q'}(q')$ can be expressed as:

$$\psi_{q'}(q') = \begin{bmatrix} \psi_{q'}(1,1) & \psi_{q'}(1,2) & \psi_{q'}(1,3) & \psi_{q'}(1,4) \\ \psi_{q'}(2,1) & \psi_{q'}(2,2) & \psi_{q'}(2,3) & \psi_{q'}(2,4) \\ 1 & 0 & 0 & 0 \\ 0 & 1 & 0 & 0 \end{bmatrix} \tag{2.12}$$

where

$$\psi_{q'}(1,1) = -L_1 \sin(q_1) - L_3 \sin(q_1 + q_3),$$

$$\psi_{q'}(1,2) = L_2 \sin(q_2) + L_4 \sin(q_2 + q_4),$$

$$\psi_{q'}(1,3) = -L_3 \sin(q_1 + q_3),$$

$$\psi_{q'}(1,4) = L_4 \sin(q_2 + q_4),$$

$$\psi_{q'}(2,1) = L_1 \cos(q_1) + L_3 \cos(q_1 + q_3),$$

$$\psi_{q'}(2,2) = -L_2 \cos(q_2) - L_4 \cos(q_2 + q_4),$$

$$\psi_{q'}(2,3) = L_3 \cos(q_1 + q_3), \text{ and}$$

$$\psi_{q'}(2,4) = -L_4 \cos(q_2 + q_4)$$

Using Equation (2.1), $\rho(q')$ can be expressed as follows:

$$\rho(q') = \psi_{q'}^{-1}(q') \begin{bmatrix} 0 & 0 \\ 0 & 0 \\ 1 & 0 \\ 0 & 1 \end{bmatrix} = \psi_{q'}^{-1}(q') \begin{bmatrix} o_{2x2} \\ I_{2x2} \end{bmatrix} \tag{2.13}$$

Since $\rho(q')$ is related to an inverse matrix, it is not easy to take the time derivative. However, the following expression for $\dot{\rho}(q', \dot{q}')$ can be obtained by pre-multiplying (2.13) with $\psi_{q'}(q')$ and taking the time derivative:

$$\dot{\rho}(q', \dot{q}') = -\psi_{q'}^{-1}(q')\dot{\psi}_{q'}(q', \dot{q}')\rho(q') \tag{2.14}$$

where $\dot{\psi}_{q'}(q', \dot{q}')$ can be obtained by differentiating (2.12) with respect to time and can be written in the following form:

$$\dot{\psi}_{q'}(q', \dot{q}') = \begin{bmatrix} \psi(1,1) & \psi(1,2) & \psi(1,3) & \psi(1,4) \\ \psi(2,1) & \psi(2,2) & \psi(2,3) & \psi(2,4) \\ 0 & 0 & 0 & 0 \\ 0 & 0 & 0 & 0 \end{bmatrix} \tag{2.15}$$

where

$$\psi(1,1) = -L_1 \cos(q_1)\dot{q}_1 - L_3 \cos(q_1 + q_3)(\dot{q}_1 + \dot{q}_3)$$

$$\psi(1,2) = L_2 \cos(q_2)\dot{q}_2 + L_4 \cos(q_2 + q_4)(\dot{q}_2 + \dot{q}_4)$$

$$\psi(1,3) = -L_3 \cos(q_1 + q_3)(\dot{q}_1 + \dot{q}_3)$$

$$\psi(1,4) = L_4 \cos(q_2 + q_4)(\dot{q}_2 + \dot{q}_4)$$

$$\psi(2,1) = -L_1 \sin(q_1)\dot{q}_1 - L_3 \sin(q_1 + q_3)(\dot{q}_1 + \dot{q}_3)$$

$$\psi(2,2) = L_2 \sin(q_2)\dot{q}_2 + L_4 \sin(q_2 + q_4)(\dot{q}_2 + \dot{q}_4)$$

$$\psi(2,3) = -L_3 \sin(q_1 + q_3)(\dot{q}_1 + \dot{q}_3)\text{, and}$$

$$\psi(2,4) = L_4 \sin(q_2 + q_4)(\dot{q}_2 + \dot{q}_4)$$

To derive the analytical expression for the parameterization $q' = \rho(q)$ is a difficult and challenging task and numerical methods are often employed. However, in the case of the 2-DOF five bar linkage closed loop mechanism it is possible to derive this expression analytically. Given the angles of the two input links L_1 and L_2, the angles of the other two links L_3 and L_4 can be derived and given by

$$q_4 = 2\tan^{-1}\left[\frac{\pm\sqrt{A(q_1,q_2)^2 + B(q_1,q_2)^2 - C(q_1,q_2)^2}}{C(q_1,q_2)}\right] + \tan^{-1}\left[\frac{B(q_1,q_2)}{A(q_1,q_2)}\right] \tag{2.16}$$

$$q_3 = \tan^{-1}\left[\frac{\mu(q_1,q_2) + L_4\sin(q_2+q_4)}{\lambda(q_1,q_2) + L_4\cos(q_2+q_4)}\right] - q_1 \tag{2.17}$$

$A(q_1,q_2) = 2L_4\lambda(q_1,q_2)$,

$B(q_1,q_2) = 2L_4\mu(q_1,q_2)$,

$C(q_1,q_2) = L_3^2 - L_4^2 - \lambda(q_1,q_2)^2 - \mu(q_1,q_2)^2$,

$\lambda(q_1,q_2) = L_2\cos(q_2) - L_1\cos(q_1) + L_5$,

$\mu(q_1,q_2) = L_2\sin(q_2) - L_1\sin(q_1)$

2.4 Control Schemes for Multi-DOF Closed-loop Mechanisms

Control Schemes play an essential role in the trajectory tracking of robot manipulators. There are two types of control schemes which are of interest in the present study, i.e., (i) proportional-derivative (PD) based control and (ii) model based control.

2.4.1 PD based control methods

PD-based control has been widely used in the industry. It has a simple structure, given by

$$T = K_p e(t) + K_d \dot{e}(t) \tag{2.18}$$

where e and $\dot{e}$ are the vectors representing the errors between the desired and the actual position and velocity, respectively, K_p and K_d are the control gains and are given in terms of positive definite matrices, and T is the applied torque.

The traditional PD controller is a simple linear controller. Due to this, it is still the most widely used control method for the majority of industrial robots despite the presence of many advanced control laws. For the control of nonlinear systems, a practical approach usually involves the design of a linear controller (e.g. the PD controller) based on the linearization of the system at the operating point.

Much work has been done in the design of PD-based control methods and the modified traditional PD control approaches have been developed (Rugh, 1987; Shahruz and Schwartz, 1994; Xu et al., 1995; Seraji, 1998; Armstrong and Wade, 2000). The PD control method with desired gravity compensation proved to provide global and asymptotic stability for point-set tracking problems (Craig, 1986 and 1988; Kelly, 1997). Qu (1994) and Chen et al., (2001) have also investigated the global stability of PD-based control methods for the trajectory tracking of robot manipulators.

The non-linear PD (NPD) control law is one of the modifications to the fixed-gain traditional PD controller. In this control scheme, the control parameters, i.e., K_p and K_d, are not constant but functions of the errors of the system. For the purposes of force control applications, Xu *et al*. (1995) developed a NPD controller, while mentioning that it is also applicable to position control tasks as well. The non-linear proportional-integral-derivative (NPID) control scheme is another modification developed by Rugh (1987), in which the three gains of the controller, i.e, K_p, K_d, and K_I, are functions of the errors. There are only a very few studies considering the effectiveness of NPD control for the trajectory tracking of parallel manipulators. Also, it is noted that point-set control of linear systems has been the primary focus of most of the previous works involving this control method. This thesis considers the effectiveness of the NPD control method for the trajectory tracking of a closed-loop mechanism. The details of this control algorithm and the results as applied to trajectory tracking will be considered in chapters 4 and 5 respectively.

2.4.2 Model based control methods

Unlike the PD based control methods which are based solely on the errors of the system, some other control approaches take the dynamic model of the plant into account, which are called model based control. In general, the dynamic model of a closed loop mechanism can be stated as follows

$$D(q)\ddot{q} + C(q,\dot{q})\dot{q} + G(q,\dot{q}) = T \tag{2.19}$$

The meanings of the terms in the above equation have been discussed in the preceding section.

On the basis of the model-based control concept, Craig (1986) developed a control scheme, called the Computed Torque Control (CTC), for the control of robots. This scheme is summarized as follows:

$$T = D(q)\ddot{q}_d + C\dot{q} + G + D(q)(K_p e + K_d \dot{e}) \tag{2.20}$$

The toque in the above equation can be broken down into two components. The first component, $D(q)\ddot{q}_d + C\dot{q} + G$, evaluated from the system dynamic model, provides the necessary torque to drive the system along its desired path. This term is the feedforward part of the control law. The second component, $D(q)(K_p e + K_d \dot{e})$, is the feedback

component and is evaluated from the system errors, which provides an additional torque to reduce the errors in the trajectory tracking.

It is obvious that the effectiveness of the CTC law strongly depends on the dynamic model developed for a plant. For precise trajectory tracking performance, an accurate dynamic model is essentially needed. Since the CTC control law is heavily affected by the dynamic model, any inaccuracies in this model can result in unsatisfactory performance. It is also noted that the CTC control law has some inherent disadvantages that are associated with the torque calculation from the model. This is particularly true for the case where a closed loop mechanism is running at high speed. For such a case, due to the high nonlinearity and complexity of the dynamics, considerable computation resources are necessary which lead to difficulty in physical implementations (Lin and Chen, 1996).

2.5 Previous works developed at the AEDL at the University of Saskatchewan

In the past several years, a number of control algorithms and methods have been developed for the control of parallel mechanisms at the AEDL. Mechanisms such as robot manipulators which operate in a repetitive manner are very common in the industry. Due to the fact that the desired or reference trajectory is repeated, one may use iteration learning control (ILC) to improve the tracking performance from iteration to iteration. For this purpose, at AEDL several iteration learning control approaches, including adaptive evolutionary switching PD control (AES-PD) and adaptive nonlinear PD

learning control (NPD-LC), have been developed (Ouyang et al., 2004). These approaches are discussed in detail in Chapter 4.

Base on the existing Nonlinear PD control and the computed torque control method, an evolutionary PD-based (EPD) control method was also proposed at the AEDL. In this method, the plant dynamics is integrated into the control law by using the measured torque profiles of the previous run (i.e., iteration). Thus, the controller is capable of learning from its previous iteration (Ouyang, 2002). This control method, termed as a type of ILC learning control, will be discussed in more details in Chapter 4.

Much effort has also been put in the modelling and control of hybrid actuation systems in recent years at the AEDL. As a result, the dynamic model of a hybrid actuation system driven by a CV motor and a servo motor was developed (Ouyang, 2005), taking the dynamics of both mechanism and motors used to drive the system into account. As well, a hybrid controller has been proposed and then validated based on simulations. This control algorithm will be discussed in more details in Chapter 6.

2.6 Trajectory planning methods

Trajectory planning and tracking of a mechanism can be done in either Cartesian or joint coordinates (Tondue and Bazaz, 1999; Constantinescu and Croft, 2000; Macfarlane and Croft, 2001). Lin et al. (1983) introduced a trajectory planning algorithm in which the trajectory planning is done at the joint level. Based on the initial, intermediate and the

final path specifications, Paul (1979) developed a time schedule for the end-effector and the joint position, velocity, and acceleration. Although it is simple to develop a Cartesian space trajectory planning for the endeffector, to execute a trajectory in Cartesian space, the conversion of Cartesian coordinates to joint coordinates in real time is required. This is due to the fact that the control of a mechanism is performed at the joint level. In this thesis, the term “trajectory” refers to the joint or actuator trajectory.

2.7 Summary

This chapter is to provide a basis for the remaining chapters by reviewing the significant developments in this area. The dynamic model outlined in section 2.3 is to be used in the following chapters for the control of the closed loop mechanism. PD-based control approaches and model-based control algorithms were introduced in section 2.4 with the aim to give the reader an introduction to the control algorithms that will later be discussed in this thesis. Section 2.5 briefly discussed the previous works relevant to this research that are developed at the AEDL. The effectiveness of the dynamic model and control algorithms discussed in this chapter has mostly been explored only through simulations in the previous literature, leaving a lot to be desired in experimental verification. This study is to meet the need by carrying out an experimental study on the effectiveness of these control approaches and strategies.

Chapter 3

Test Beds for Experimental Study

3.1 Introduction

This chapter presents the two main test beds developed for the experimental study in this thesis, namely, the RTC mechanism and the hybrid machine. In particular, Section 3.2 discusses the five bar 2-DOF closed-loop mechanism in detail. In Section 3.3, the RTC mechanism test bed is presented. The 2-DOF hybrid machine test bed is presented in Section 3.4. Section 3.5 discusses the control part of the test beds, including a control program with its user-interface. The approach for obtaining position and velocity information used in this study is discussed in Section 3.6. Finally, a summary is given in Section 3.7.

3.2 Two DOF Five Bar Linkage Close-loop Mechanism

A two DOF five-bar linkage closed loop mechanism has been developed for the experimental study. With reference to research objective 1 defined in Chapter 1, this two DOF mechanism is planar and the simplest of multi-DOF and closed-loop mechanical structures. This mechanism is generic in that the results obtained from it would be of generalized implications. In other words, the control algorithms and strategies applied to this mechanism can be applied to closed loop mechanisms with a higher number of DOF. Figure 3.1 shows the design of the five-bar linkage mechanism, which was created by using SolidWorks® 2005. It is important to note that links 3 and 4 in Figure 3.1 do not slide with respect to one another. The lengths of links 3 and 4 are adjustable and can be adjusted to the desired length and then locked with a screw and bolt at that position.

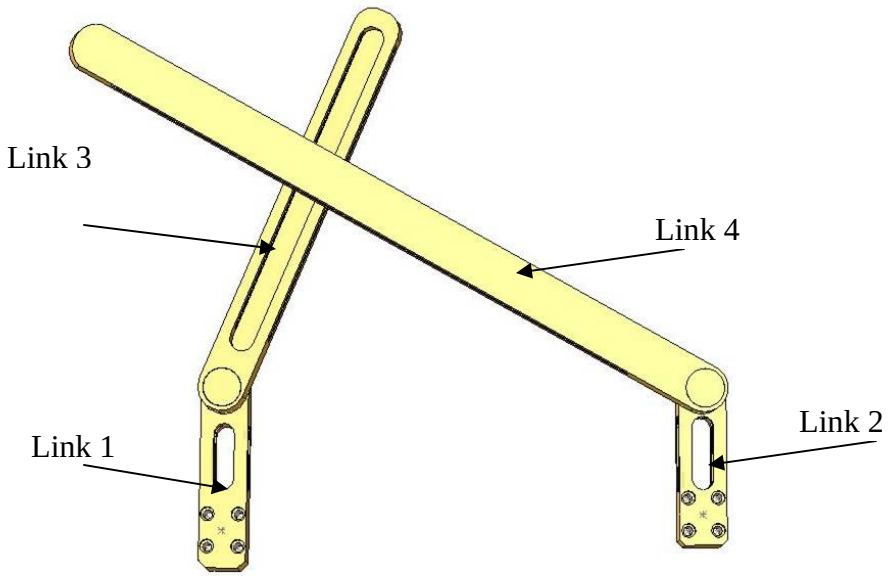

Figure 3.1: Five-bar linkage mechanism

For the convenience of the following discussion, the schematic diagram of this 2-DOF mechanism from chapter 2 is repeated in Figure 3.2 with the angles $\delta_i \neq 0, i \in 4$.

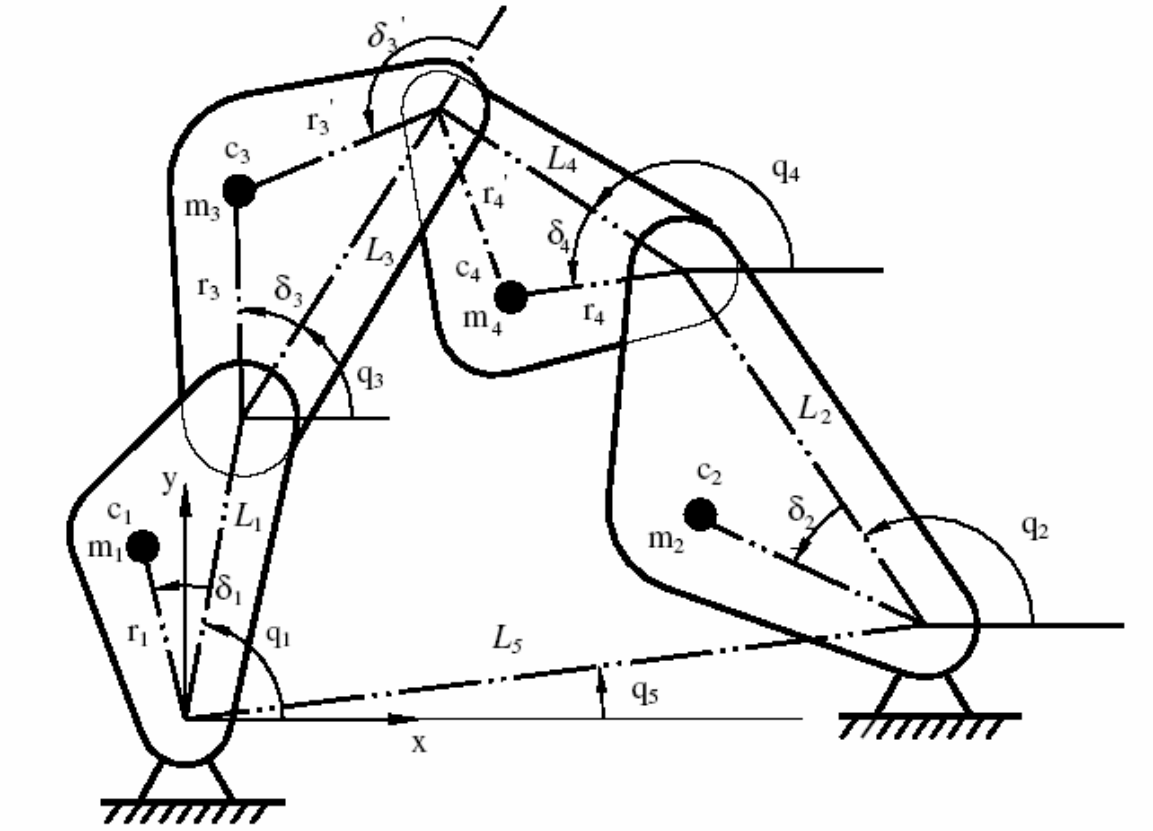

Figure 3.2: Schematic of a five-bar linkage mechanism (Ouyang, 2002)

The individual linkages of the five-bar mechanism, created by using SolidWorks® 2005, are shown in Figure 3.3. The parameters of the five-bar linkage are listed in Table 3.1, in which m_i is the mass of the individual linkages in kilograms (kg), r_i the distance to the center of mass from the joint of link i in meters (m), L_i the length of link i in meters (m), I_i the inertia of link i in kgm^2 about the z axis, and δ_i the angle to the center of mass of link i in *radians*.

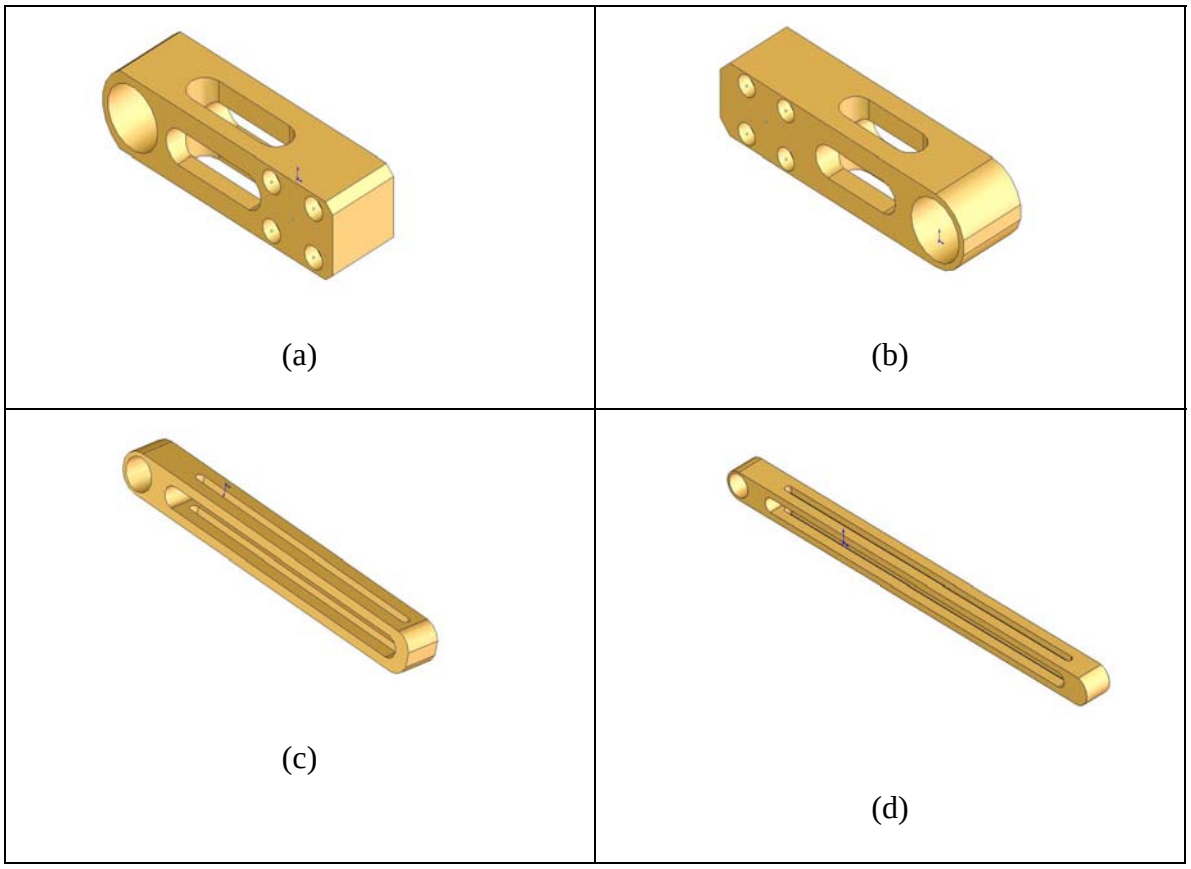

Figure 3.3: Individual links of the five-bar mechanism: (a) Link 1, (b) Link 2, (c)Link 3, and (d) Link 4.

Table 3.1 Parameters of the five-bar mechanism

	m_i	r_i	L_i	I_i	δ_i
Link 1	0.2258	0.0342	0.0894	0.0217×10^{-2}	0
Link 2	0.2623	0.0351	0.0943	0.0314×10^{-2}	0
Link 3	0.4651	0.1243	0.2552	0.3105×10^{-2}	0

Link 4	0.7931	0.2454	0.2352	1.6713×10^{-2}	0

The distance between the axes of joints 1 and 2, denoted by L_5, is also adjustable. In this study, it is set to 0.211 *m* in order to ensure the full rotatability of the mechanism, which is discussed as follows.

To ensure that the mechanism is fully rotatable, the two input or driving links should be able to revolve completely around their rotating shafts and also be able to operate independently of one another. In other words, the motion relationship between the driving links should depend on the desired trajectory of the end-effector, but not on the geometrical configuration of the mechanism. Ting and Liu (1991) proposed a theorem for the full rotatability of closed-loop linkages. Based on this theorem, Ouyang (2002) described the conditions of full-rotatability for a five-bar linkage mechanism, which is given in the following.

Conditions:

(1) The inequality equations

$$L_{\max} + L_{\min 2} + L_{\min 1} \le L_m + L_n \tag{3.1}$$

and

$$L_{\max} \ge L_m \ge L_n \ge L_{\min 2} \ge L_{\min 1}$$

where $L_{\max}$, $L_{\min 2}$, and $L_{\min 1}$ are the lengths of the longest and the two shortest links of the five-bar linkage. L_m and L_n are the lengths of the other two links.

(2) From the two coupler links, one must be among ($L_{\max}, L_m, L_n$).

The coupler links are the two links that are attached to the driving links of the mechanism that connect together and form the closed-loop linkage. These are the links that are not directly connected to the ground.

The mechanical parameters of the five-bar linkage presented in Table 3.1 were chosen such that the above conditions are satisfied.

3.3 RTC mechanism test bed

The RTC mechanism test bed consists of the five-bar linkage discussed above, two servomotors, two amplifiers, and a motion analyzer. The test bed is presented in Figure 3.4 on the following page. The control mechanism of the test bed includes the following components.

1. Intel Pentium III 600 MHz PC with 256 MB RAM;

2. Galil motion analyzer– DMC 1840 controller with ICM/AMP 1900 interconnect module;

3. Two incremental encoder brushless servomotors (SANYO DENKI, P30B06040D, 400W, 1.37 Nm) with servo amplifier (PE2A030, 30A); and

4. Programmable 8255 I/O card;

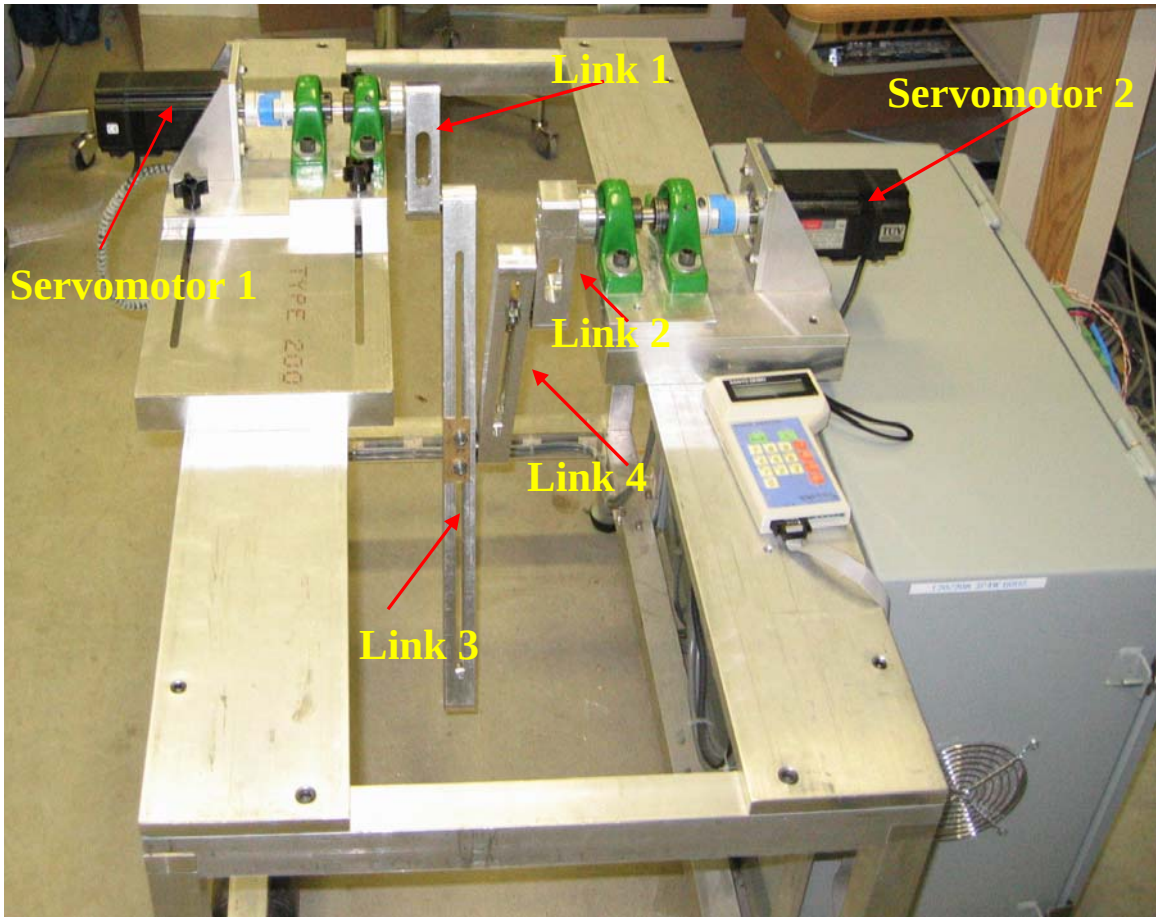

Figure 3.4: RTC mechanism test bed

The control diagram of the RTC mechanism is shown in Figure 3.5. The sensors are incremental encoders with a resolution of 8000 pulses per revolution and used to measure the shaft position of both motors. The measured position is fed back and compared to the desired input. The difference between the desired position and the measured one is termed the position error. The velocity information is obtained from the measured

positions by using the backwards finite-difference method, which is discussed in Section 3.6. Based on the position error and the velocity information, the computer generates a voltage signal by using a given control law. This voltage signal is in turn sent to the Galil™ motion analyzer, the servo amplifiers, and then to the servomotors to generate the torque required.

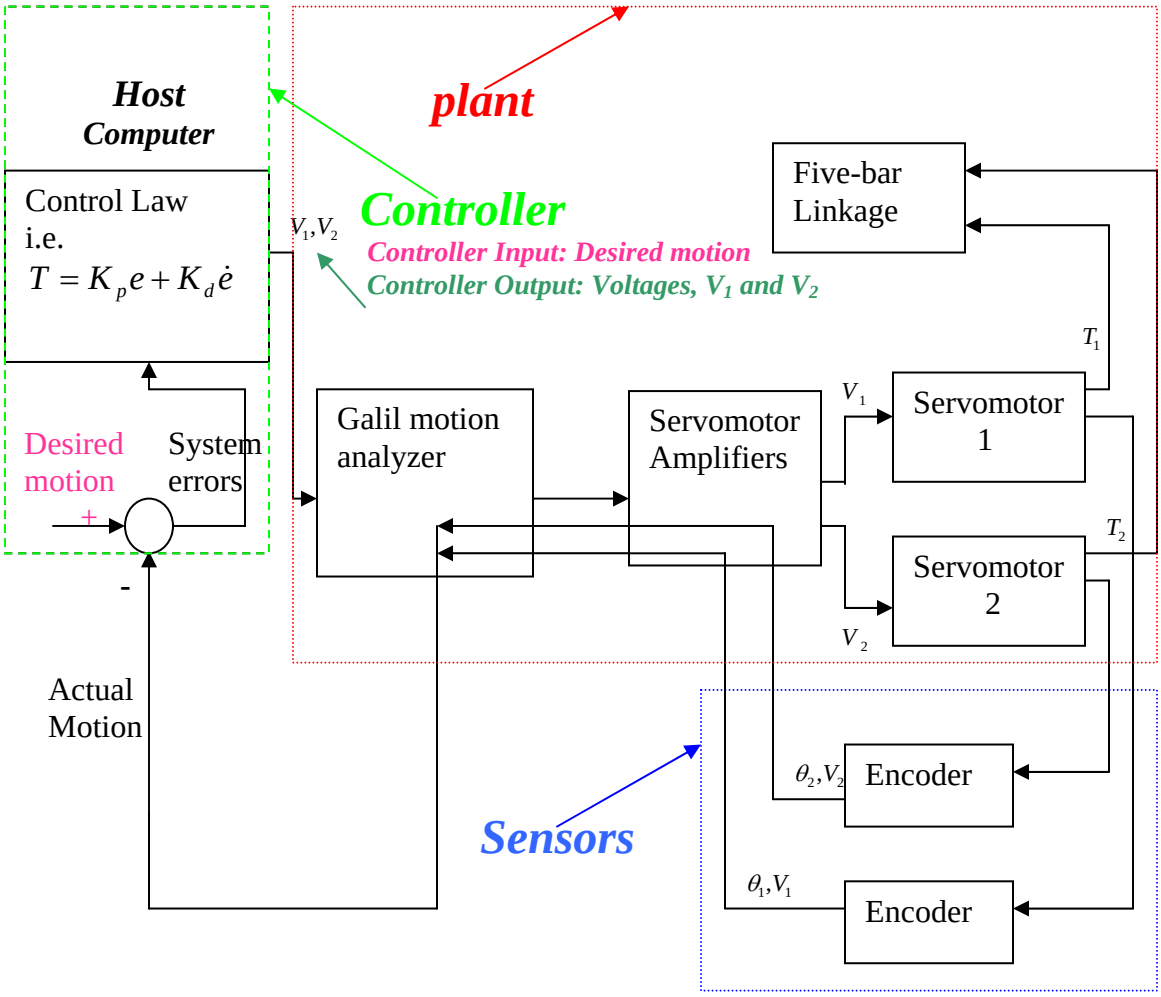

Figure 3.5: Control diagram of the RTC mechanism

3.4 Hybrid Actuation system test bed

The hybrid actuation system (HAS), as shown in Figure 3.6, includes the five-bar linkage discussed previously, a CV motor, a servomotor, and a frequency controller for the CV motor. The control mechanism of the test bed consists of the following components.

1. Intel Pentium III 600 MHz PC with 256 MB RAM;

2. Galil motion analyzer– DMC 1840 controller with ICM/AMP 1900 interconnect module;

3. Incremental encoder brushless servomotor (SANYO DENKI, P30B06040D, 400W, 1.37 Nm) with servo amplifier (PE2A030, 30A);

4. Three phase inverter duty AC induction motor ($SD18^{+}$, 190 W, 2800 rpm) with a Mitsubishi frequency controller (FR-A024-S0.4K-EC, 220-240 V, 0.2-400 Hz, Sinusoidal PWM control system);

5. Incremental shaft encoder attached to the shaft of the CV motor (8000 pulses/rev); and

6. Programmable 8255 I/O card;

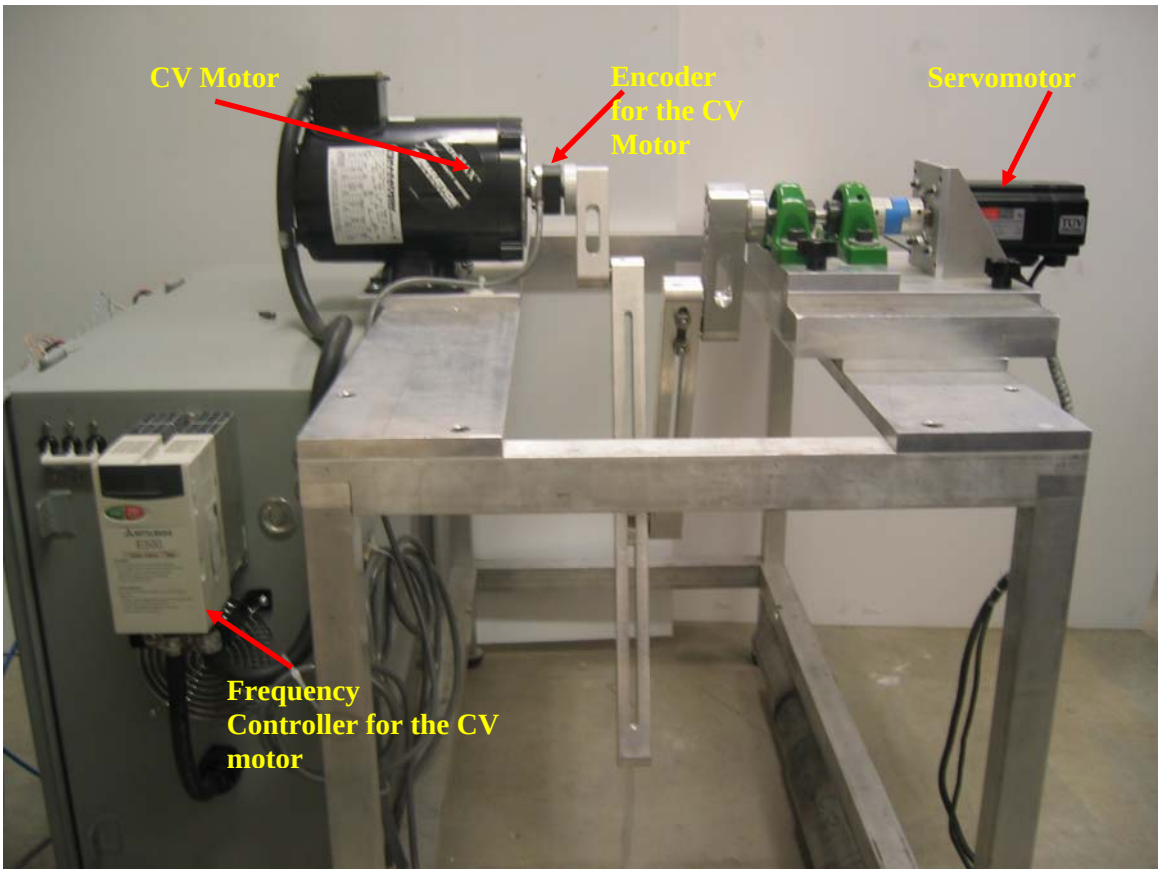

Figure 3.6: Hybrid actuation system test bed

In the HAS test bed, the CV motor and the servomotor work together to produce the torques required to run the five-bar linkage closed-loop mechanism. Specifically, the CV motor provides the majority of the power required to run the five-bar linkage, whilst the servomotor works as a low torque-modulating device. Due to the lack of a control mechanism in the CV motor, closed loop position control of the servomotor is essential for the system's controllability. The servomotor has a built-in incremental encoder, whilst an incremental shaft encoder is attached to the shaft of the CV motor. The function of these encoders is to simply sense the shaft position of their respective motors. Figure 3.7 shows the basic control system for the HAS test bed.

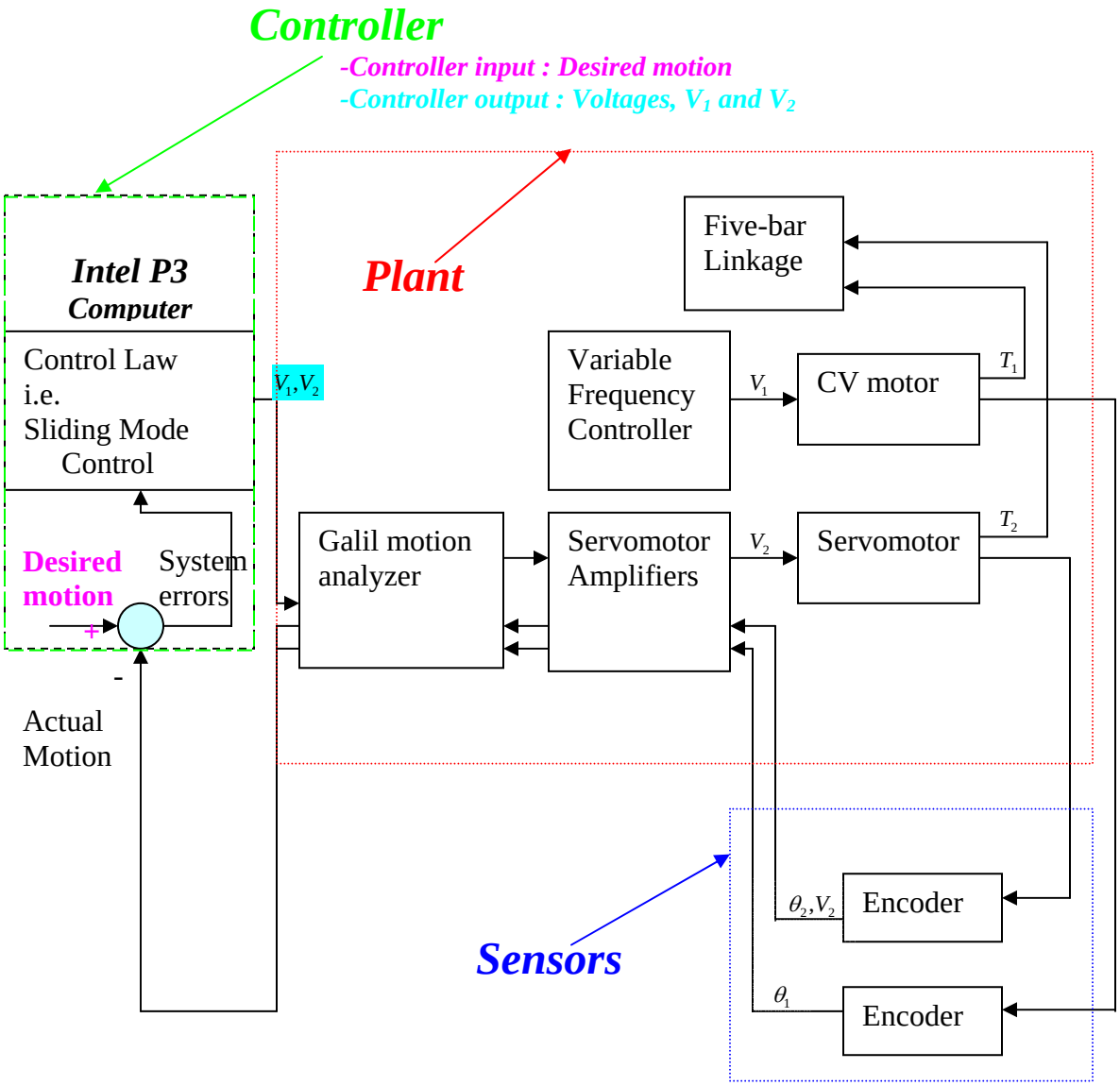

Figure 3.7: Control diagram of the HAS mechanism

In order for the HAS prototype to achieve the desired motion, an effective control strategy is required. This control strategy can be divided into two different levels. In the case of the servomotor, closed-loop position control is compulsory. As mentioned previously, the encoder measures the output position and this position is then fed back

and compared with the desired input. The difference between the desired position and actual position is the error, which is used in the control algorithm to update the next input torque to the system. In comparison to the servomotor, the CV motor lacks a control mechanism. In other words, open-loop position control is applied to the CV motor. It is important to realize that the accuracy of the angular displacement of both motors is essential since the output position of the end-effector depends on the angular positions of the two input links driven by both motors.

As can be seen in Figure 3.7, the CV motor is connected to a frequency inverter which adjusts the speed of the motor by means of applying variable frequency. The greater that the frequency of the inverter is set to, the higher the rotational velocity of the motor will be. There are two outputs at the shaft of the CV motor. The first one is the mechanical output or the torque driving the five-bar linkage. The second one is the data feedback read by an incremental encoder attached to the shaft of the CV motor. The CV motor is not originally equipped with an encoder, therefore, the incremental encoder is an add-on later attached to the shaft of this motor. For simplicity and cost, and to be able to use the same hardware and approach of sending the data feedback to the computer as the servomotor, the same type of encoder as the servomotor is purchased for the CV motor. The arrangement of the hardware described above is the basic HAS test bed that will be used for the purposes of this thesis.

3.5 User interface of the test beds

The test beds described in the previous sections require a command source to send a signal to the motion analyzer for the motors to operate. For this purpose, a user interface containing this command source is required. Therefore, for the control part of the test beds, a user interface is developed with in the host computer which contains the specific control law of interest. The user interface designed for the control of the RTC and the HAS test beds is developed using the C^{++} programming language, version 6.0. This user interface is shown in Figure 3.8.

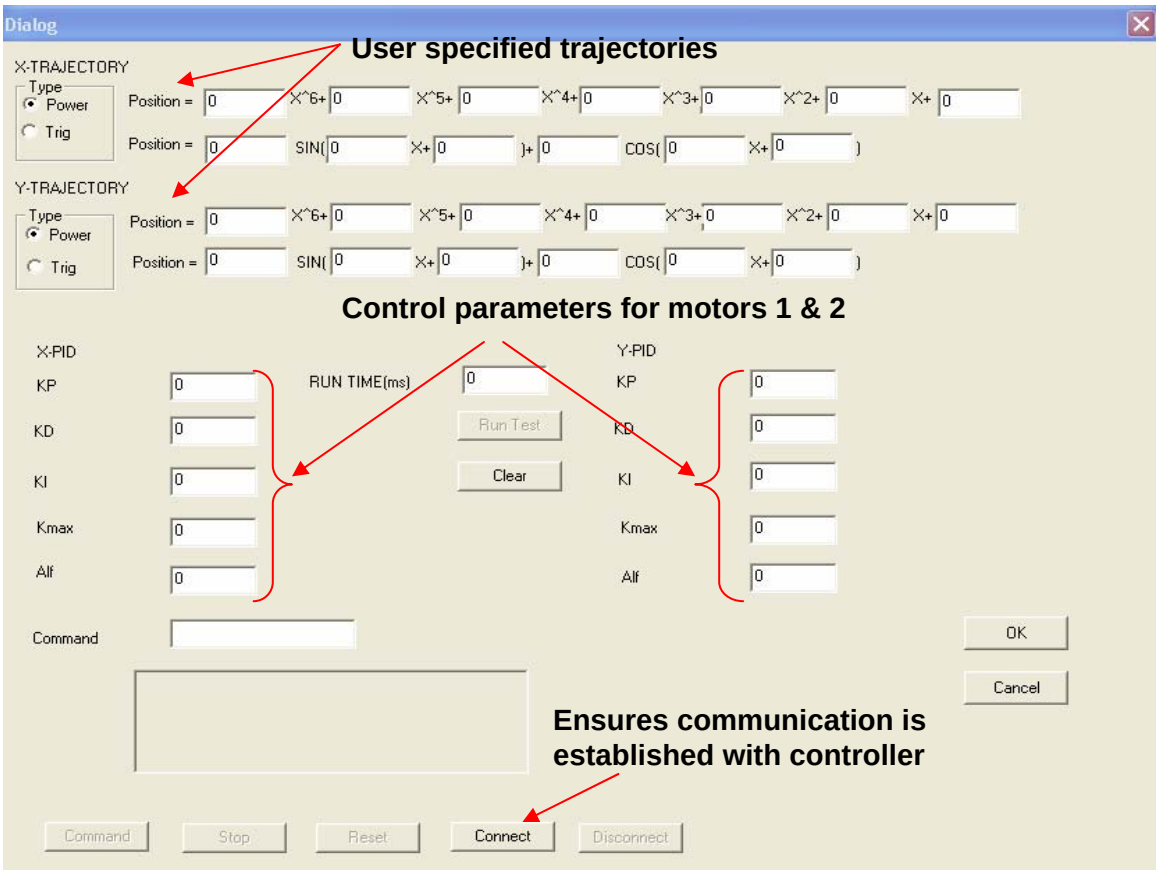

Figure 3.8: User Interface developed in C^{++} in the case of the RTC mechanism

The program code for the user interface is included in Appendix A of this thesis. It should be noted that the user interface developed for the HAS test bed is very similar to the one shown in Figure 3.8, with the exception that the user interface in this case can only accept input trajectories and control parameters for the one servomotor and not the CV motor.

As can be seen in Figure 3.8, the user interface allows a user to input the desired trajectories for the two motors connected to the controller. The *connect* button is used to establish connection with the controller. If connection with the controller is established, the other buttons and input boxes of the user interface are enabled. The user must then specify the desired trajectories for the motors. The trajectories can be either polynomials of up to the 6^{th} degree or a trigonometric function. The user should first select the type of trajectory for the motors to follow using the radio buttons, and then input numbers in the edit boxes corresponding to the desired trajectory.

The user may also input values for the control parameters (i.e., gains) and the run time for the motors. When the *run test* button is pressed, the motors will then try to follow the desired trajectories for a period of time equal to the runtime the user inputs. Afterwards, the program will graph out the desired trajectories, the errors, the actual trajectories and the torques on a separate window. These values are also saved into text files for further analysis.

3.6 Position and Velocity measurements

For the purposes of control of the five-bar mechanism, the angular positions and velocities of Links 1 and 2 are essentially needed. The position of both Links 1 and 2 are measured by means of incremental encoders. In general, incremental encoders are available in two basic output types, single channel and quadrature. A single channel encoder, often called a tachometer, is normally used in a system that rotates in one direction only. In contrast, a quadrature encoder has dual channels (A and B) to produce two output signals representing the direction and rotation, respectively. It is known that the accuracy of encoders depends on their resolution, which is a term used to describe the cycles per revolution (CPR) for incremental encoders or the total number of unique positions per revolution for an absolute encoder. Each incremental encoder has a defined number of cycles that are generated for each full 360 degree revolution. These cycles are monitored by a counter and converted to counts for position or velocity control. The encoders used in this study have a resolution of 8000 counts per revolution.

To obtain velocity information from the measurements of angular position, one straightforward approach is to use the finite-difference method (Kreyzsig, 2002). In this study, the velocity information is estimated from the position data by using the backwards finite-difference method. The mathematical expression for the backwards finite-difference method is given as follows.

$$q'(x_i) = \frac{3q(x_i) - 4q(x_{i-1}) + q(x_{i-2})}{2\Delta t} \tag{3.2}$$

where $q'(x_i)$ is the estimated velocity at the measuring point i, $q(x_i)$, $q(x_{i-1})$, and $q(x_{i-2})$ are the measured positions at the points i, i-1, and i-2, respectively, and Δt is the sampling time interval. There are some limitations to using this approach for obtaining velocity information due to the introduction of noise into the estimations, which will be discussed in Chapter 5.

3.7 Summary

The test beds of the HAS and the RTC mechanism are presented in this chapter. These test beds are developed for the experimental study presented in the following chapters of this thesis. The 2-DOF closed-loop mechanism created is generic in that it is the simplest of multi-DOF closed-loop mechanisms. In other words, the results collected from the experimental study of this system are of generalized implications and can be extended to closed-loop mechanisms with larger number of degrees of freedom. As well, the user interface developed in C^{++} for the purposes of this research is introduced. The interface allows users to define and input the desired trajectories and control parameter. The errors, actual and desired trajectories and torques are then saved into text files for further analysis. Incremental encoders are used to measure the angular position of both actuators. Thereafter, the velocity information is obtained from the position measurements by using the backwards finite difference method.

Chapter 4

Control Algorithms

4.1 Introduction

Real time control of robot manipulators, especially in the case of closed-chain mechanisms, is a difficult and challenging task. The most widely used method for the control of industrial robots is based on the measurement of joint displacement, so called joint-space control. In this chapter, different control strategies or algorithms used in this study are presented. These control algorithms include: the traditional Proportional Derivative (PD) Control, Nonlinear PD (NPD) control, Computed Torque Control (CTC), as well as several Iteration Learning Control (ILC) techniques. Sliding Mode Control (SMC), which is known as a powerful control approach for nonlinear systems with uncertainty, is also applied to the closed-loop mechanism in this study. This control approach is, however, only used for the control of the HAS prototype due to the uncontrollability of the CV motor, which is addressed in Chapter 6.

4.2 PD and NPD control laws

For the control of complex systems such as the RTC closed-loop mechanism, PD or NPD control laws are practically viable. The PD control law has demonstrated its effectiveness as applied to the position control of robot manipulators (Craig, 1986). For the five-bar linkage closed-loop mechanism considered in this study, the following PD control scheme is employed:

$$T(t) = K_P e(t) + K_d \dot{e}(t) \tag{4.1}$$

where $T(t)$ is the actuator torque, K_p and K_d are the proportional and derivative gains, and $e(t)$ and $\dot{e}(t)$ are the error and the rate of change of error, respectively. In general, both K_p and K_d are $n \times n$ symmetric positive definite matrices if the error, $e(t)$, is a *n*-dimension vector. These gains are both fixed and do not change with respect to time.

Studies have shown that a NPD controller can result in superior performance in comparison to the above fixed-gain PD controller in terms of reduced rise time, disturbance rejection, improved trajectory tracking accuracy and friction compensation (Rugh, 1987; Shahruz and Schwartz, 1994). The general expression of the NPD control law takes the following form:

$$T(t) = K_P(\cdot) e(t) + K_d(\cdot) \dot{e}(t) \tag{4.2}$$

where $K_p(\cdot)$ and $K_d(\cdot)$ are the time-varying proportional and derivative gains. These gains depend on the system state and input. In this study, the following nonlinear gain functions are used, which is adopted from (Ouyang, 2002):

$$\begin{aligned} K_p &= K_{p0} \times K(t) \\ K_d &= K_{d0} \times K(t) \end{aligned} \tag{4.3}$$

where $K(t) = K_{\max} - K_{\min} \sec h(\alpha \times e(t))$, in which K_{mas}, $K_{\min}$, and α are user-defined positive constants.

By using time-varying gain, the NPD control algorithm allows the controller to adapt to its response through changing its control parameters, i.e., gains. This controller has numerous advantages over the fixed-gain PD control. As can be seen from equation (4.3), the non-linear gains of the controller are functions of the errors of the system. Depending on the magnitude of the errors, the gains of the NPD controller are modified to generate the torque required to drive the system. When the errors of the system are large, the gains amplify the errors significantly to achieve a large corrective action. On the other hand, the gains are automatically decreased as the errors reduce in order to achieve a steady response without excessive overshoots and large oscillations.

4.3 Iteration Learning Control (ILC)

4.3.1 Iterative learning

Mechanisms such as robot manipulators which perform their tasks in a repetitive manner are very common in the industry. Although the use of the traditional fixed-gain feedback PD control for the control of these robots is common; however, with the fixed-gain PD control method it is not always easy to find a suitable control gain. As well, the increase of the control gains may also cause the oscillation of the required torques which is harmful to the actuators (Craig, 1988; Qu, 1995; Kerry, 1997). For the control of such robot manipulators, one may take advantage of iterative learning control (ILC) to improve the trajectory tracking performance from one iteration to the next (i.e., reduce the trajectory tracking errors).

ILC takes advantage of performing the same task over a given operation time to determine its control action. In particular, the torque profile in the current iteration is determined from the one in the previous iteration based on given learning rules. In the following, ILC control method is outlined and examined (Arimoto et al., 1984; Kuc et al., 1991; Chen and Moore, 2002; Tayebi, 2003). In general, ILC control can be written by the following mathematical expression.

$$T^{j+1}(t) = T^{j}(t) + \Delta T^{j}(e(t), \dot{e}(t)) \tag{4.4}$$

where $T^{j+1}(t)$ is the torque profile of the $j+1$ iteration, $T^{j}(t)$ is the torque profile of the j[th] iteration, and $\Delta T^{j}(e(t),\dot{e}(t))$ is the torque generated by the so called "learning rule" of the control law. The specific learning rule depends on the certain type of ILC control that is used, as will be discussed in the following sections. The general iterative scheme of the ILC algorithm is shown in Figure 4.1.

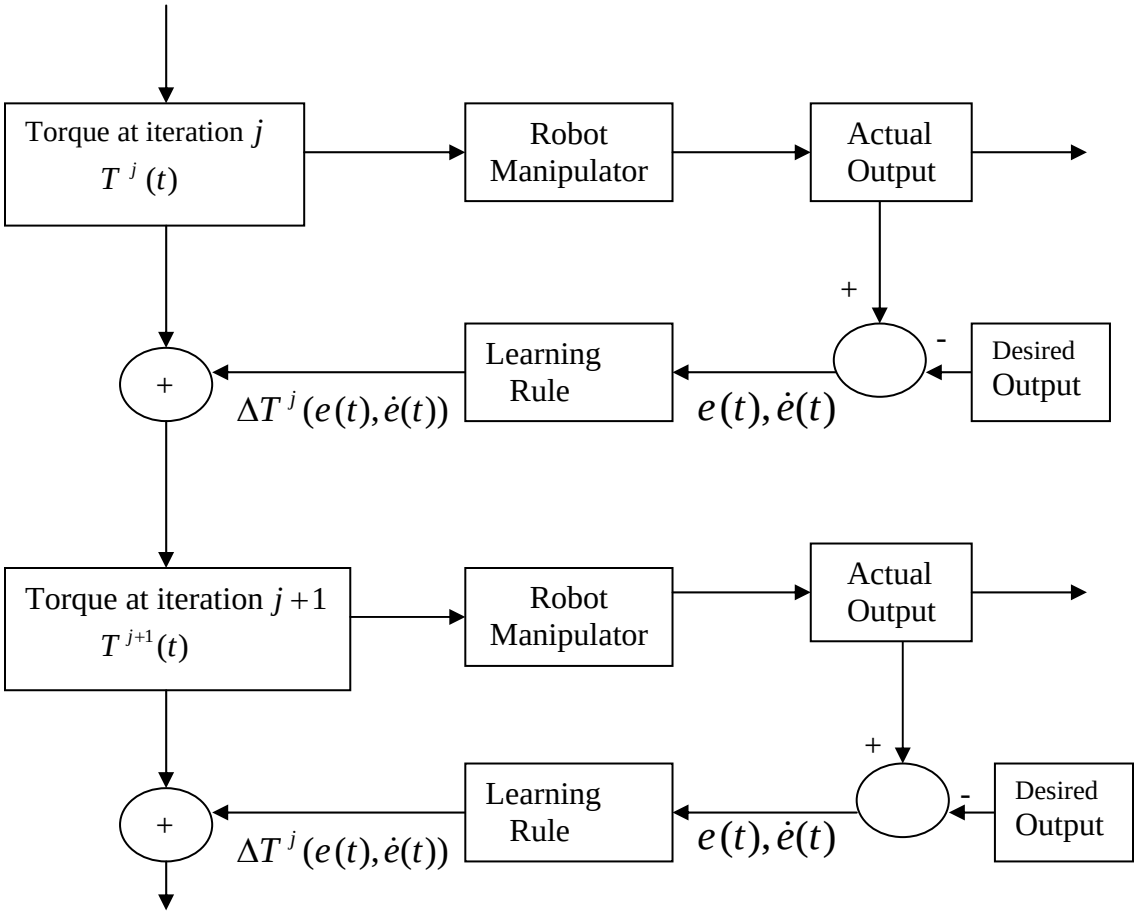

Figure 4.1: Iterative scheme of the iteration learning control algorithm

As can be seen from Figure 4.1, the torque at iteration *j+1* is a combination of the torque profile at iteration *j* and the torque generated by the learning rule. In the traditional ILC

control, information in the current torque profile does not come from the present iteration but from the previous one, hence the traditional ILC control algorithm is a feedforward or off-line learning control. In other words, the learning rule in the traditional ILC control approach is off-line in that it uses errors from the previous iterations to generate the torques for the present iteration. Even though the measurements from the previous iteration are important, in real-time or on-line control strategies the information from the present iteration is much more significant than the previous one. The following sections will discuss the different ILC control methods used in this study.

4.3.2 Evolutionary PD (EPD) control law

The idea behind the EPD control law is to incorporate the information regarding the plant dynamics into a PD-based control algorithm. On this basis, Ouyang (2002) proposed the following formulation of a PD-based control method:

$$T(t) = K_P e(t) + K_d \dot{e}(t) + \tilde{T} \tag{4.5}$$

where $\tilde{T}$ is the torque associated with the plant dynamics. Discretizing the above equation and then combining with ILC yields:

$$T_i^{\,j} = K_P e_i^{\,j} + K_d \dot{e}_i^{\,j} + T_i^{\,j-1} \tag{4.6}$$

where i is the discrete time and j has the same meaning as mentioned previously. The control algorithm starts with iteration $j = 1$; where the initial torque, T_i^0 is zero. Hence, in the first iteration this control method is reduced to the fixed-gain PD method. This control algorithm terminates once the desired performance is achieved. In other words, if the difference between the desired performance and the actual one is smaller than a prescribed small positive number, ε, the scheme will end.

It is noted that the above EPD control law is different from the PD-based iteration learning control strategies reported in the literature, which in general have the following form (Arimoto et al., 1984; Kuc et al., 1991; Chen and Moore, 2002; Tayebi, 2003):

$$T_i^j = K_P e_i^{j-1} + K_d \dot{e}_i^{j-1} + T_i^{j-1} \tag{4.7}$$

In comparison to the EPD control law, this algorithm uses the errors from the previous iteration rather than the present one, hence it is an offline control approach.

4.3.3 Adaptive Evolutionary Switch Gain PD Control (AES-PD)

The adaptive evolutionary switching PD (AES-PD) control design is based on two operational modes. These two modes are the single and evolutionary operation modes. In the first operation mode, the traditional PD control feedback with gain-switching is used and thus the information from the present operation is utilized. In the evolutionary operational mode, the information from previous iterations is used with a simple iterative

learning control. With these two operational modes, the information from both the current and previous operations is utilized. The AES-PD control method is outlined as follows (Ouyang, 2005).

Consider the *j*th iterative operation of the 5 bar linkage with the two servo motors under the following control law:

$$T^{j}(t) = K_p^{j} e^{j}(t) + k_d^{j} \dot{e}^{j}(t) + T^{j-1}(t) \qquad j = 0,1,\ldots\ldots, N \tag{4.8}$$

where the control algorithm repeats from iteration 0 to *N*.

The gains of the controller are determined by using the following rule:

$$\begin{cases} K_p^{j} = \beta(j) K_p^{0} \\ K_d^{j} = \beta(j) K_d^{0} \\ \beta(j+1) > B(j) \end{cases} \qquad j = 0,1,\ldots\ldots, N \tag{4.9}$$

In the above equations,

$$\begin{cases} T^{-1}(t) = 0; \\ e^{j}(t) = q_d(t) - q^{j}(t) \\ \dot{e}^{j}(t) = \dot{q}_d(t) - \dot{q}^{j}(t) \end{cases} \tag{4.10}$$

where K_p^0 and K_d^0 are the initial PD control gain matrices, which are diagonal and positive definite. These matrices are referred to as the initial proportional and derivative gains. As well, K_p^j and K_d^j are the control gains of the *j*th iteration. These gains are obtained by multiplying the initial PD control gains, K_p^0 and K_d^0, by $\beta(j)$, which is a

function of the iteration number. In general, $\beta(j)$ is assumed to be greater than one for j = 1, 2, ..., N.

The above control method is a hybrid one in that it combines several control methods and therefore takes advantages of each of them. The structural design of this control method has 3 parts. First of all, the control is evolutionary through several generations of changes. Secondly, the control model consists of two parts, a PD feedback part and a feedforward part. This allows the use of torque profiles obtained from the present and the previous iteration. Finally, the gains in the PD feedback law are changed according to the switching gain principle. Therefore, it can be observed that this control method is a simple combination of the traditional PD control with gain switching and the traditional ILC control (Ouyang, 2005).

4.3.4 Adaptive Nonlinear PD learning control (NPD-LC)

NPD-LC is a combination of a nonlinear PD control and an iterative learning structure which holds both adaptive and on-line learning properties. This type of control can be developed by following the same strategy that was discussed previously for the adaptive PD learning control (AES-PD). The major difference between the NPD-LC and AES-PD control laws is that the control gains are not constant in the NPD-LC controller, but are functions of error. The NPD-LC algorithm is outlined in the following.

$$T^{j}(t) = K_{p}^{j}(t)e^{j}(t) + K_{d}^{j}(t)\dot{e}^{j}(t) + T^{j-1}(t) \tag{4.11}$$

where

$$K_p(t) = K_{p0} * K_p(t)$$
$$K_d(t) = K_{d0} * K_d(t) \qquad (4.12)$$

In the above equations,

$$K_p(t) = K_{\max} - K_{\min} \sec h(\alpha * e(t))$$

$$K_d(t) = K_{\max} - K_{\min} \sec h(\alpha * e(t))$$

where K_{mas}, $K_{\min}$, and α are user-defined positive constants.

In Eq. (4.11), the term $K_p^j(t)e^j(t) + K_d^j(t)\dot{e}^j(t)$ represents the feedback portion and the term $T^{j-1}(t)$ is the feedforward portion of the control algorithm. Hence, NPD-LC method is an on-line learning control strategy, while the ILC is an off-line learning control. Consequently, the NPD-LC method is expected to have a faster convergence speed. In other words, a fewer number of iterations are required using the NPD-LC method in order to obtain the same or superior trajectory tracking (i.e., a greater reduction in trajectory tracking errors).

4.4 Computed Torque Control (CTC) algorithm

The CTC control algorithm has been briefly discussed previously in chapter 2. Based on the dynamic model presented in that chapter, the following CTC control law is applied to the closed-loop mechanism in this study.

$$T = D(q')(\ddot{q}_d + K_p e + K_d \dot{e}) + C(q', \dot{q}')\dot{q} + g(q') \quad (4.13)$$

where $\ddot{q}_d$ is the desired acceleration and $\dot{q}$ is the actual velocity vector. The expressions for the inertia term, $D(q')$, the centripetal and centrifugal effects, $C(q', \dot{q}')$, and the gravitational term, $g(q')$, have been developed earlier in this thesis (refer to chapter 2).

4.5 Summary and Discussion

Various control laws for the control of the 2-DOF closed-loop RTC mechanism are presented in this chapter. At first, the traditional fixed-gain PD control law and the NPD control algorithm are reviewed and outlined. In the NPD control law, the gains are not constant but adjusted based on the errors of the trajectory tracking. The use of the traditional PD control is popular due to its simple structure and implementation as well as its acceptable performance for some applications in robotics. However, the inherent difference between the nonlinear dynamics behaviour of a manipulator and the linear regulating behaviour of a PD controller makes these types of control strategies unsuitable for more complex control applications.

Then, ILC control approaches are examined and outlined. Traditional ILC algorithms are feedforward or offline learning control strategies. In contrast, the EPD control algorithm is an online iterative learning control strategy, which incorporates the plant dynamics into its control law by taking into account the torques from the previous iteration.

Next, the CTC control law is discussed. In this control law, the dynamic model of the plant is essentially required. As a result, the dynamic model plays a significant role in the performance of the CTC control law. Also, it is noted that, for a complex system, the dynamic model is usually complicated. In such a case, the CTC control law, sometimes, prove to be impractical due to the time required for computation. In comparison, the AES-PD control algorithm does not need the system model, thereby requiring much less computational time.

Finally, the NPD-LC iterative learning control strategy is examined. This control incorporates the system dynamics into the control law. Experiments to verify the effectiveness of the control approaches examined in this chapter are presented in Chapter 5.

Chapter 5

EXPERIMENTS AND RESULTS ON THE RTC MECHANISM

5.1 Introduction

This chapter presents an experimental study on the closed-loop RTC mechanism described previously, by applying the different control approaches reviewed in the preceding chapter. The objective of this experimental study is to verify and compare the effectiveness of these control approaches, as applied to the closed-loop RTC mechanism. In Section 5.2, the trajectories of the two servomotors are presented. Presented in Sections 5.3 to 5.7 are the experiments and results of applying the PD and NPD control laws at both low and high speeds, EPD control, NPD-LC control, and AES-PD control, respectively. In Section 5.7, the results of applying the above five different control laws are compared with each other, followed by Section 5.8 that compares the effectiveness of applying feedback ILC control to that of feedforward ILC control. Section 5.9 presents the results of applying CTC control, as compared to the traditional PD control. In Section

5.10, the limitations of the experimental study are discussed. Finally, Section 5.11 provides the conclusions drawn from this chapter.

5.2 Trajectory planning for the two servomotors

As mentioned previously, the trajectory tracking of a mechanism can be performed in either Cartesian space (i.e., trajectory of the end-effector) or joint space (i.e., trajectory of the motors). However, regardless of the trajectory tracking approach, since the control of a mechanism is performed at the joint level, the conversion of the end-effector coordinates to joint coordinates is essentially required. This thesis is concerned with the joint or actuator trajectory tracking. For the purposes of this study, the desired trajectories of the two actuators are planed as functions of time. In particular, this function is a Hermite polynomial of the fifth degree with continuous bounded conditions for position, velocity, and acceleration, which is adopted from (Ouyang, 2005). The mathematical expression of the trajectories for the two actuators are given by, respectively,

$$q_1^d(t) = q_{10}^d + (6\frac{t^5}{t_f^5} - 15\frac{t^4}{t_f^4} + 10\frac{t^3}{t_f^3})(q_{1f}^d - q_{10}^d) \tag{5.1}$$

$$q_2^d(t) = q_{20}^d + (6\frac{t^5}{t_f^5} - 15\frac{t^4}{t_f^4} + 10\frac{t^3}{t_f^3})(q_{2f}^d - q_{20}^d) \tag{5.2}$$

where $q_1^d(t)$ and $q_2^d(t)$ are the desired trajectories of the two servomotors, q_{10}^d, q_{1f}^d, q_{20}^d, and q_{2f}^d are the desired initial and final positions of the servomotors, respectively, and

t_f represents the time period required for the actuators to reach the desired final position. In this study, the initial positions for the two actuators is set equal to zero, i.e., $q_{10}^d = 0$ and $q_{20}^d = 0$ for simplification; and two cases with different operating speeds are investigated experimentally. In the first case, the RTC mechanism is operated at a lower speed with

$$t_f = 4\,\text{sec} \qquad q_{1f}^d = \frac{\pi}{2}, \qquad \text{and } q_{1f}^d = \frac{\pi}{2} \tag{5.3}$$

Thus, the motor speed is $\omega = 60/(4\times 4) = 3.75$ rpm for this case. In the second case, the mechanism is operated at a higher speed with

$$t_f = 2\,\text{sec} \qquad q_{1f}^d = \pi, \qquad \text{and } q_{2f}^d = \pi \tag{5.4}$$

Thus, the motor speed is $\omega = 60/(2\times 2) = 15$ rpm for this case. For convenience, the first case is also referred to as the low speed case and the second one as the high speed case in the rest of the chapter.

5.3 PD and NPD control laws

For the PD control law, via trial and error, the proportional and derivative gains, K_p and K_d, are chosen such that they result in the lowest possible maximum position tracking errors whilst there is no excessive torque fluctuations in the actuators. The control gains and parameters of all of the control laws used throughout this thesis are chosen based on the same criteria. For the PD control law, their values are given as follows for both low and high speed cases.

The low speed case:

Actuator 1: $K_{p1} = 0.00022,\ K_{d1} = 0.00002$

Actuator 2: $K_{p2} = 0.00036,\ K_{d2} = 0.00004$

The high speed case:

Actuator 1: $K_{p1} = 0.00052,\ K_{d1} = 0.000052$

Actuator 2: $K_{p2} = 0.00048,\ K_{d2} = 0.000062$

Similar to the PD controller, for the NPD control law, the nonlinear gains of the controller are selected via trial and error such that the lowest maximum position tracking errors are obtained. These gains are as follows.

$$K_1(t) = 3 - 2\sec h(alf_1 e_1(t)) \qquad (5.3)$$

$$K_2(t) = 3 - 2\sec h(alf_2 e_2(t))$$

where alf_1 and alf_2 are user-defined constants. In this study, their values are set as 1.5 and 1.3 for the low speed case, and 4.3 and 3.7 for the high speed case, respectively. In addition, it is seen from the above equations that, if alf_1 and alf_2 are set as zeros, both K_1 and K_2 have a value of 1. In such a case, the NPD controller reduces to a PD controller. It is also seen that the values of both gains, $K_1(t)$ and $K_2(t)$, are in the range from 1 to 3.

The PD and NPD control schemes with the above determined gain values were applied to the closed-loop RTC mechanism test bed, respectively, in order to track the trajectories presented in Section 5.2. In the experiments, the angular positions and velocities of both actuators were measured by using the approaches discussed in Chapter 3, with a sampling period of 4ms. This sampling period is used for all the PD-based control algorithms employed in this study. The error or the difference between the measured angular position and the desired ones were then evaluated. The results are presented in Figure 5.1 for the low speed case, and Figure 5.3 for the high speed case, respectively. In these figures, the solid lines represent the results of the PD controller and the dashed lines the results of the NPD controller. Also, in the experiments, the actuator torques are obtained from the control law by recording the voltage output signal sent to the amplifiers. As the actuator torque is determined by the voltage signal applied to the actuator, in the study this voltage signal is used to 'represent' the actuator torques. The so-represented torque is shown in Figure 5.2 for the low speed case, and Figure 5.4 for the high speed case, respectively.

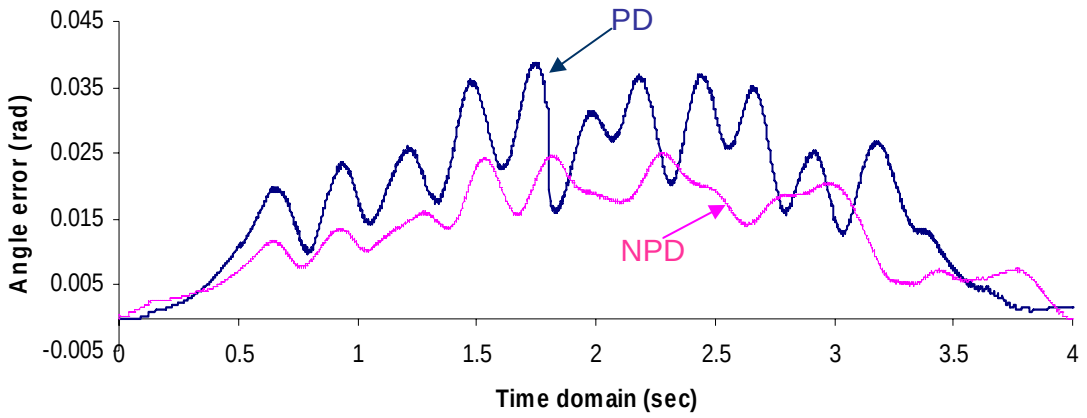

(a)

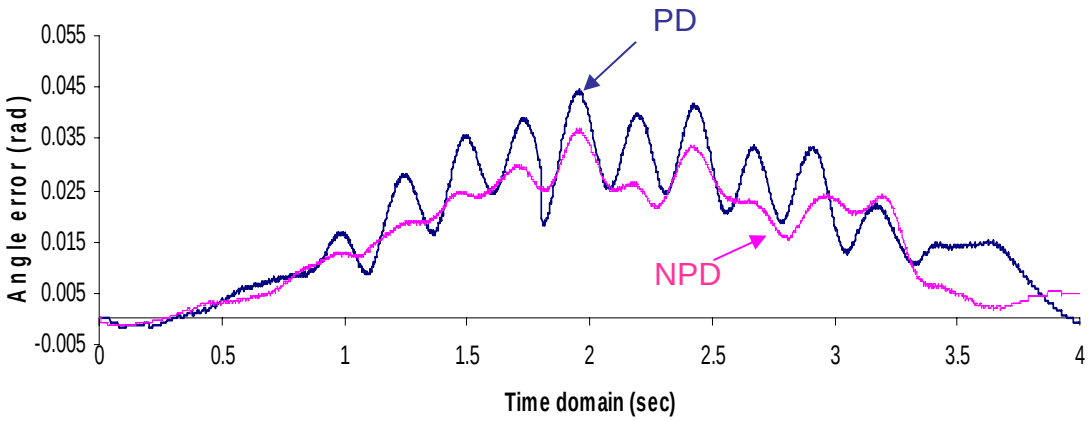

Note: Solid lines: PD control law; Dotted lines: NPD control law

(b)

Figure 5.1: Experimental results by applying PD and NPD controllers for the low speed case: (a) angle error of Actuator 1 and (b) angle error of Actuator 2.

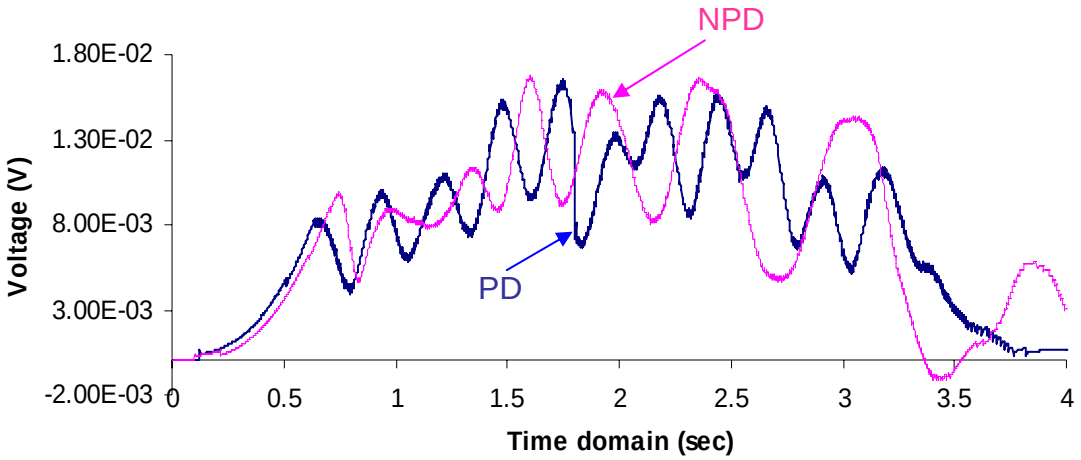

(a)

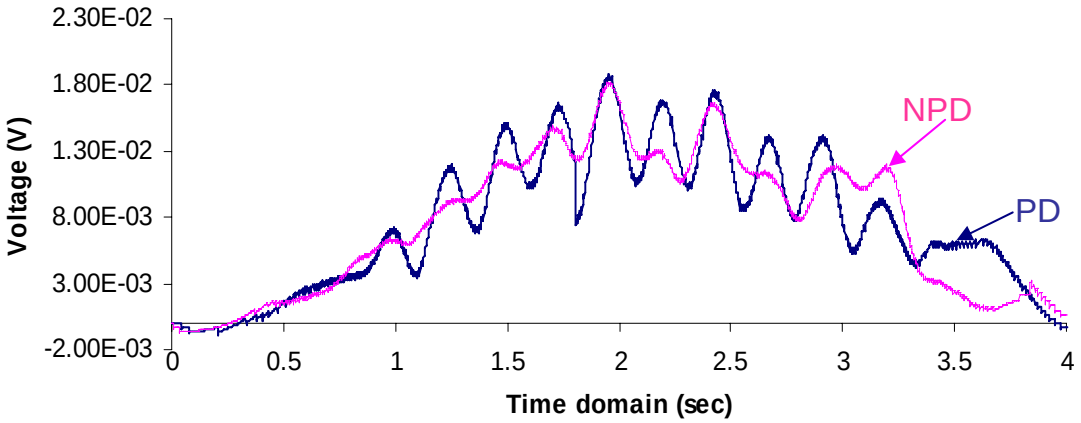

Note: Solid lines: PD control law; Dotted lines: NPD control law

(b)

Figure 5.2: Experimental results by applying PD and NPD controllers for the low speed case: (a) voltage applied to Actuator 1 and (2) voltage applied to Actuator 2.

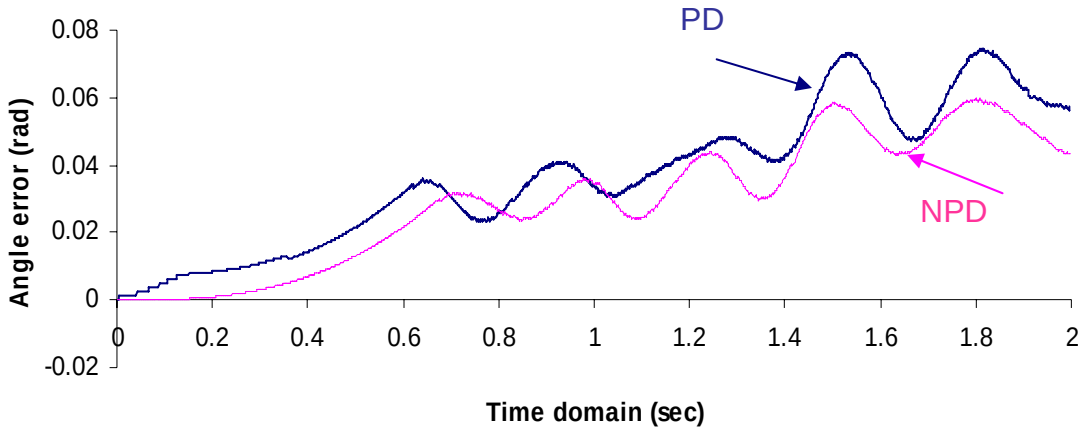

(a)

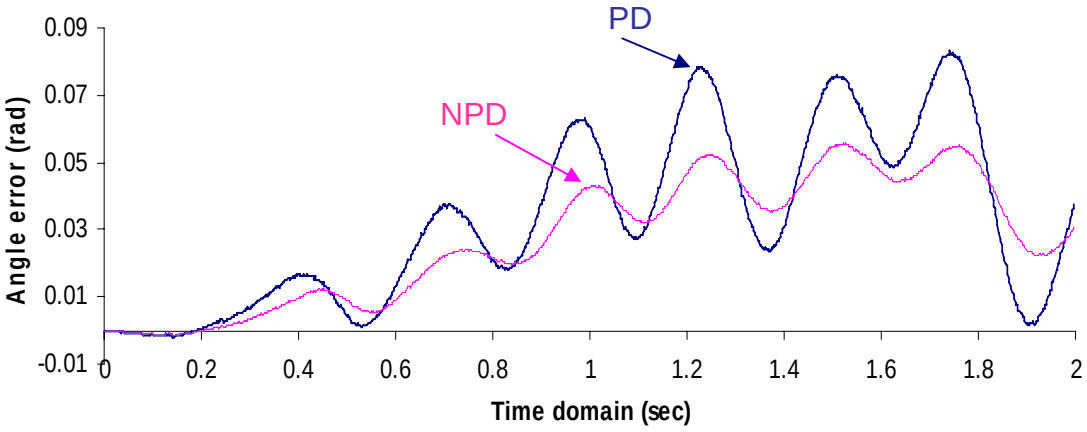

Note: Solid lines: PD control law; Dotted lines: NPD control law

(b)

Figure 5.3: Experimental results by applying PD and NPD controllers for the high speed case: (a) angle error of Actuator 1 and (b) angle error of Actuator 2.

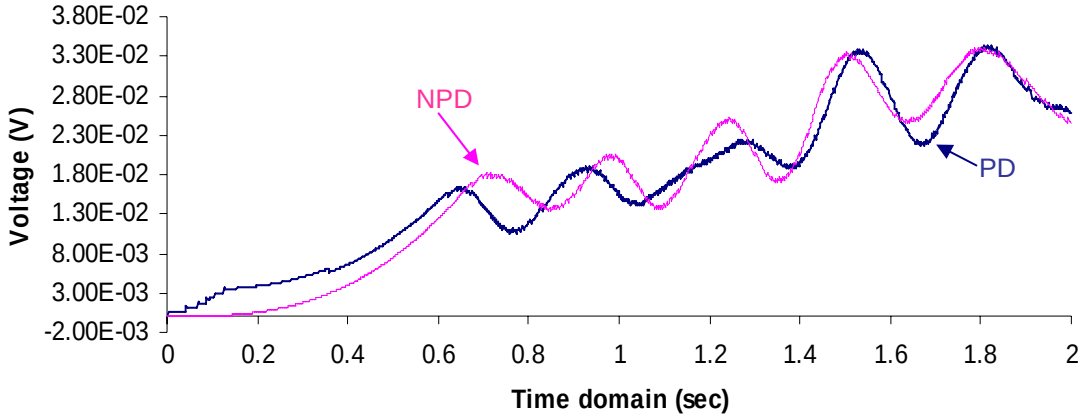

(a)

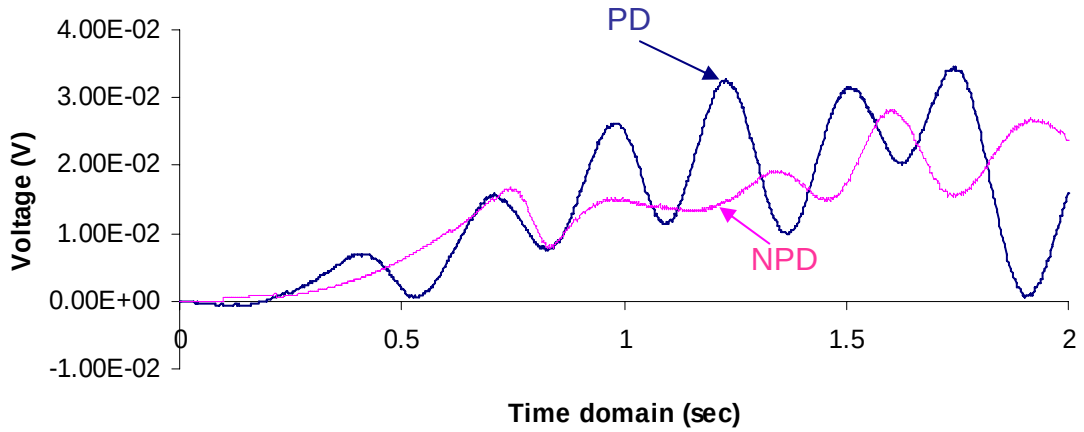

Note: Solid lines: PD control law; Dotted lines: NPD control law

(b)

Figure 5.4: Experimental results by applying PD and NPD controllers for the high speed case: (a) voltage applied to Actuator 1 and (2) voltage applied to Actuator 2.

From the results shown in Figures 5.1 and 5.3, it is observed that the NPD controller generally improves the performances in terms of reduction of trajectory tracking errors. It is interesting to compare Figures 5.1 and 5.3, which leads to the observation that with the increase of the velocities in the actuators, the position tracking errors will increase as well. This is expected since as the velocity and acceleration of the mechanism increase, the bigger effect the inertia forces will have, thus the more likely errors occur in the trajectory tracking. As well, the sampling period is the same for both the low speed and high speed cases. With an increase in the velocity of the mechanism, a higher sampling rate is also required as the controlled torque should also be updated more frequently. However, with the current system set-up, the 4ms sampling period is the lowest sampling rate that can be used. Regardless of the operating speed, at both high and low speeds the NPD controller results in reduced trajectory tracking errors in comparison to the PD controller. As for the torque profiles shown in Figures 5.2 and 5.4, it is difficult to comment on the differences between the PD and NPD controllers as they are very similar to one another in terms of the profile smoothness and the peak torque.

5.4 EPD control law

In the EPD control law, the control gains in each iteration are selected to be the same, which are given by, for the low speed case,

Actuator 1: $K_{p1} = 0.000022,\ K_{d1} = 0.000002$

Actuator 2: $K_{p2} = 0.000036,\ K_{d2} = 0.000004$

and for the high speed case:

Actuator 1: $K_{p1} = 0.000052,\ K_{d1} = 0.0000052$

Actuator 2: $K_{p2} = 0.000048,\ K_{d2} = 0.0000062$

Using the EPD control method, trajectory tracking performance for each generation was recorded, as in the experiments presented in the preceding section. Figures 5.5, 5.6, and 5.7 illustrate the performance improvement by using the EPD control law, one generation by one generation in an evolutionary process.

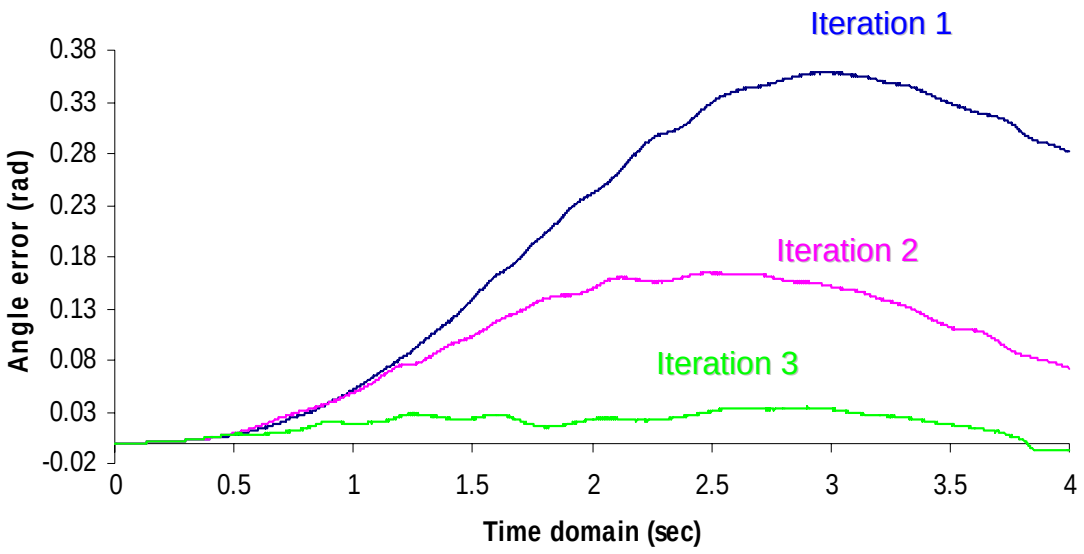

(a)

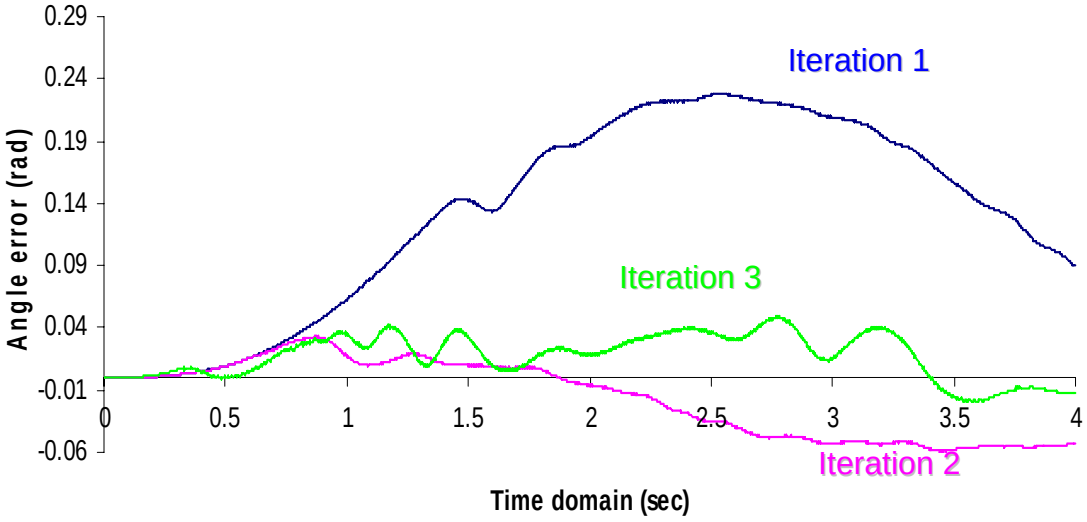

(b)

Figure 5.5: Experimental results by applying EPD controller for the low speed case (Iterations 1 to 3): (a) angle error of Actuator 1 and (b) angle error of Actuator 2.

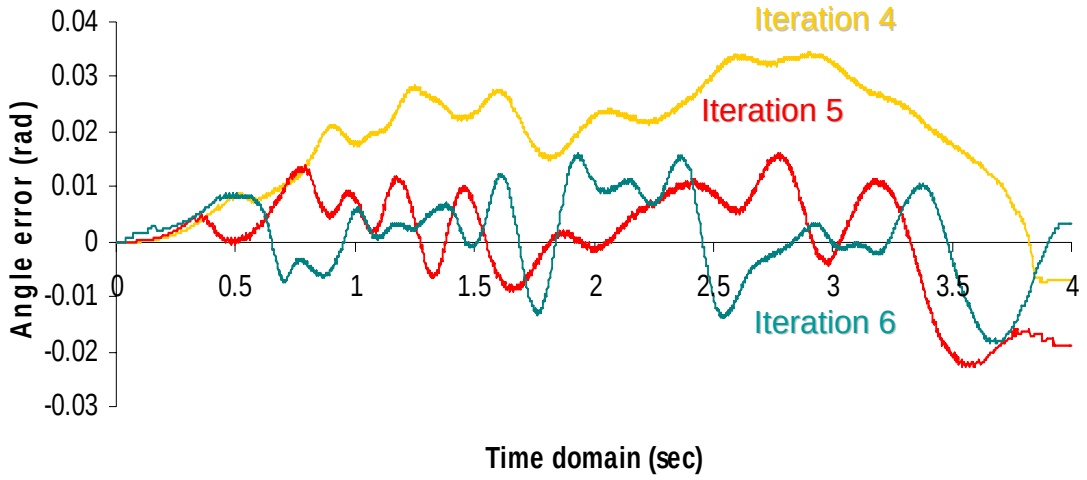

(a)

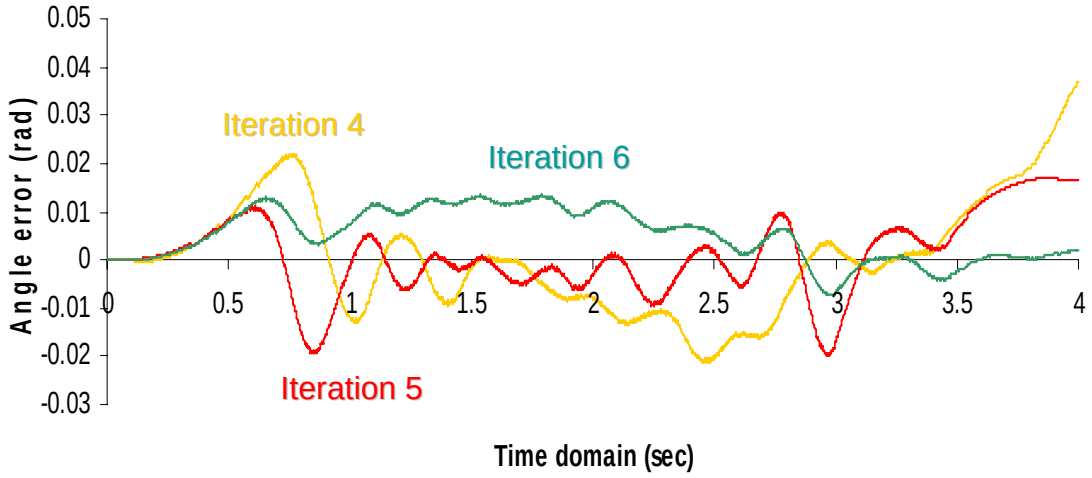

(b)

Figure 5.6: Experimental results by applying EPD controller for the low speed case (Iterations 3 to 6): (a) angle error of Actuator 1 and (b) angle error of Actuator 2.

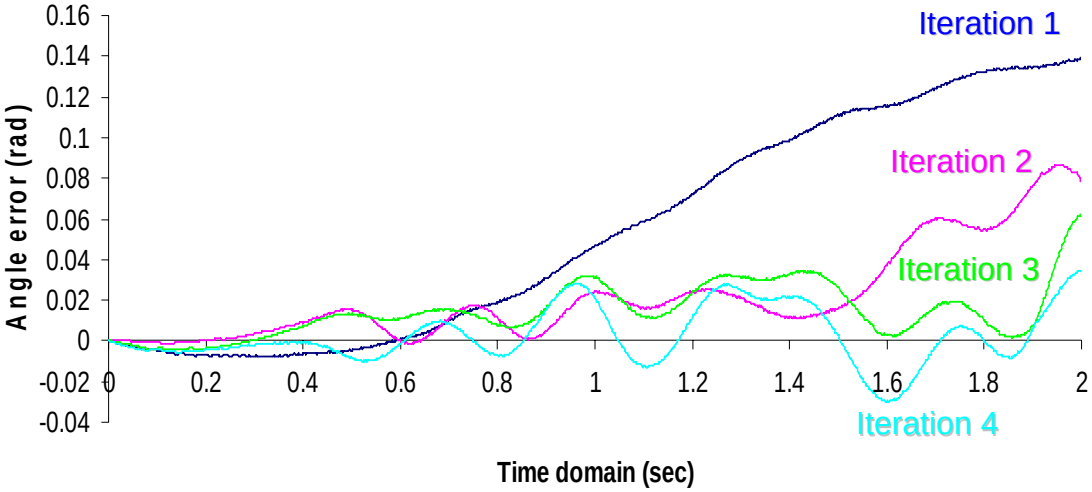

(a)

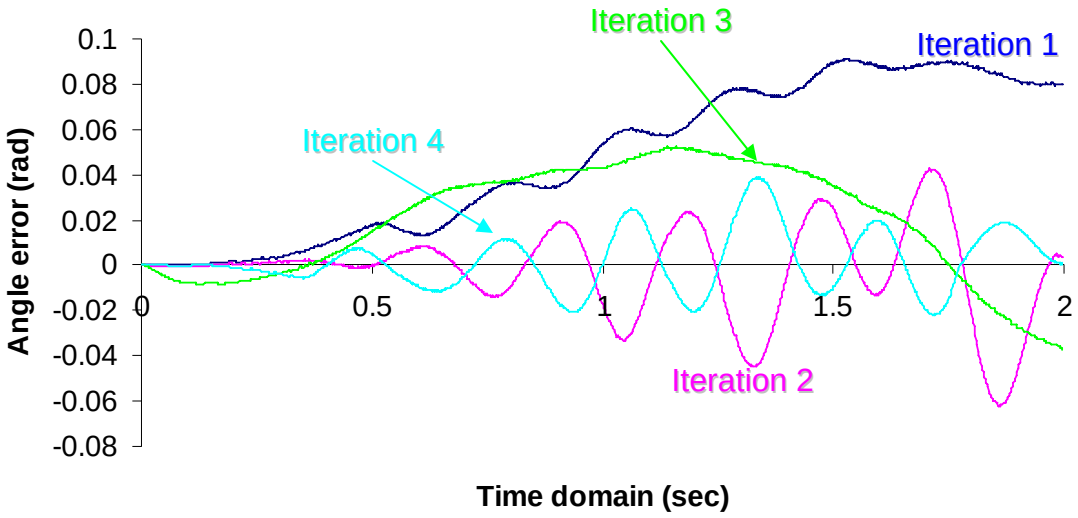

(b)

Figure 5.7: Experimental results by applying EPD controller for the high case (Iterations 1 to 4): (a) angle error of Actuator 1 and (b) angle error of Actuator 2.

The experimental results produced at both low and high speeds are also documented in Tables 5.1 and 5.2, respectively, to give a more clear presentation of the performance improvement from one iteration to the next (only the maximum values of each performance index are given). It should be noted that the units of the performance indexes in all the tables are as follows:

Position error (e_i): rad; Torque (T_i): V

Table 5.1 Performance improvement with the EPD control at the low speed case

Generation	e_1	e_2	T_1	T_2

Iteration 1	0.358	0.227	0.022	0.026
Iteration 2	0.164	0.056	0.020	0.023
Iteration 3	0.035	0.045	0.021	0.022
Iteration 4	0.031	0.030	0.022	0.029
Iteration 5	0.022	0.019	0.023	0.027
Iteration 6	0.018	0.016	0.024	0.028

Table 5.2 Performance improvement with the EPD control at the high speed case

Generation	e_1	e_2	T_1	T_2
Iteration 1	0.139	0.091	0.038	0.052
Iteration 2	0.086	0.059	0.041	0.047
Iteration 3	0.061	0.050	0.043	0.049
Iteration 4	0.035	0.038	0.040	0.051

Figures 5.5 through 5.7 show the EPD results from iteration to iteration for actuators 1 and actuator 2, respectively. At low speeds, for the first iteration, the maximum tracking errors were about 0.358rad and 0.227rad for actuators 1 and 2, respectively. After 6 iterations, the maximum tracking error was about 0.018rad for actuator 1 and 0.016rad for actuator 2, respectively. From these figures, one can see the trajectory tracking performance improvement from iteration 1 to iteration 6 at low speeds. The test at high speed also demonstrated a similar conclusion. At high speeds, for the first iteration, the maximum tracking errors were 0.139rad and 0.091rad for actuators 1 and 2, respectively. After 4 iterations, the maximum tracking errors were 0.035rad and 0.038rad for actuators 1 and 2, respectively. The above figures and discussion provide a clear presentation of the effectiveness of the EPD control law at both high and low speeds.

5.5 NPD-LC control law

Similar to the previous control laws, for the NPD-LC control law study, experiments are carried out at low and high speeds. As it was discussed in Chapter 4, the control gains are kept the same for each generation, i.e.,

At the low speed case:

Actuator 1: $K_{p1} = 0.000022$, $K_{d1} = 0.000002$, $K_{\max 1} = 3$, and $\alpha_1 = 1.5$

Actuator 2: $K_{p2} = 0.000036$, $K_{d2} = 0.000004$, $K_{\max 2} = 3$, and $\alpha_2 = 1.5$

At the high speed case:

Actuator 1: $K_{p1} = 0.000055$, $K_{d1} = 0.0000052$, $K_{\max 1} = 3$, and $\alpha_1 = 3.2$

Actuator 2: $K_{p1} = 0.000048$, $K_{d1} = 0.0000062$, $K_{\max 2} = 3$, and $\alpha_2 = 3.2$

The experiments were conducted from iteration to iteration and the experimental results produced using this control method are presented in Figures 5.8 through 5.10 and Tables 5.3 and 5.4.

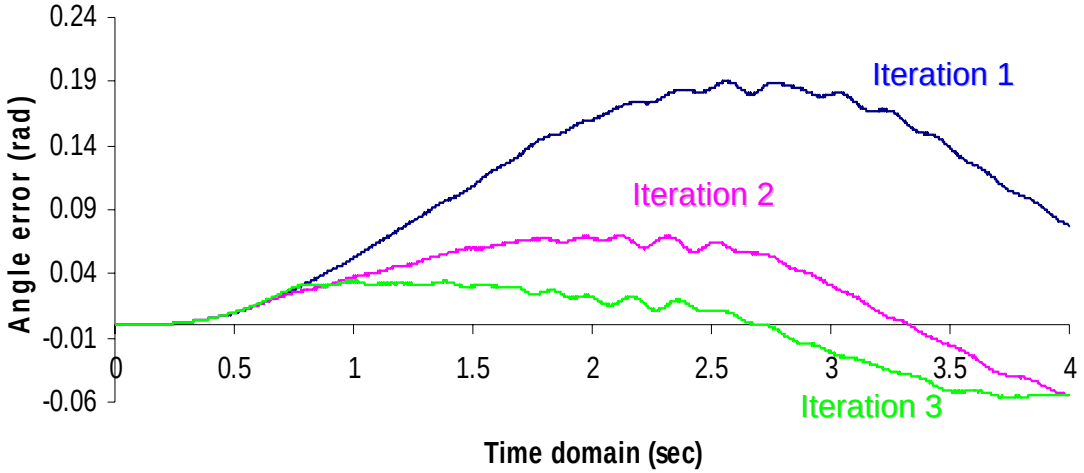

(a)

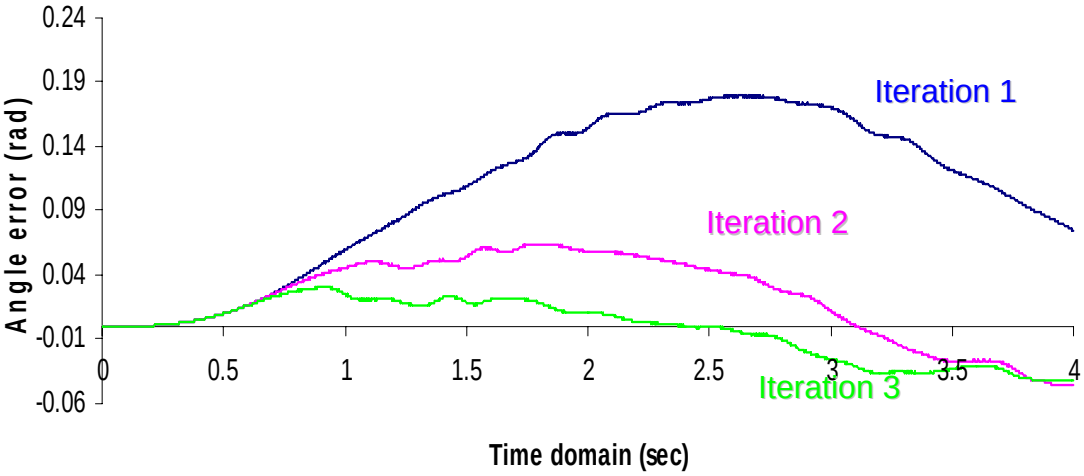

(b)

Figure 5.8: Experimental results by applying NPD-LC controller for the low speed case (Iterations 1 to 3): (a) angle error of Actuator 1 and (b) angle error of Actuator 2.

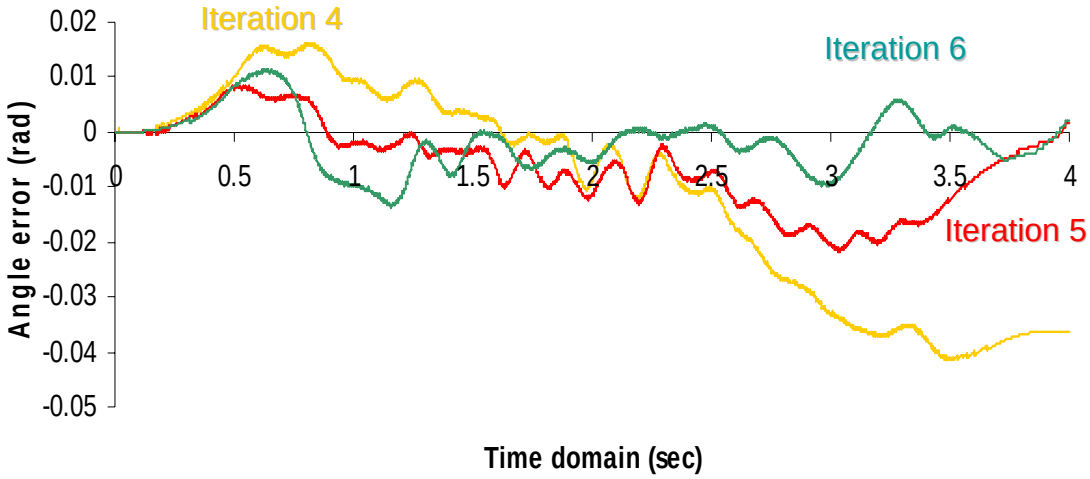

(a)

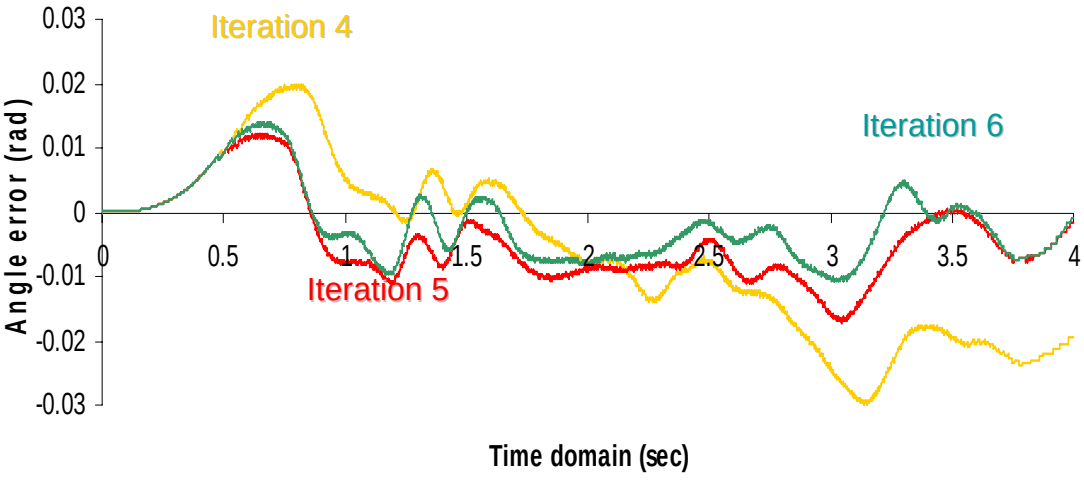

(b)

Figure 5.9: Experimental results by applying NPD-LC controller for the low speed case (Iterations 3 to 6): (a) angle error of Actuator 1 and (b) angle error of Actuator 2.

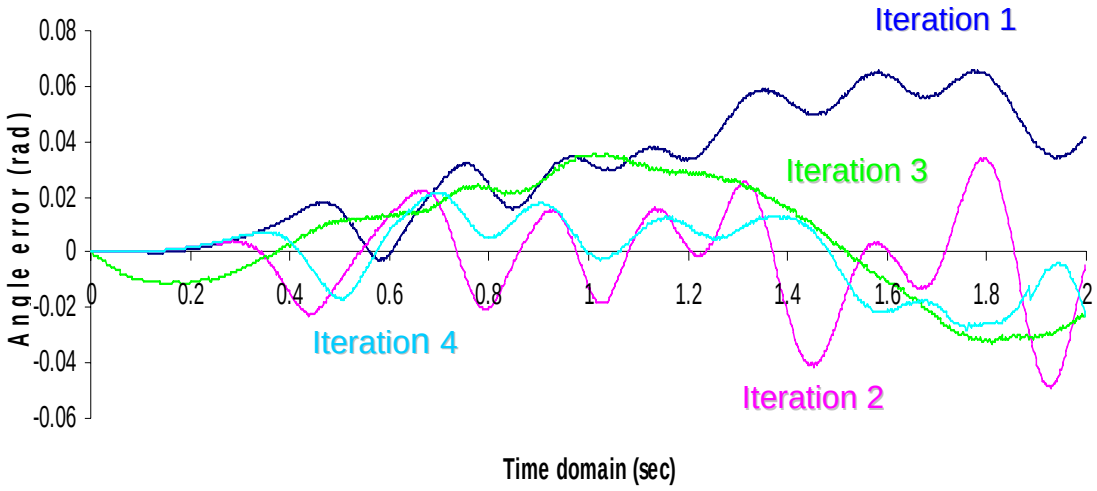

(a)

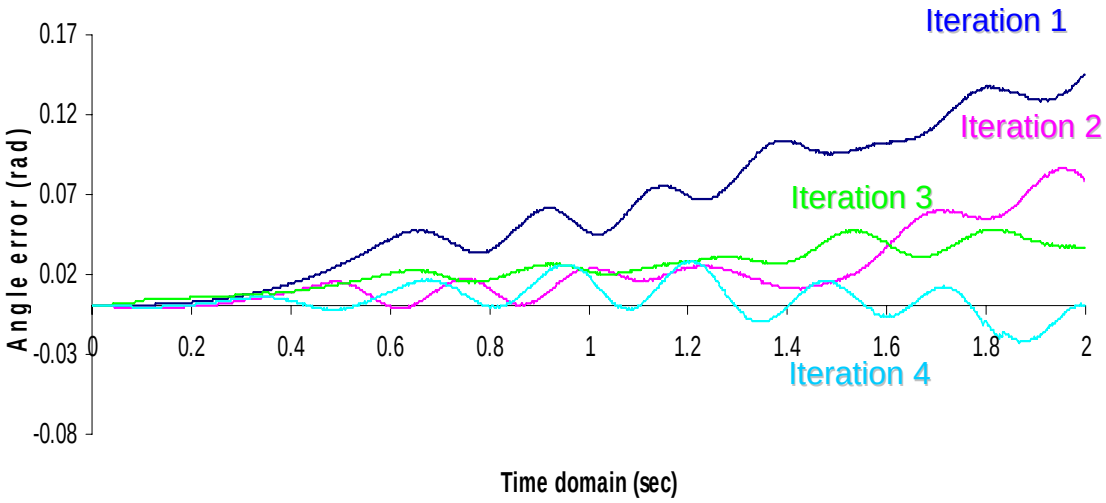

(b)

Figure 5.10: Experimental results by applying NPD-LC controller for the high speed case (Iterations 1 to 4): (a) angle error of Actuator 1 and (b) angle error of Actuator 2.

Table 5.3 Performance improvement with the NPD-LC control at the low speed case

Generation	e_1	e_2	T_1	T_2
Iteration 1	0.189	0.179	0.020	0.023
Iteration 2	0.068	0.064	0.023	0.021
Iteration 3	0.055	0.031	0.022	0.019
Iteration 4	0.041	0.027	0.022	0.019
Iteration 5	0.020	0.016	0.024	0.020
Iteration 6	0.013	0.013	0.025	0.022

Table 5.4 Performance improvement with the NPD-LC control at the high speed case

Generation	e_1	e_2	T_1	T_2
Iteration 1	0.066	0.144	0.042	0.049
Iteration 2	0.048	0.086	0.040	0.052
Iteration 3	0.035	0.049	0.041	0.048
Iteration 4	0.026	0.027	0.043	0.050

To show the effectiveness of the NPD-LC control method, Figures 5.8 through 5.10 illustrate the performance improvement of trajectory tracking from one iteration to the next. At low speeds, for the first iteration, the maximum tracking errors were 0.189rad and 0.179rad for actuators 1 and 2, respectively. After 6 iterations, the maximum tracking error was about 0.013rad for both actuators. From these figures, it is easy to observe the trajectory tracking performance improvement from iteration to iteration at low speeds using the NPD-LC iterative learning control. Similar conclusions can be made about the test at high speeds. At high speeds, for the first iteration, the maximum tracking errors were 0.086rad and 0.144rad for actuators 1 and 2, respectively. After 4 iterations, the maximum tracking errors were 0.026rad and 0.027rad for actuators 1 and 2, respectively. The above figures and discussion provide a clear presentation of the effectiveness of the NPD-LC control law at both high and low speeds.

5.6 AES-PD control law

In the experiments for the AES-PD control, the initial PD control gains and the switching factor, β, are selected as follows:

At the low speed case:

Actuator 1: $K_{p1} = 0.000022$, $K_{d1} = 0.000002$, $\beta = 2.5$

Actuator 2: $K_{p1} = 0.000036$, $K_{d1} = 0.000004$, $\beta = 2.5$

At the high speed case:

Actuator 1: $K_{p1} = 0.000052$, $K_{d1} = 0.0000052$, $\beta = 2$

Actuator 2: $K_{p1} = 0.000048$, $K_{d1} = 0.0000062$, $\beta = 2$

It can be seen that the initial PD control gains of the AES-PD control are selected to be the same as that of the adaptive NPD-LC control and the EPD control. The reason for this is to be able to compare the performance improvement and the convergence rate of these different ILC control techniques. Figures 5.11 through 5.13 and Tables 5.5 and 5.6 show the experimental results at low and high speeds from iteration to iteration.

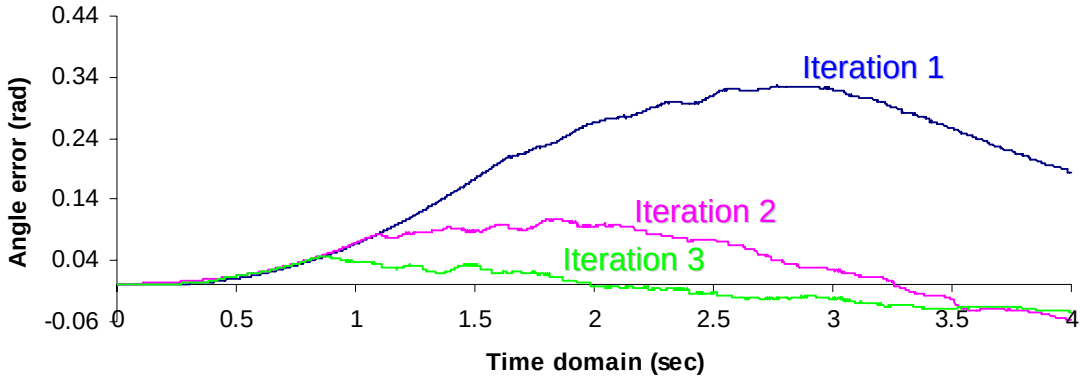

(a)

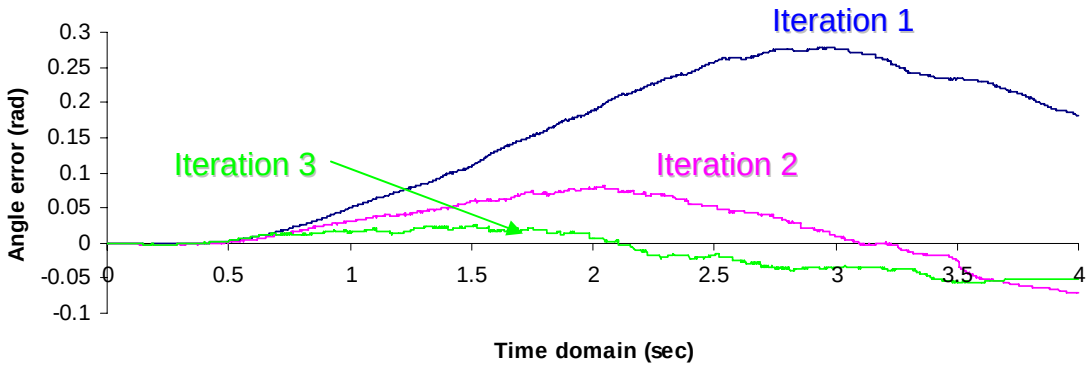

(b)

Figure 5.11: Experimental results by applying AES-PD controller for the low speed case (Iterations 1 to 3): (a) angle error of Actuator 1 and (b) angle error of Actuator 2.

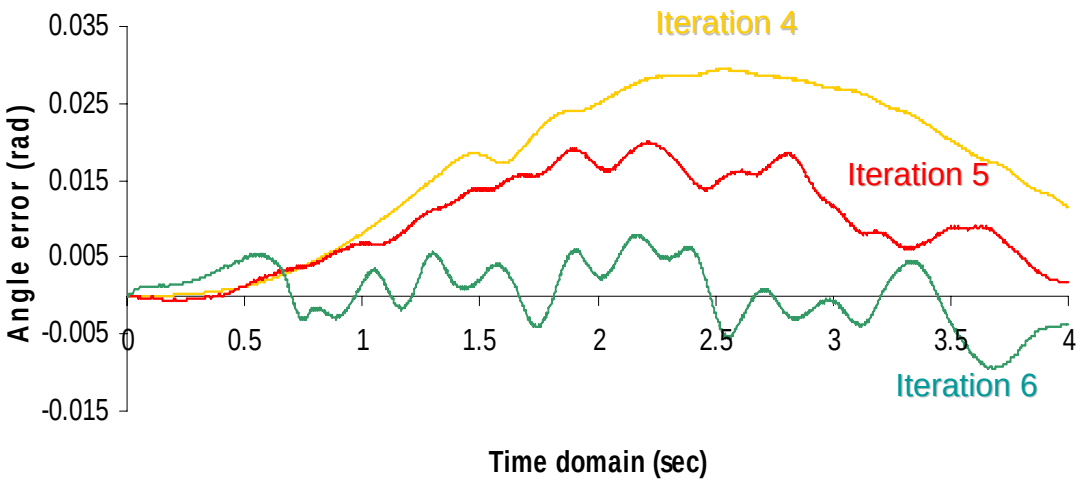

(a)

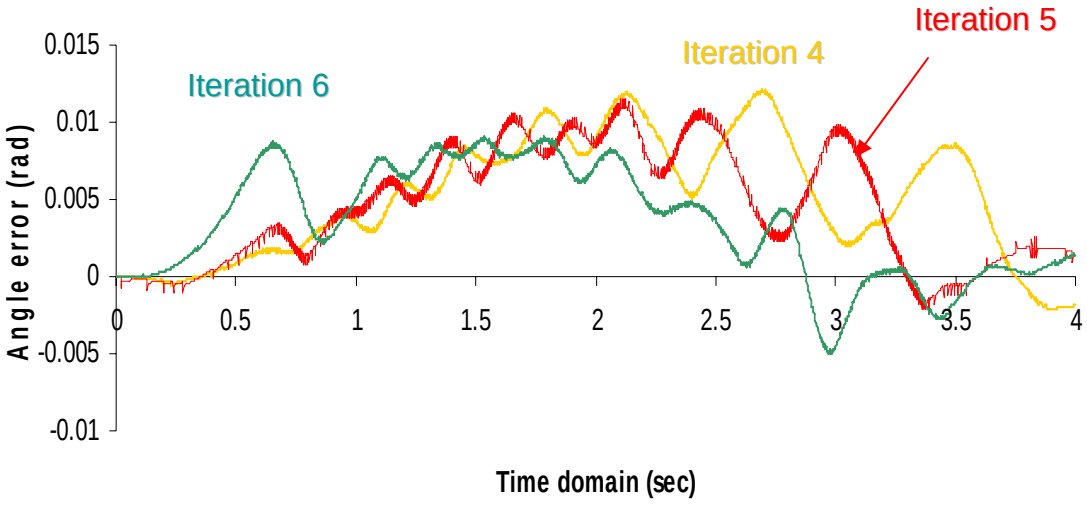

(b)

Figure 5.12: Experimental results by applying AES-PD controller for the low speed case (Iterations 3 to 6): (a) angle error of Actuator 1 and (b) angle error of Actuator 2.

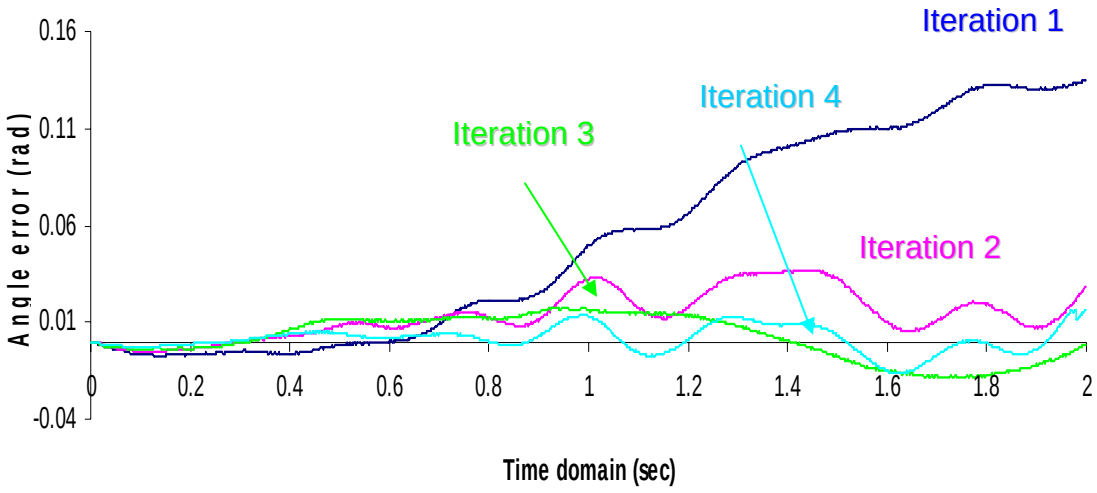

(a)

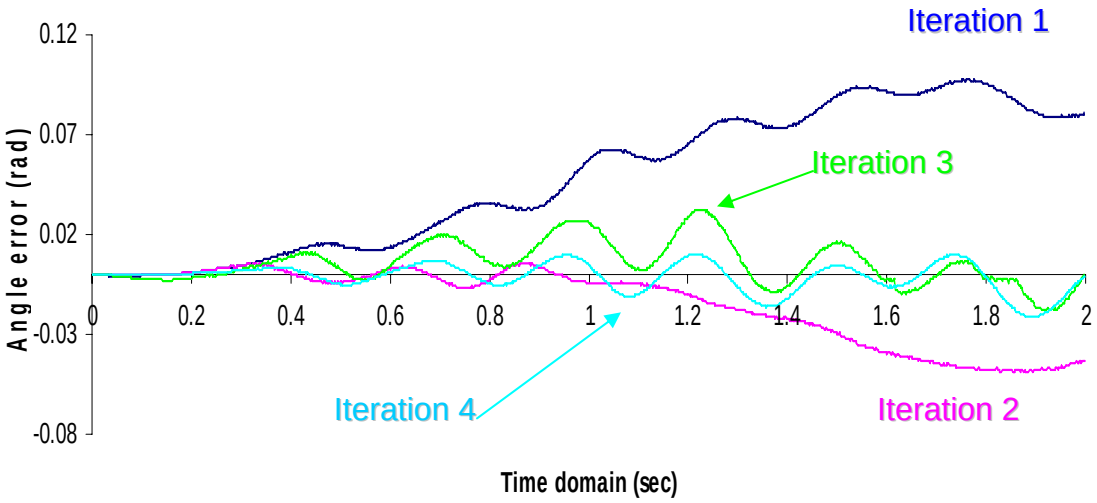

(b)

Figure 5.13: Experimental results by applying AES-PD controller for the high speed case (Iterations 1 to 4): (a) angle error of Actuator 1 and (b) angle error of Actuator 2.

Table 5.5 Performance improvement with the AES-PD control at the low speed case

Generation	e_1	e_2	T_1	T_2
Iteration 1	0.324	0.278	0.023	0.027
Iteration 2	0.107	0.076	0.021	0.025
Iteration 3	0.045	0.055	0.022	0.022
Iteration 4	0.029	0.012	0.020	0.019
Iteration 5	0.019	0.010	0.021	0.020
Iteration 6	0.009	0.009	0.022	0.020

Table 5.6 Performance improvement with the AES-PD control at the high speed case

Generation	e_1	e_2	T_1	T_2
Iteration 1	0.135	0.110	0.054	0.051
Iteration 2	0.034	0.047	0.052	0.052
Iteration 3	0.020	0.032	0.049	0.048
Iteration 4	0.017	0.016	0.050	0.051

To show the effectiveness of the AES-PD control method, Figures 5.11 through 5.13 illustrate the performance improvement in the position tracking errors. From these results it is clear how the position tracking errors are reduced from one iteration to the next. At low speeds, for the first iteration, the maximum tracking errors were 0.324rad and 0.278rad for actuators 1 and 2, respectively. After 6 iterations, the maximum tracking error was about 0.009rad for both joints 1 and 2. The tests at high speeds also demonstrated similar conclusions regarding the reduction in errors using the AES-PD control method. In this case, for the first iteration, the maximum tracking errors were 0.135rad and 0.110rad for actuators 1 and 2, respectively. After 4 iterations, the maximum tracking errors were 0.017rad and 0.016rad for joints 1 and 2, respectively. The above figures and discussion provide a clear presentation of the effectiveness of the AES-PD control law at both high and low speeds.

5.7 Comparison of the PD, NPD, EPD, AES-PD, NPD-LC Control methods

In the previous sections of this chapter, PD-based control schemes, including fixed gain PD control, NPD control, EPD control, NPD-LC control, and AES-PD control, for the trajectory tracking of the RTC closed loop mechanism are investigated experimentally. This section is to present a comparison of the experimental results to understand how the different control laws affect the trajectory tracking performance.

For the purposes of comparison, Figures 5.14 and 5.15 show the trajectory tracking errors by applying all the 5 aforementioned control algorithms, while Tables 5.7 and 5.8 summarize the maximum errors and torques of the actuators. For the EPD, NPD-LC, and AES-PD iterative control techniques, the last iteration (i.e., 4th and 6th iteration) of the learning process is presented for the high and low speed operating cases, respectively.

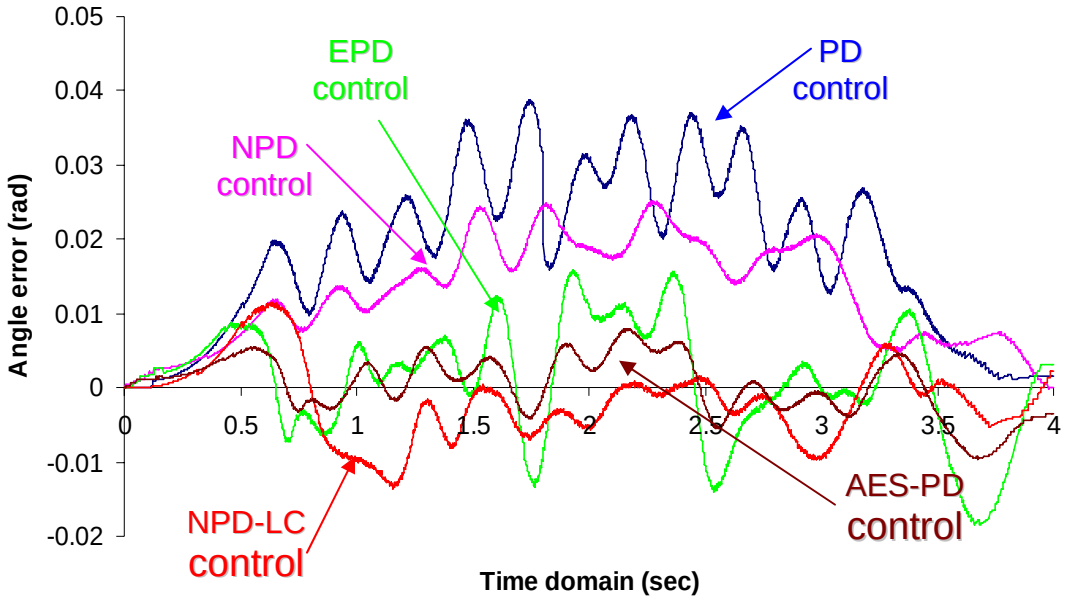

(a)

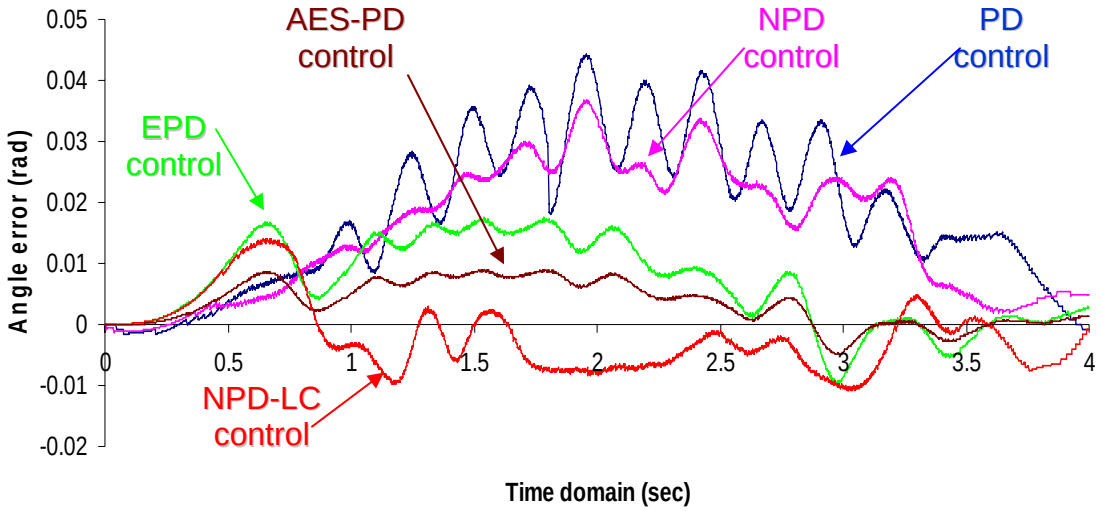

(b)

Figure 5.14 Comparison of the trajectory tracking performance with PD-based controllers at the low speed case: (a) angle error of Actuator 1 and (b) angle error of Actuator 2.

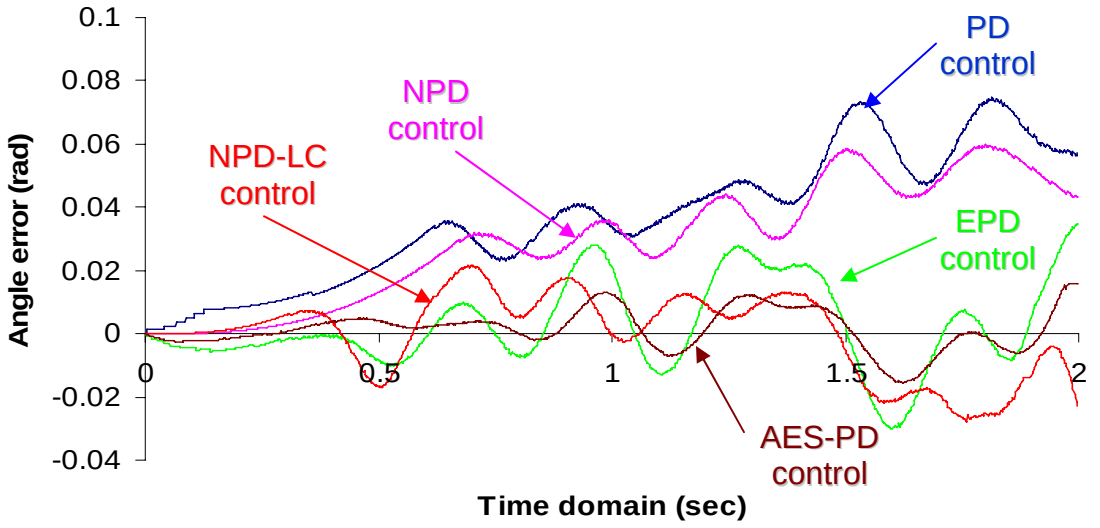

(a)

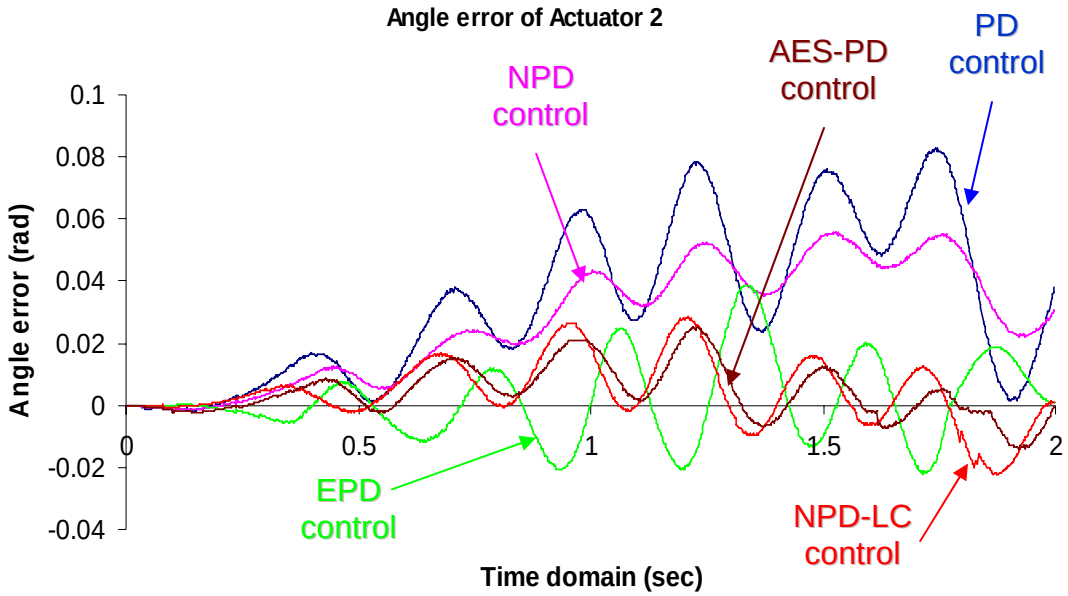

(b)

Figure 5.15 Comparison of the trajectory tracking performance with PD-based controllers at the high speed case: (a) angle error of Actuator 1 and (b) angle error of Actuator 2.

Table 5.7: Experimental Results for PD, NPD, EPD, NPD-LC, AES-PD at the low speed case (maximum errors and torques in the actuators)

	e_1	e_2	T_1	T_2
PD Control	0.038	0.043	0.016	0.018
NPD Control	0.025	0.036	0.015	0.018
EPD Control	0.018	0.016	0.024	0.028
NPD-LC Conrol	0.013	0.013	0.025	0.022

AES-PD Control	0.009	0.009	0.022	0.020

Table 5.8: Experimental Results for PD, NPD, EPD, NPD-LC, AES-PD at the high speed case (maximum errors and torques in the actuators)

	e_1	e_2	T_1	T_2
PD Control	0.079	0.081	0.035	0.038
NPD Control	0.058	0.055	0.032	0.028
EPD Control	0.035	0.038	0.040	0.051
NPD-LC Conrol	0.026	0.027	0.043	0.050
AES-PD Control	0.017	0.016	0.050	0.051

From the results shown in Figures 5.14 and 5.15 it is seen that in both high and low operating speed cases, AES-PD resulted in the lowest trajectory tracking errors, followed by NPD-LC, EPD, NPD and PD. Also from Tables 5.7 and 5.8 it is seen that in using the ILC control approaches, there is an increase in the peak actuator torques in comparison to that of the PD and NPD control methods. Although all ILC control techniques in general can be used to improve the trajectory tracking of the closed-loop manipulator, NPD-LC control and AES-PD control proved to have better trajectory tracking performance in comparison to EPD control. From Tables 5.4 and 5.6, one can observe that the AES-PD control method has lower position tracking errors after the second iteration compared to

those obtained after the third iteration using NPD-LC. The maximum trajectory tracking errors using AES-PD control after the second iteration are 0.034rad and 0.047rad for actuators 1 and 2, respectively, while the maximum trajectory tracking errors using NPD-LC control after the third iteration are 0.035rad and 0.049rad, respectively. Therefore, generally speaking, the AES-PD control has a faster convergence rate than the NPD-LC control approach. These finding are in agreement with the simulation results of (Ouyang 2002 and 2005).

5.8 Comparison of Feedforward ILC control to Feedback ILC control

In Chapter 4, the difference between feedforward ILC control and Feedback ILC control were discussed. In this section, the experimental results of using EPD control, which is a feedback control technique, are compared to that of the traditional feedforward control technique. The gains of the feedforward ILC control are selected to be the same as that of the feedback ILC control and are kept to be the same from one iteration to the next, i.e.,

At low speeds:

Actuator 1: $K_{p1} = 0.000022,\ K_{d1} = 0.000002$

Actuator 2: $K_{p2} = 0.000036,\ K_{d2} = 0.000004$

At high speeds:

Actuator 1: $K_{p1} = 0.000052,\ K_{d1} = 0.0000052$

Actuator 2: $K_{p2} = 0.000048,\ K_{d2} = 0.0000062$

The trajectory tracking performance for each generation using feedforward ILC control is presented in Figure 5.16 and is recorded and compared to that of feedback ILC control in Table 5.9. It should be noted that the following symbols are used for the performance indexes:

Maximum feedforward Position error (e_{ifw}): rad;

Maximum feeback Position error (e_{ifb}): rad;

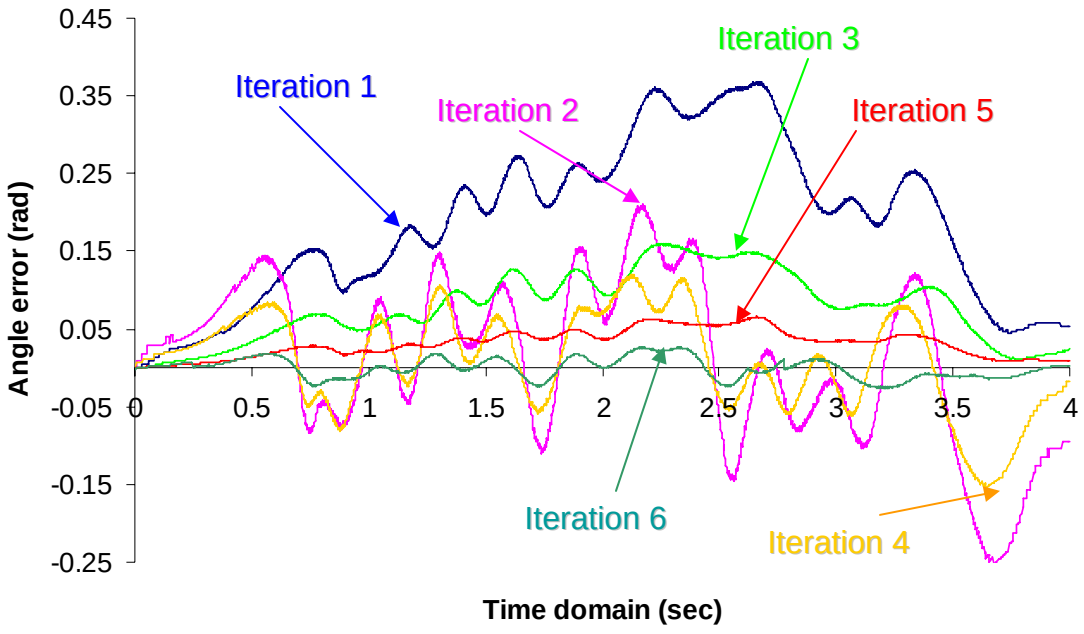

(a)

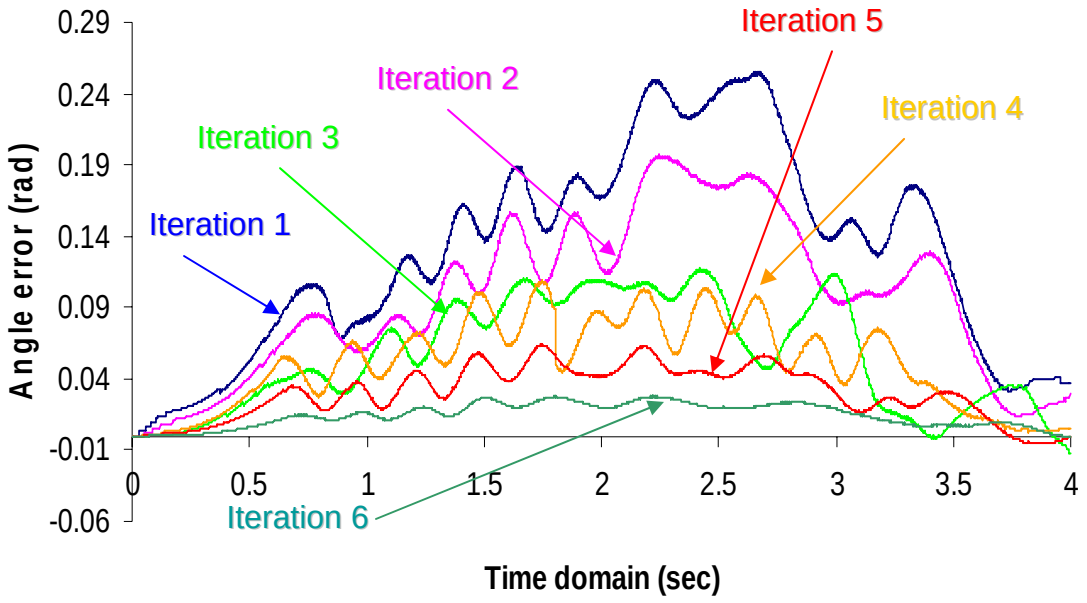

(b)

Figure 5.16: Experimental results by applying Feedforward ILC for the low speed case (Iterations 1 to 6): (a) angle error of Actuator 1 and (b) angle error of Actuator 2.

Table 5.9 Performance improvement comparison of feedforward ILC and feedback ILC

Generation	$e_{1\,fw}$	$e_{2\,fw}$	$e_{1\,fb}$	$e_{2\,fb}$
Iteration 1	0.361	0.245	0.358	0.227
Iteration 2	0.246	0.194	0.164	0.056
Iteration 3	0.160	0.110	0.035	0.045
Iteration 4	0.145	0.099	0.031	0.030

Iteration 5	0.063	0.062	0.022	0.019
Iteration 6	0.027	0.029	0.018	0.016

From Table 5.9, it can be seen that the feedback ILC control has a much faster convergence rate than the feedforward ILC control. The maximum position errors after the 3rd iteration of feedback ILC are 0.035rad and 0.045rad for actuators 1 and 2, respectively. Comparatively, the maximum position errors after the 5th iteration of feedforward ILC are 0.063rad and 0.062rad for actuators 1 and 2, respectively. It can easily be observed that the position tracking errors after the third iteration of feedback ILC are smaller than those of the fifth iteration of feedforward ILC. Such a conclusion is expected since from a real time control point of view, feedback or online learning control is much more efficient than feedforward or offline learning control. The experiments at the high speed operating condition provided similar conclusions.

5.9 Comparison of CTC control law to PD control law

The purpose of this section is to compare the effectiveness of the CTC control law which is a model based control method to that of the traditional PD control law which is an error based control approach at low and high speeds. The same PD control gains as the PD controller in Section 5.3 are chosen for the CTC controller for both operating speeds. Figures 5.18 and 5.19 illustrate the performance of CTC and PD control approaches at low and high speeds, respectively. In these figures, the solid lines indicate the results of

the PD controller and the dashed lines represent the results of applying the CTC control law to the closed-loop mechanism. The dynamic model component of the CTC control law is calculated in real time using the dynamic model developed earlier in Chapter 2.

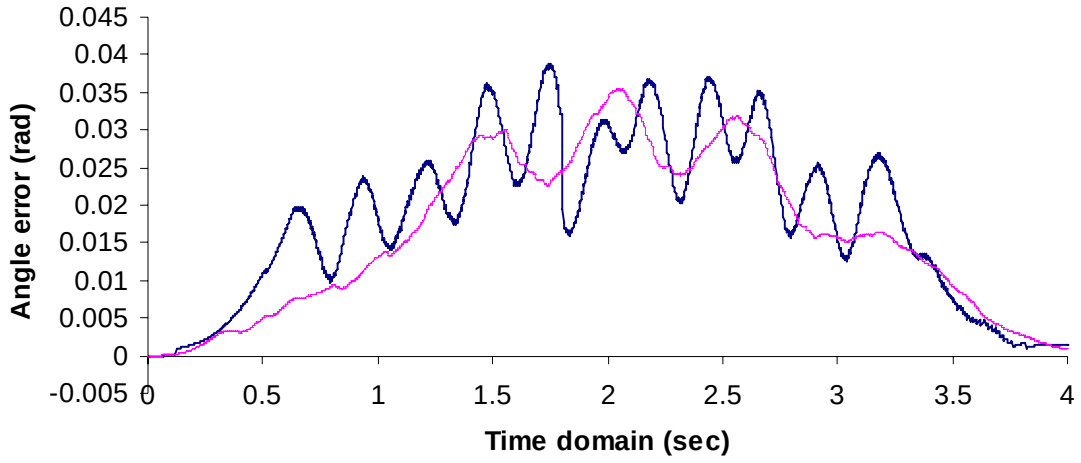

(a)

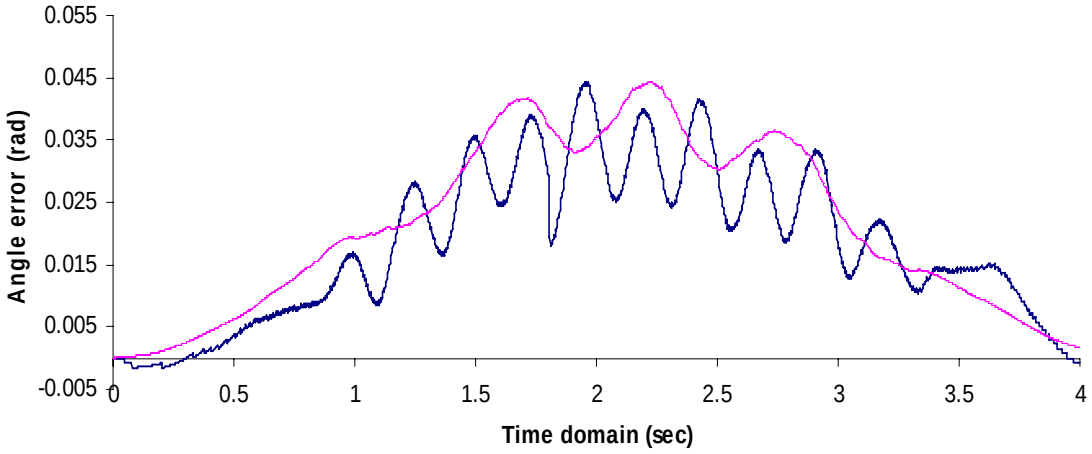

(b)

Figure 5.17: Experimental results by applying CTC and PD control for the low speed case: (a) angle error of Actuator 1 and (b) angle error of Actuator 2.

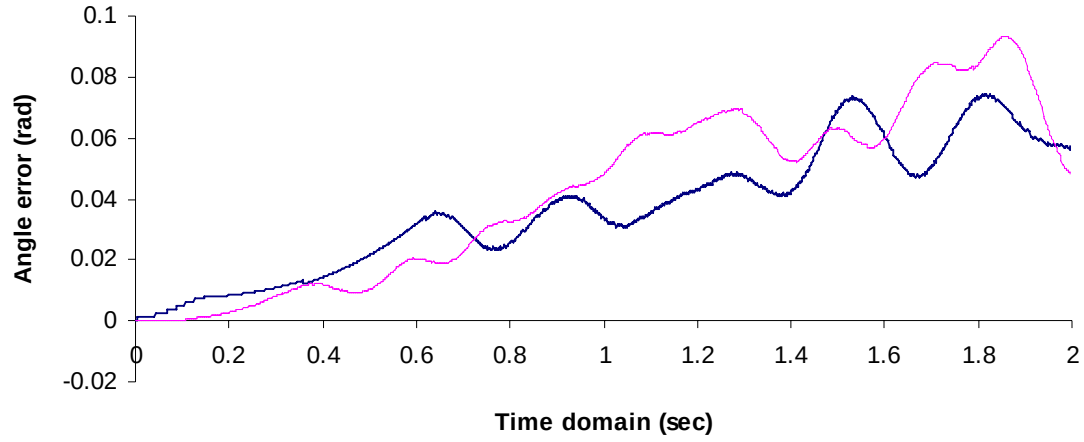

(a)

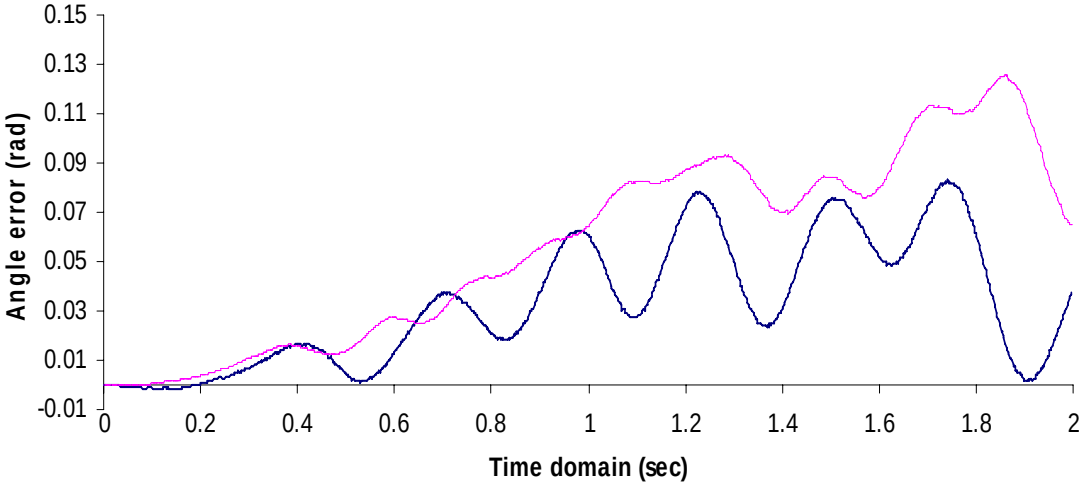

(b)

Figure 5.18: Experimental results by applying CTC and PD control for the high speed case: (a) angle error of Actuator 1 and (b) angle error of Actuator 2.

From Figure 5.17, it can be observed that at the low speed operating conditions, the maximum position tracking errors using both CTC and PD control approaches are close to one another. As the speed increases, the position tracking errors in both actuators increases as well, however, using the CTC control approach a greater increase in the position tracking errors is observed. Such an observation is expected since the performance of the CTC control approach is highly dependant on the accuracy of the dynamic model, with an increase in speed (i.e., less precise calculation of the dynamic model), the performance of this control approach becomes inferior to that of the traditional PD control in terms of the trajectory tracking performance.

5.10 Comments on the experiment

The experiments discussed in the previous sections are based on some simplifications. The results presented are acceptable for the purposes of demonstrating the effectiveness of the control algorithms examined. As applied to the real situations, however, some issues need to be further addressed, which are briefly discussed as follows.

5.10.1 Initial position error

The encoders used in this study are only relative position encoders. It is important in the iteration running mode that the initial position is the same from one iteration to the next. However, with relative encoders one cannot ensure this condition. This situation results in some initial position errors when the EPD, NPD-LC and AES-PD iterative learning

control techniques are used. The initial position errors in the actuators will affect the control of the system for the subsequent iterations and further impact the overall trajectory tracking of the actuators. One solution for this problem is the use an absolute position encoder.

5.10.2 Sampling period

The accuracy of the sampling period is the second problem in this experimental study. In the control strategies examined in this thesis, it is desired that the sampling period be the same from one iteration to the next. However, in reality it is hard to do so due to the nature of the Windows XP operating system used for data acquisition and processing in this study. Windows XP is designed to run and manage different tasks at the same time. The rate at which an application can execute commands depends on the system's clock speed and how fast it can retrieve messages from the message queue. The solution to this problem is the use of a hardware device such as dSPACE, which is able to provide a more accurate and smaller sampling period (Ouyang, 2005).

5.10.3 Estimations of velocity

For the control methods examined in this study, whether they are model based or error based control approaches, not only the position information but also the velocity information is essentially required. In this study, the position information was obtained from the relative encoders; while the velocity was estimated from the measured position

data. Using this approach, only the average velocity is obtained. It is known that a smaller sampling period can make the so-estimated velocities closer to the true instantaneous velocity; however, a smaller sampling period also might introduce large noise into the estimations, thereby degrading the tracking performance of the control approach examined. The possible solution to this problem is either the use of tachometers to directly measure the velocity or the use of filters (e.g. low pass filter, Kalman filter) to improve the velocity estimation from the measured position data.

5.11 Conclusion

In this chapter, PD-based control algorithms are investigated experimentally. In particular, the traditional PD control, NPD control, and iterative learning control methods were examined and compared in terms of trajectory tracking performance. The experimental results show that the AES-PD iterative control technique is superior to the other PD-based control methods. This conclusion is based on the reduction in the position tracking errors at both high and low speed operating conditions. The results of the experiments also show that ILC control techniques are promising control approaches compared to the PD and NPD control methods. These experimental results are in agreement with the simulation results reported in the previous literature.

Feedback ILC control and Feedforward ILC control were compared in terms of the reduction in trajectory tracking errors and also in their convergence rate, and the results indicate that feedback ILC control is superior to the Feedforward ILC control. In general,

Feedback ILC control proved to have a faster convergence rate than the Feedforward ILC control. Also, the well known CTC control technique (i.e. model based control algorithm) is compared to the traditional PD control approach (i.e. error based control algorithm). It is observed that at the lower speed, both of these control approaches provide similar results. However, as the speed increases, due to the difficulty in the precise calculation of the dynamic model, the position tracking errors using the CTC control approach become larger than that of the traditional PD control.

Chapter 6

EXPEIMENTS AND RESULTS ON THE HAS MECHANISM

6.1 Introduction

As described in chapter 3, the hybrid actuation system (HAS) test bed is driven by a CV motor and a servomotor. Previous studies have shown that the traditional PD control and other PD-based control methods applied to such a system might not yield to satisfactory performance due to the uncontrollability of the CV motor. Therefore, a more advanced control approach is needed for the improved trajectory tracking performance of the HAS. This is addressed in this chapter. Particularly, in Section 6.2 the dynamic model of the HAS is developed by integrating the dynamic model of the five-bar mechanism previously introduced in Chapter 2 and the dynamic model of the motors. Sliding Mode Control (SMC), which is known as an effective control technique for nonlinear systems is introduced in Section 6.3, as applied to the HAS. Section 6.4 presents the trajectory planning of the servomotor and the CV motor of the HAS mechanism. The experiments and results by applying the traditional PD control law and the SMC technique to the HAS are presented in Section 6.5. Finally, Section 6.6 gives the conclusions drawn from this chapter.

6.2 Dynamic model of the hybrid actuation system

The HAS test bed has 2 DOFs, one of which is controllable. As seen in Figure 3.9 in Chapter 3, the torque applied to link 1 is produced by a constant velocity motor and the torque applied to link 2 is produced by a servomotor. In order to be able to apply the SMC method to the HAS, the dynamic model of the system is essential. For the development of such a model, the model of the motors is presented in the following, and then integrated with the dynamic model of the parallel mechanism previously introduced in Chapter 2.

Consider a load driven by a motor, the dynamics is governed by (Nasar and Unnrewhr, 1979; Pillay and Krishnam, 1989)

$$\tau_e = \tau_L + B_m \omega_r + J_m \dot{\omega}_r \tag{6.1}$$

where τ_e is the torque generated by the motor, B_m the viscous damping coefficient, J_m is the moment of inertia of the motor, τ_L is the load torque, and ω_r is the motor's angular speed. It is known that the motor torque is proportional to the current going through the motor, i.e.,

$$\tau_e = k_\tau i_q \tag{6.2}$$

Rearranging equation (6.1), one has

Rearranging equation (6.1) leads to

$$\tau_e - \tau_L = B_m \omega_r + J_m \dot{\omega}_r \tag{6.3}$$

From equation (6.3), it is clear that the motor can only start to accelerate if the electromagnetic torque τ_e is larger than the load torque τ_L. At the start-up, the motor is at rest (i.e., speed is zero) and the left-hand side of (6.3) is greater than the right-hand side, therefore, the electric machine starts to accelerate. The motor continues to accelerate as long as this condition is held. When the steady state of the system is reached, the time derivatives in its dynamic model goe to zero, meaning the CV motor reaches steady state when $\tau_e - \tau_L = B_m \omega_r$; where $\dot{\omega}_r = 0$ (i.e., acceleration is zero) and the motor operates at a constant speed.

As mentioned previously, the CV motor is not real-time programmable, implying that its electromagnetic torque, τ_e , is constant throughout its motion. From the above discussion, one can clearly observe that in order for the CV motor to operate at constant speed, the load torque τ_L must be constant through out the entire operation time of the CV motor. However, in the case of the HAS prototype, the load torque τ_L varies periodically, therefore the speed fluctuation in the CV motor will be present, regardless of the fact that the machine is driven by the constant speed motor. This is the main reason why the traditional PD control approaches do not result in satisfactory trajectory tracking performance in the case of the HAS prototype.

Integrating the above motor dynamic equation (6.3) into the dynamic model of the closed-loop mechanism equation (2.1), a dynamic model of the HAS can be derived and is given by (Ouyang, 2005):

$$\begin{cases} \overline{D}(q')\ddot{q} + C(q', \dot{q}')\dot{q} + B\dot{q} + g(q') = \tau \\ \dot{q}' = \rho(q')\dot{q} \\ q' = \sigma(q) \end{cases} \tag{6.4}$$

where $\overline{D}(q')$ is the inertia matrix and is given by $\overline{D}(q') = (D(q') + J)$, $J = diag[J_{m1}\ J_{m2}]$, and $B = diag[B_{m1}\ B_{m2}]$. J_{mi} and B_{mi} (i = 1 or 2) are the moment of inertia and the viscous damping coefficient of the ith motor, respectively.

It should be noted that for the dynamic model of the HAS given in Equation (6.4), one has the following properties (Ghorbel, 1995; Ghorbel and Gunnawardana, 1997):

(1) The inertia matrix $\overline{D}(q')$ is asymmetric and positive definite.

(2) $\dot{\overline{D}}(q') - 2C(q', \dot{q}')$ is a skew symmetric matrix.

(3) $\dot{\overline{D}}(q')$, $C(q', \dot{q}')$ and $g(q')$ are bounded

(4) $\dot{\overline{D}}(q')$, $C(q', \dot{q}')$ and $g(q')$ are only partially known, implying that there exists uncertainty in modeling.

Properties 1 and 2 can be proved as follows. Given that both $\overline{D}(q')$ and J are symmetric and positive definite (Ghorbel, 1995; Ghorbel and Gunnawardana, 1997), the matrix $\overline{D}(q') = (D(q') + J)$ is also symmetric and positive definite because J does not change in time and is constant. The term $\dot{\overline{D}}(q') - 2C(q', \dot{q}') = \dot{D}(q') - 2C(q', \dot{q}')$ is skew (Ghorbel, 1995; Ghorbel and Gunnawardana, 1997; Ouyang 2005).

6.3 Sliding Mode Control (SMC) for nonlinear systems

For the control of nonlinear systems with parameter uncertainties, SMC is known as an effective control approach. This approach originated in Russia in the late 1960's and has since been studied extensively for the control of nonlinear systems with modeling uncertainties as well as the presence of time varying- parameter fluctuation and external disturbances (Utkin, 1977; Slotine and Li, 1991; Edwards and Spurgeon, 1998; Ouyang 2005). The goal of this control approach is to constrain the states of the controlled system to reach a given manifold in the state-space and thereafter slide towards an equilibrium condition along this manifold (Ouyang, 2005). As applied to the control of the HAS, the goal is to drive the joint position q to the desired position q_d as close as possible, despite the presence of the speed fluctuation $\dot{q}_1$ on the CV motor. As did previously, the tracking errors are defined as the difference between the actual position and the desired one, i.e.,

$$\begin{cases} e = q - q_d \\ \dot{e} = \dot{q} - \dot{q}_d \end{cases} \tag{6.5}$$

where $q_d = [q_{1d} \quad q_{2d}]^T$ and $\dot{q}_d = [\dot{q}_{1d} \quad \dot{q}_{2d}]^T$. As mentioned previously, link 1 is connected to the CV motor, so $q_{1d} = \omega_d t$ and $\dot{q}_{1d} = \omega_d$. For SMC, the following sliding surface is defined:

$$s = \dot{e} + \lambda e \tag{6.6}$$

where $\lambda = diag[\lambda_1 \quad \lambda_2]$ in which λ_1 and λ_2 are positive constants (i.e., control gains). In addition, the following reference states are defined for the SMC:

$$\begin{cases} \dot{q}_r = \dot{q} - s = \dot{q}_d - \lambda e \\ \ddot{q}_r = \ddot{q} - \dot{s} = \ddot{q}_d - \lambda \dot{e} \end{cases} \tag{6.7}$$

As discussed in the preceding section, for the SMC control approach, it is assumed that the dynamic model components, $\overline{D}(q')$, $C(q', \dot{q}')$, and $g(q')$ are only partially known. Let, let $\hat{\overline{D}}(q')$, $\hat{C}(q', \dot{q}')$, and $\hat{g}(q')$ denote the estimations of $\overline{D}(q')$, $C(q', \dot{q}')$, and $g(q')$, respectively. Also let, $\Delta\overline{D}(q') = \hat{\overline{D}}(q') - \overline{D}(q')$, $\Delta C(q', \dot{q}') = \hat{C}(q', \dot{q}') - C(q', \dot{q}')$, and $\Delta g(q') = \hat{g}(q') - g(q')$. Substituting Equations (6.5)-(6.7) into Equation (6.4), the dynamic model of the hybrid mechanism in terms of the newly defined signal vector s, can be written as follows:

$$\overline{D}(q')\dot{s} + C(q', \dot{q}')s + Bs = \begin{bmatrix} \tau_1 - f_1 + \Delta f_1 - B_{m1}\dot{q}_1 + B_{m1}s_1 \\ \tau_2 - f_2 + \Delta f_2 - B_{m2}\dot{q}_2 + B_{m2}s_2 \end{bmatrix} \tag{6.8}$$

where

$$f_1 = \hat{\bar{d}}_{11}(q')\ddot{q}_{r1} + \hat{\bar{d}}_{12}(q')\ddot{q}_{r2} + \hat{c}_{11}(q',\dot{q}')\dot{q}_{r1} + \hat{c}_{12}(q',\dot{q}')\dot{q}_{r2} + \hat{g}_1(q') \tag{6.9}$$

$$f_2 = \hat{\bar{d}}_{21}(q')\ddot{q}_{r1} + \hat{\bar{d}}_{22}(q')\ddot{q}_{r2} + \hat{c}_{21}(q',\dot{q}')\dot{q}_{r1} + \hat{c}_{22}(q',\dot{q}')\dot{q}_{r2} + \hat{g}_2(q') \tag{6.10}$$

$$\Delta f = [\Delta f_1 \;\; \Delta f_2]^T = \Delta\bar{D}(q')\ddot{q}_r + \Delta C(q',\dot{q}')\dot{q}_r + \Delta g(q') \tag{6.11}$$

For the CV motor it is assumed that the motor torque is constant. If the CV motor is running at its operating speed, λ_1 is equal to 0; and the motor torque is given by

$$\tau_1 = B_{m1}\omega_d \tag{6.12}$$

Further, the controlled torque for the servomotor is set as (Ouyang, 2005):

$$\tau_2 = B_{m2}\dot{q}_{2r} + f_2 - K\,\mathrm{sgn}(s_2) - as_2 + \tau_r \tag{6.13}$$

where K is a design parameter, which is a positive constant; and τ_r is the designed torque of the servomotor to compensate for the speed fluctuations in the CV motor. Assume $|\Delta f_i| < \Delta f_{bi}$, where Δf_{bi} is a positive constant, giving the boundary of Δf_i. The positive constant K is chosen such that,

$$K \geq \Delta f_{b2} \tag{6.14}$$

The designed torque τ_r is based on the following switching rule:

$$\tau_r = \begin{matrix} -|s_1|(|f_1| + \Delta f_{b1})/s_2, & if \quad s_2 \neq 0 \\ 0 & if \ s_2 = 0 \end{matrix} \tag{6.15}$$

Furthermore, several remarks are given to the above SMC control law as applied to the control of the HAS according to (Ouyang, 2005):

Remark 1. From Equation (6.13), it is observed that the torque applied to the servomotor is not continuous. A smoothing method based on Slotine (1991) is used in order to eliminate the chattering of the servomotor as follows:

$$\tau_2 = B_{m2}\dot{q}_{2r} + f_2 - Ksat(s_2/\phi) - as_2 + \tau_r\phi > 0, \tag{6.16}$$

where ϕ is called the boundary layer and must be greater than 0.

Remark 2. The designed torque for the servomotor in Equation (6.15) is discontinuous as the sliding surface *s* is discontinuous. Therefore, Equation (6.15) is modified to eliminate this chattering as follows:

$$\tau_r = \frac{-|s_1|(|f_1| + \Delta f_{b1})s_2}{\delta + s_2^2} \tag{6.17}$$

where δ is the boundary layer thickness and is greater than zero (i.e., $\delta > 0$)

6.4 Trajectory Planning for the CV and Servomotor

In this study, the CV motor is desired to rotate at a constant speed, while the servomotor is planned in terms of the Hermite polynomial of the fifth degree. It is noted that for the servomotor, such a planed trajectory results in bounded continuous position, velocity, and acceleration profiles. The desired trajectories of both motors can be expressed as

$$q_1^d(t) = \omega_d t \tag{6.18}$$

$$q_2^d(t) = q_{20}^d + (6\frac{t^5}{t_f^5} - 15\frac{t^4}{t_f^4} + 10\frac{t^3}{t_f^3})(q_{2f}^d - q_{20}^d) \tag{6.19}$$

where $q_1^d(t)$ and $q_2^d(t)$ are the desired trajectories of the two motors, q_{20}^d and q_{2f}^d are the desired initial and final positions of the input link 2 driven by the servomotor, t_f represents the time required to reach the final position from the initial one. Two cases with different operating speeds are set for experiments. As well for simplification, for both operating speeds, $q_1(0) = 0$, $q_2(0) = 0$. In the experimental results presented in the following section, the parameter values are set as, respectively:

Case 1:

$$\omega_d = 0.25\pi \text{ (rad/s)}, \ q_{20}^d = 0, \ q_{2f}^d = \pi, \text{ and } t_f = 4\text{s}. \tag{6.20}$$

Case 2:

$$\omega_d = 0.5\pi \text{ (rad/s)}, \ q_{20}^d = 0, \ q_{2f}^d = 2\pi, \text{ and } t_f = 4\text{s}. \tag{6.21}$$

As can be seen from equations (6.20) and (6.21), the speed in Case 2 has doubled compared to that of Case 1. For convenience, the first case is referred to as the low speed case and the second one as the high speed case in the rest of this chapter.

6.5 Experimental Results of the HAS

The traditional PD control and the SMC control law are applied to the HAS mechanism. The error between the desired motion and the actual motion is used to measure the performance in this experimental study, as in the case of the RTC mechanism presented in Chapter 5. The sampling periods for the traditional PD controller and the SMC are 4ms and 10ms, respectively. The increase in the sampling time of the SMC is mainly due to additional computational time required for this control law. From experimental observation, the smallest sampling period attainable for the SMC control is 6ms. However, since SMC heavily relies on velocity information, this sampling period was increased to 10ms to obtain a smoother velocity profile.

The control parameters of the PD and SMC control laws are selected via trial and error based on the criteria that was discussed in Chapter 5. In the case of the PD controller, K_p and K_p are given as follows.

The low speed case:

Actuator 1 (servomotor): $K_{p1} = 0.00035$, $K_{d1} = 0.000041$

Actuator 2 (CV motor): Not real time controllable, i.e., no control gains

The high speed case:

Actuator 1 (servomotor): $K_{p1} = 0.00065$, $K_{d1} = 0.000072$

Actuator 2 (CV motor): Not real time controllable, i.e., no control gains

For the SMC control law, the controlled torque for the servomotor is chosen as in Equation (6.16) with a = 0.00055 and $\lambda_2 = 0.00045$. Three case studies are performed at the high speed operating condition and 3 are performed at the low speed operating condition with the following control parameters:

Low Speed:

For Case 1: $\delta = 0.5$, $K = 1.5000$, and $\phi = 1.0000$

For Case 2: $\delta = 0.7$, $K = 2.5000$, and $\phi = 1.4000$

For Case 3: $\delta = 0.9$, $K = 3.0000$, and $\phi = 1.8000$

High Speed:

For Case 1: $\lambda = 1.5$, $K = 2.3000$, and $\phi = 2.0000$

For Case 2: $\lambda = 2.4$, $K = 3.5000$, and $\phi = 2.5000$

For Case 3: $\lambda = 2.5$, $K = 3.4000$, and $\phi = 2.4000$

The physical parameters of the HAS prototype are previously presented in Figures 3.3 through 3.6 in Chapter 3, while the parameters of the two motors are listed in Table 6.1.

Table 6.1 The parameters of the two motors

Motor Type	J (Kgm^2)	B_m (Nms)
CV motor	0.75	0.75
Servomotor	0.085	0.085

The position tracking errors or the difference between the measured angular position and the desired ones are evaluated using the PD and SMC control laws. Figures 6.1 through 6.4 on the following pages illustrate the position tracking errors in the actuators as a result of applying the PD and SMC controllers to the HAS, respectively. It should be noted that the results presented for the comparison of the PD and SMC control laws correspond to the parameters stated for Case 3 of the SMC at both the low and high speed operating conditions, as these parameters resulted in the lowest position tracking errors in the servomotor.

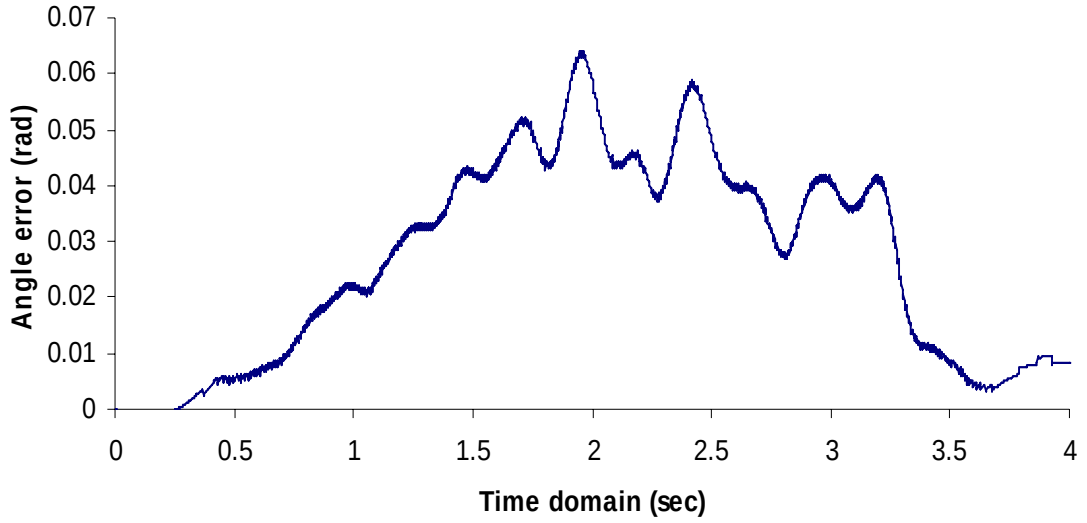

(a)

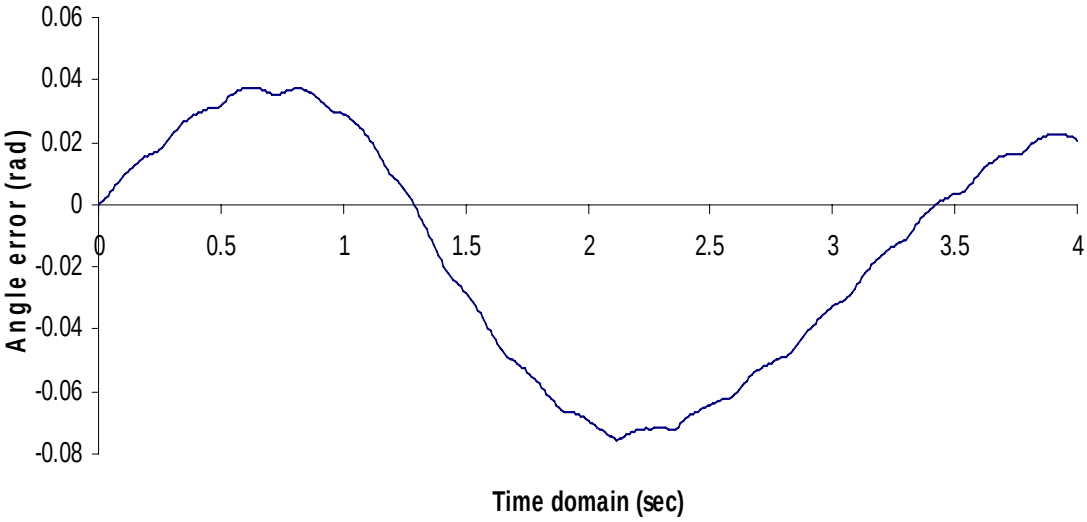

(b)

Figure 6.1: Measured position tracking errors in the motors for the low speed case using PD controller: (a) angle error of Servomotor and (b) angle error of CV motor

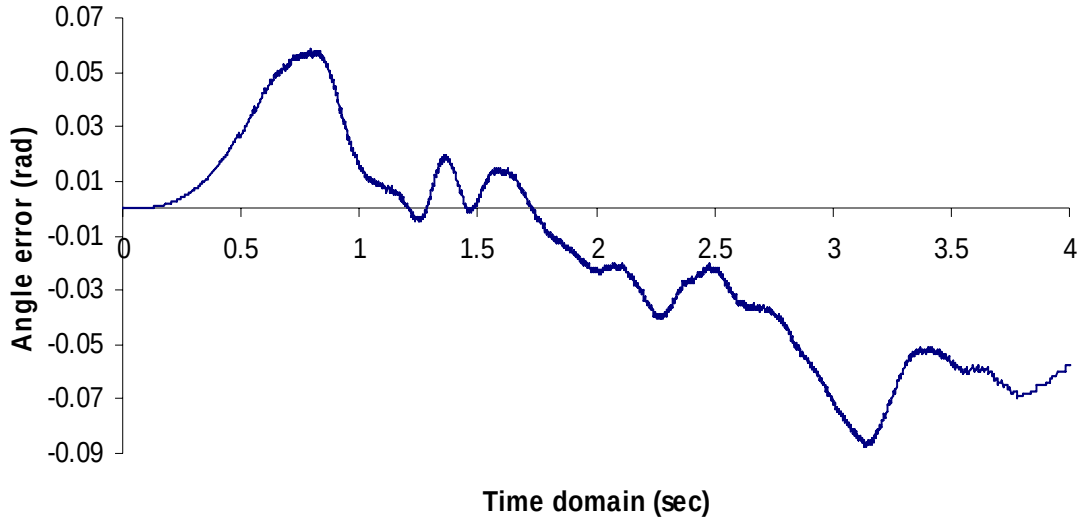

(a)

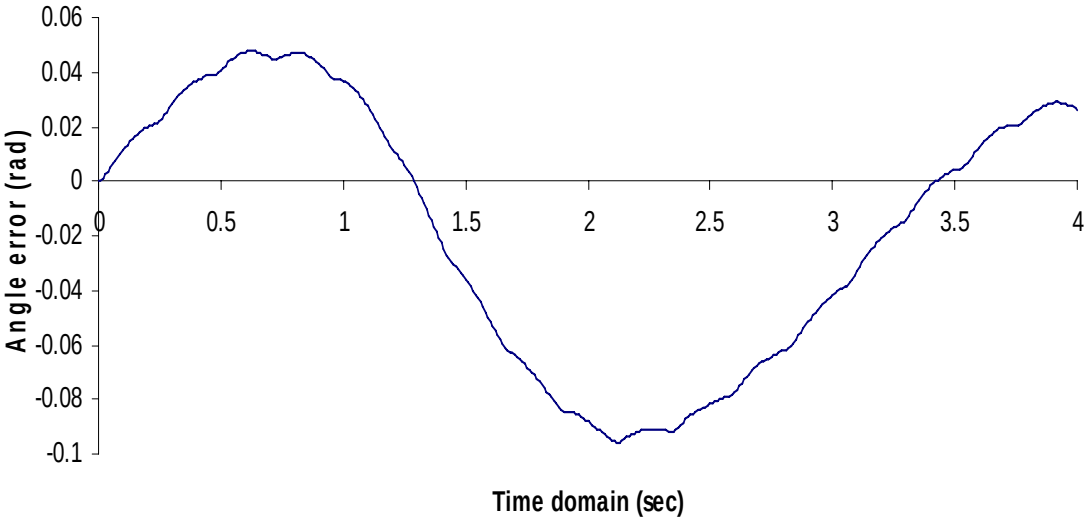

(b)

Figure 6.2: Measured position tracking errors in the motors for the high speed case using PD controller: (a) angle error of Servomotor and (b) angle error of CV motor

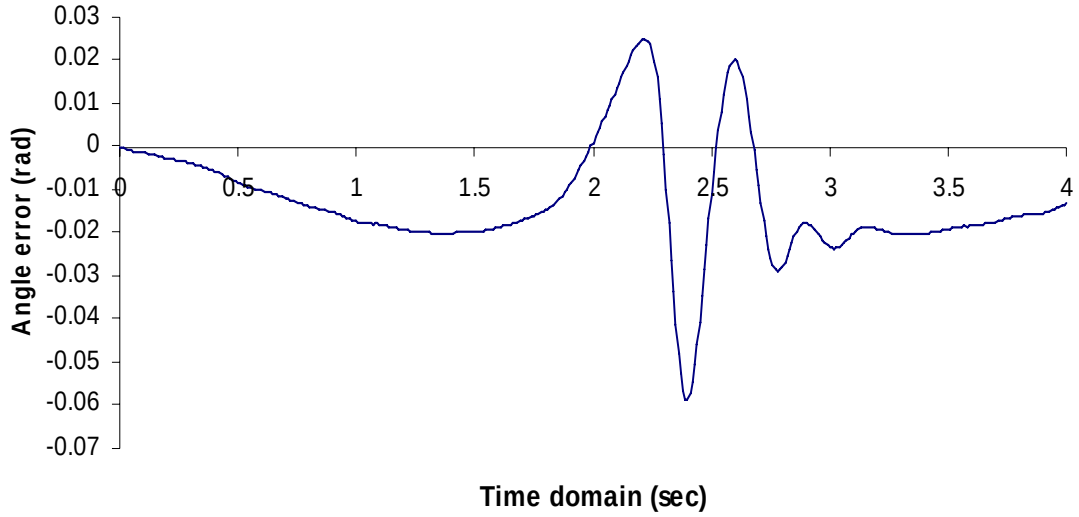

(a)

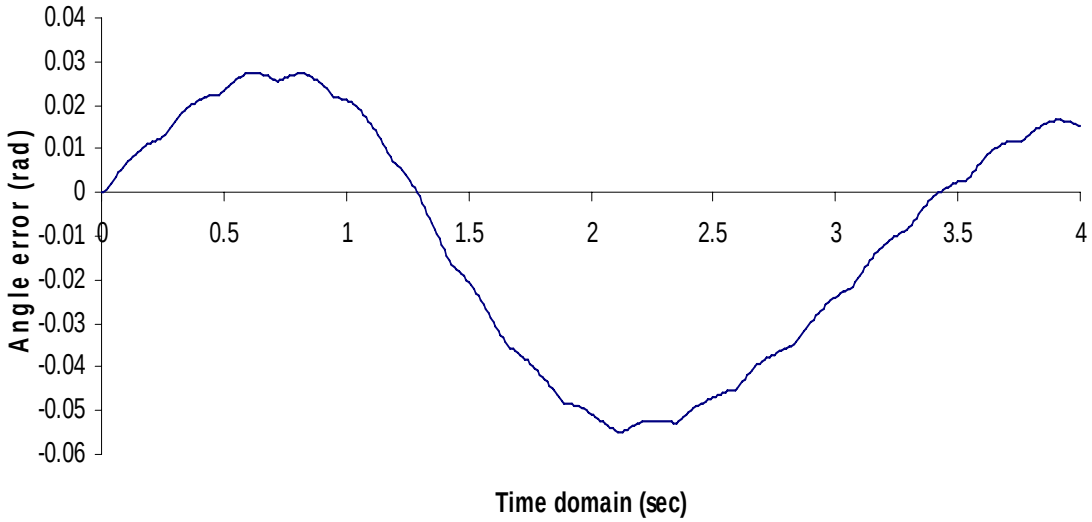

(b)

Figure 6.3: Measured position tracking errors in the motors for the low speed case using SMC: (a) angle error of Servomotor and (b) angle error of CV motor

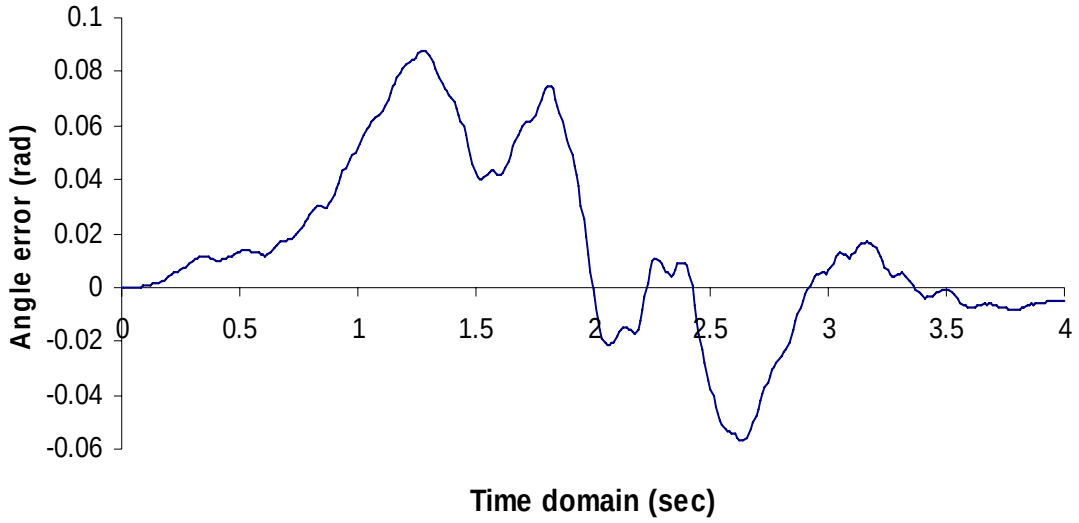

(a)

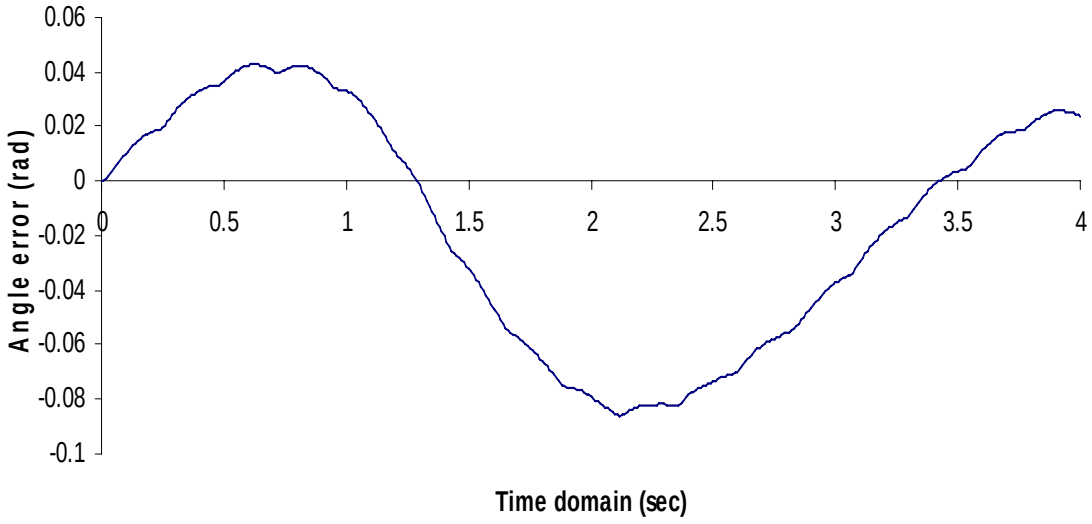

(b)

Figure 6.4: Measured position tracking errors in the motors for the high speed case using SMC: (a) angle error of Servomotor and (b) angle error of CV motor

From Figures 6.1 and 6.2, the maximum position tracking errors for the low speed operating case using PD control are 0.059 rad and 0.072 rad for the servomotor and the CV motor, respectively; and are 0.086 rad and 0.092 rad for the high speed case. The results show satisfactory trajectory tracking at these operating speeds by using PD control, although it was indicated by Ouyang (2005) that this controller is inadequate for such a mechanism. This can be explained as follows. The maximum speed that the HAS mechanism is operated at for this experimental study is 15 rpm. At this operating speed however, the speed fluctuation of the CV motor is not considerably large enough to have a significant impact on the servomotor. Nonetheless, it is interesting to note from Figure 6.1 that at lower speeds the position errors of the PD controller for the servomotor tend to converge closer to zero compared to that of the high speed case. From these figures it can be observed that the PD controller is not as effective at the higher speed case for the HAS. This is due to the reason that at the higher operating speed scenario, the velocity fluctuations of the CV motor is also larger, which the PD controller can not compensate for.

As the speed of the mechanism increases, these velocity fluctuations become too large and the PD controller becomes unstable. In such operating conditions, a controller such as SMC that takes into account the velocity fluctuations of the CV motor is necessary for the control of the HAS. From Figures 6.3 and 6.4, one can observe that the SMC control law results in satisfactory performance and acceptable errors at both the low and high speed operating conditions. Particularly, the maximum position tracking errors for the low speed cases using SMC control are 0.057 rad and 0.052 rad for the servomotor and

the CV motor, respectively and are 0.084 rad and 0.089 rad for the high speed case. It should be noted that at the higher speed operating condition, the position tracking errors of the SMC control law converge to nearly zero, whilst those of the traditional PD controller do not. This shows that the SMC controller is more effective than the PD controller at the higher speed case.

6.6 Conclusion

In this chapter, the complete dynamic model of the HAS prototype including the dynamic models of the servomotor and the CV motor are introduced. As well, SMC is reviewed and outlined for the control of nonlinear time-varying systems with parameter uncertainties. In the experimental study presented in this chapter, the traditional PD control and the SMC are applied to the HAS. It was observed that at the speed examined in this experimental study, PD control can result in satisfactory performance. It is also observed that SMC proved to be more effective than the traditional PD control at higher speeds. The reason for this is that the SMC control law can compensate for the velocity fluctuation of the CV motor, whilst the traditional PD controller does not have this capability. As the velocity fluctuation of the CV motor becomes larger at higher speeds, the traditional PD controller becomes unstable and may not be adequate for the control of the HAS.

Chapter 7

Conclusion and Recommendation

7.1 Overview of the thesis

RTC mechanisms and hybrid actuation systems are widely used in the industry. Recently, several control approaches have been developed for the control of both RTC mechanisms and hybrid actuation systems at the AEDL of the University of Saskatchewan. These control approaches have proven to be promising through simulation studies, experimental verification, however, remains to be addressed. This research is to carry out an experimental study to examine and verify their effectiveness.

One of the major contributions of this research is the development of a generic experiment environment where various control approaches can be examined and verified experimentally. Particularly, two test beds, the RTC mechanism and the HAS, were designed and developed for this purpose.

The other major contribution is the experimental examination and verification of several control approaches. As applied to the RTC mechanism, the examined control approaches include the traditional PD control, NPD control, iterative learning control techniques

(EPD, NPD-LC, and AES-PD), and the CTC approach. As applied to the HAS, the traditional PD control and the SMC control technique are examined and compared.

7.2 Major Conclusions

(1) The RTC mechanism and the HAS, developed based on a 2-DOF closed-loop mechanism is appropriate for the experimental examination and verification of different control approaches.

(2) The experiments on the five PD-based control algorithms, i.e., PD control, NPD control, EPD, NPD-LC, and AES-PD, show that the NPD controller has better performance than the PD controller in terms of the reduction in position tracking errors. It is also illustrated by the experiments that EPD, NPD-LC, and AES-PD are all effective for use in situations where the task of the robot involves a repetition of its trajectory. Moreover, AES-PD control technique was shown to be superior to both the NPD-LC and the EPD in terms of the reduction in the position tracking errors from iteration to iteration.

(3) Feedback and feedforward ILC are applied to the RTC mechanism. Experimental results show that feedback ILC is more effective than the feedforward ILC and has a faster convergence rate. In addition, the results of the comparative study of the traditional PD and the CTC control technique at both low and high speeds show that at lower speeds, both of these controllers provide similar results. However, with an

increase in speed, as the accuracy in the calculation of the dynamic model decreases, the position tracking errors using the CTC control approach become larger than that of the traditional PD control

(4) The experimental results of the HAS show that for the control of the hybrid machine for the range of speed used in this experimental study, the traditional PD control can result in satisfactory performance. However, with an increase in speed, SMC proved to be more effective. SMC has the capability to cope with the velocity fluctuation present in the system as a result of the presence of the CV motor. As the speed increases and thereof a larger velocity fluctuation will be present, the traditional PD controller can no longer compensate for this velocity fluctuation and will become unstable. Therefore, at higher speeds a more sophisticated controller such as SMC is required.

7.3 Future Work

The experiments and results presented in this thesis are based on some simplifications. The results presented are acceptable for the purposes of demonstrating the validity and effectiveness of the proposed control algorithms. For applications to the real situations, however, some issues need to be further addressed, which include the initial position error, the sampling period, and the estimation of velocity. In particular, for the problem related to the initial position error, one solution would be to use an absolute position encoder. As well, to reduce the sampling period for future possible improvement of the

control performance, one may use a hardware device such as dSPACE. In addition, for the estimation of velocity, a low pass filter could be used for possible improvements.

In the experiments presented in this thesis, the motor speed to drive the mechanism was set up to 15 rpm. With the current settings, the system was found to be inappropriate to run at speeds higher than this speed due to the presence of the un-balanced forces. To alleviate this problem, the individual linkages of the five-bar structure should be redesigned so that the force balancing conditions can be achieved in the mechanism, thereby possibly further improving the trajectory tracking performance.

REFERENCES

Armstrong, B., and Wade, B. A., 2000, Nonlinear PID Control with Partial State Knowledge: Damping without Derivatives, The International Journal of Robotics Research, Vol.19, No. 8, pp. 715-731.

Arimoto, S., Kawamura, S., and Miyasaki, F., 1984, Bettering operation of robots by learning, Journal of Robotic Systems, Vol.1, No.2, pp. 123-140.

Chen, Q.J., Chen, H. T., Wang, Y.J., and Woo, P.Y., 2001, Global stability analysis for some trajectory tracking control schemes of robotic manipulators, Journal of Robotic Systems, Vol. 18, No. 2, pp. 69-75.

Chen, Y. Q., and Moore, K. L., 2002, An optimal design of PD-type iterative learning control with monotonic convergence, Proceedings of the 2002 IEEE International symposium on Intelligent Control, pp. 55-60.

Codourey, A., 1998, dynamic modeling of parallel robots for computed-torque control implementation, The International Journal of Robot Research, Vol. 17, No. 12, pp. 1325-1136.

Constantinescu, D., and Croft, E.A., 2000, Smooth and time-optimal trajectory planning for industrial manipulators along specified paths, Journal of Robotic Systems, Vol. 17, No. 5, pp. 233-249.

Craig, J. J., 1986, Introduction to robotics: mechanics and control. Reading, Addison Wesley, MA.

Craig, J.J., 1988, Adaptive control of mechanical manipulators, Addison-Wesley.

Edwards, C. and Spurgeon, S. K., 1998, Sliding Mode Control Theory and Application, Taylor & Francis Ltd, Padstow, UK.

Fitcher, E.F., 1986, A Stewart platform based Manipulator: General Theory and Practical Construction, International Journal of Robotics Research, pp. 157-182.

Gautrier, M., Khalil, P., and Restrepo P., 1995, Identification of the dynamic parameters of a closed-loop robot, in Proceedings of IEEE International Conference of Robot Automat, pp. 3045-3050.

Ghorbel, F., 1995 Modeling and PD control of a closed-chain mechanical system, Proceeding of 34th Conference on Decision & Control, New Orleans, LA, USA, pp. 540 542.

Ghorbel, F., 1997, A validation study of PD control of a closed chain mechanical system, Proceeding of the 36th Conference on Decision & Control, San Diego, California, USA,

Dec., 1997, pp. 1998-2004.

Ghorbel, F., and Gunawardana, R., 1997, A validation study of PD control of a closed chain mechanical system, Proceeding of the 36th Conference on Decision & Control, San Diego, California, USA, Dec., 1997, pp. 1998-2004.

Ghorbel, F., and Srinivasan, B., 1998, On the uniform boundedness of the inertia matrix of serial robot manipulators, Journal of Robotic Systems, Vol. 15, No. 1, pp. 17-28.

Ghorbel, F., Chetelat, O., and Longchamp, R., 1994, A reduced model for constrained rigid bodies with application to parallel mechanical systems, Proceeding of the 4th IFAC Symposium on Robot Control, Capri, Italy, pp. 45-50.

Greenough, J. D., Bradshaw, W. K., and Gilmartin, M. J., 1995, Design of hybrid machines, Proceedings of the 9th World Congress on the Theory of Machines and Mechanisms, pp. 2501-2505.

Guo, L. S., Zhang, W. J., Li, Y. F., and Li, Q., 1999, Design, Modelling and Control of a Hybrid Machine, IEEE/ASME Trans on Mechatronics, Vol. 14, pp.324-332.

Hall, Jr., Allen S., 1981. Notes on Mechanism Analysis, Waveland Press, Prospect Heights, Illinois.

IFToMM, 1991, Terminology for the theory of machines and mechanisms, Mechanism and Machine Theory, Vol. 26, No. 5, pp. 435-439.

Kelly, R., 1997, PD control with desired gravity compensation of robotic manipulators: a Review, The international Journal of Robotics Research, Vol. 16, No. 5, pp. 660-672.

Kerry, R., 1997, PD control with desired gravity compensation of robotic manipulators: a review, The International Journal of Robotics Research, Vol.16, No. 5, pp. 660-672.

Klein, B. A. J., 1987, Kinematic optimization of mechanisms, a finite element approach, Dissertation, Delft University of Technology, the Netherlands.

Kreyszig, E., 2002, Advanced Engineering Math, John Wiley and Sons.

Kuc, T. Y., Nam, K., and Lee, J. S., 1991, An iterative learning control of robot manipulators, IEEE Trans. on Robotics and Automation, Vol. 7, No. 6, pp. 835-842.

Li, Q., and Wu, F. X., 2004, Control performance improvement of a parallel robot via the design for control approach, Mechatronics, Vol.14, pp.947-964.

Li, Q., Tso, S. K., Guo, L. S., and Zhang, W. J., 2000, Improving motion tracking of servomotor-driven closed-loop mechanisms using mass-redistribution, Mechanism and Machine Theory, Vol. 35, No. 7, pp. 1033-1045.

Lin, C.S., Chang P.R., and Luh, J.Y.S., 1983, formulation and optimization of cubic polynomial joint trajectories for industrial robots, IEEE trans. On Automatic Control, Vol. AC-28, No. 12, pp. 1066-1074.

Liu, K., Lebret, G., and Lewis, F.L., 1993, Dynamic Analysis and Control of a SP Manipulator, Journal of Robotic Systems, Vol. 10, No. 5, pp. 629-655.

Macfarlane, S., and Croft, E.A., 2001, Design of jerk bounded trajectories for on-line industrial robot applications, Proceedings of the 2001 IEEE International Conference on Robotics and Automation, Seoul, Korea, pp. 979-984.

Nasar, S. A., and Unnewehr, L. E., 1979, Electromechanics and Electric Machines, John Wiley & Sons, New York.

Nguyen, P., and Cipra, R. J., 1999, Dynamic analysis of five-bar mechanism with torsional springs using Lagrange's equation and kinematic coefficients, 1999 ASME Design Engineering Technical Conferences, DAC-8621, Las Vages, Nevada, USA.

Ouyang, P., 2002, "Force balancing design and trajectory tracking control of real-time controllable mechanisms", M.Sc. thesis, University of Saskatchewan.

Ouyang, P., 2005, "Hybrid Intelligent Machine Systems: Design, Modelling and control", Ph.D. thesis, University of Saskatchewan.

Ouyang, P. R., and Zhang, W. J., 2004, Comparison of PD-based Controllers for Robotic Manipulators, Proceedings of the ASME Design Engineering Technical Conference, Vol. 2, pp. 23-31.

Ouyang, P. R., Zhang, W. J., and Gupta, M. M., 2004, Adaptive Nonlinear PD Learning Control for Robot Manipulators, Proceedings of the ASME Design Engineering Technical Conference, Vol. 2, pp. 357-365.

Ouyang, P. R., Zhang, W. J., and Gupta, M. M., 2004, A Robust PD-type Evolutionary Learning Control for Nonlinear Time-varying systems, the 2004 IEEE International Symposium on Intelligent Control, September 1 - 4, Taipei, Taiwan, pp. 90-95.

Paul, R. P., 1979, Manipulator Cartesian path control, IEEE Trans. System, Man, Cybern., Vol. SMC-9, Nov., pp. 702-711.

Qu, Z. H., 1994, Global stability of trajectory tracking of robot under PD control, Dynamics and Control, Vol. 5, No. 1, pp. 59-71.

Qu, Z. H., 1995, Global stability of trajectory tracking of robot under PD control, Dynamics and Control, Vol. 5, No. 1, pp. 59-71.

Raghavan, M., Waldron, K.J., and Roth, B., 1989, Kinematics of a Hybrid Series-Parallel Manipulation System, AMSE J. of DMC., Vol.111, pp. 211-221.

Reboulet, C., and Berthomieu, T., 1991, Dynamic models of a Six Degree of Freedom Parallel Manipulators, Proc. Of the Conf. ICAR 91, pp. 377-394.

Rugh, W. J., 1987, Design of nonlinear PID controllers, AIChE Journal, Vol. 33, No. 10, pp. 1738-1742.

Seraji, H., 1998, Nonlinear and adaptive control of force and compliance in manipulators, International Journal of Robotics Research, Vol. 17, No. 5, pp. 467-484.

Shahruz, S. M., and Schwartz, A. L., 1994, Design and optimal tuning of nonlinear PI compensators, Journal of Optimization Theory and Applications, Vol. 83, No. 1, pp. 181-198.

Slotine, J. E., and Li, W. P., 1991, Applied Nonlinear Control, Prentice Hall, Eaglewood Cliffs, N. J.

Tayebi, A., 2003, Adaptive iterative learning control for robot manipulators, Proceedings of the American Control Conference, pp.4518-4523.

Thomson, W. T., 1993, Theory of vibration with Applications, Prentice Hall, Englewood Cliffs, New Jersey.

Tokuz, L.C. and Jones, J.R., 1991, Programmable modulation of motion using hybrid machines, Proceedings of ImechE, C414/071, pp.85-91.

Tondu, B., and Bazaz S. A., The three-cubic method: an optimal online robot joint trajectory generator under velocity, acceleration, and wandering constraints, The International Journal of Robotics Research, Vol. 18, No. 9, pp. 893-901.

Utkin, V. I., 1977, Variable structure systems with sliding modes, IEEE Trans. On Automatic Control, Vol. 22, No. 2, pp. 212-222.

Wang, Z. H., 2000, "Mechatronic design to real-time controllable mechanical systems: force balancing and trajectory tracking", M.Sc. thesis, University of Saskatchewan.

Xu, Y. M., Hollerbach, J. M., and Ma, D. H., 1995, A Nonlinear PD Controller for Force and Contact transient control, IEEE Control Systems Magazine, Vol. 15, No. 1, pp. 15-21.

Youcef-Toumi, J., and Kuo, A. T. Y., 1993, High-speed trajectory control of a direct drive manipulator, IEEE Trans. On Robotics and Automation, Vol. 9, pp. 102-108